FINAL REPORT

NEIWPCC Job Code: 0346-002-001

Project Code: LS-2020-063

Contractor: Stone Environmental, Inc.

Prepared By:
Dave Braun, M.S., Stone Environmental, Inc.
Andrew Schroth, Ph.D., University of Vermont
Ashton Kirol, M.S., University of Vermont
Clelia Marti, Ph.D., University of Western Australia
Ken Wagner, Ph.D., Walter Resource Services, Inc.

Project Period: 5/26/2020 to 8/30/2024

Date Final Version Submitted: August 30, 2024

Date Approved: August 30, 2024

EVALUATING ALTERNATIVES TO CONTROL INTERNAL PHOSPHORUS LOADING IN MISSISQUOI BAY USING A 3-DIMENSIONAL COUPLED HYDRODYNAMIC-AQUATIC ECOSYSTEM MODEL

CONTACT INFORMATION

Stone Environmental, Inc.
535 Stone Cutters Way, Montpelier, Vermont 05602
802-272-8819; dbraun@stone-env.com

This project was funded by an agreement awarded by EPA to NEIWPCC in partnership with LCBP.

The viewpoints expressed here do not necessarily represent those of LCBP, NEIWPCC, EPA, or the Great Lakes Fishery Commission, nor does mention of trade names, commercial products, or causes constitute endorsement or recommendation for use.

Executive Summary

Existing Conditions in Missisquoi Bay

Persistent and relatively severe cyanobacteria blooms that occur in late summer and early fall in Missisquoi Bay (MB) degrade surface water quality and decrease ecosystem services (*Isles et al.,* 2017a). Whereas the long-term eutrophication of MB was driven by increased riverine nutrient loads, the build-up of legacy phosphorus (P) in the sediments, and subsequent release of immediately bioavailable sediment P to the water column (internal P loading), can drive cyanobacteria bloom initiation, duration, and severity (e.g., *Smith et al.*, 2011; *Pearce et al.*, 2013; *Giles et al.*, 2016; *Isles et al.*, 2017a).

Due to MB's particularly high surface area relative to its volume, coupled with its robust inventory of legacy P in surface sediment, nutrient dynamics in MB are strongly impacted by internal P loading. Much of the internal P loading to MB occurs during summer months, when the majority of water column P is likely derived from internal loading, although this relative contribution fluctuates each year due to variability in weather patterns (*Giles et al.*, 2016; *LimnoTech*, 2012; *Isles et al.*, 2017a,b). Summer internal P loading occurs during periods when water residence times in the bay are longest, temperatures are favorable for cyanobacteria growth, and the water column is stratified, which allows cyanobacteria to outcompete other phytoplankton for P due to their buoyancy regulation (*Huisman et al.*, 2018).

A stable water column with minimal vertical mixing promotes reducing conditions at the sediment-water interface (SWI) as dissolved oxygen (DO) in the bottom water is depleted, which leads to release of P from redox-sensitive mineral phases, primarily iron oxyhydroxides in the case of MB (*Schroth et al.*, 2015; *Giles et al.*, 2016). Conversely, riverine inputs and wind promote mixing of the water column, input of riverine sediments, and reoxidation of the SWI, all of which promote accumulation of sediment P (*Giles et al.*, 2016). Because the system has such a high surface area to volume ratio, MB is particularly sensitive to wind speed and orientation, completely turning over in response to relatively minor wind events (e.g., 4 m/s, *Isles et al.,* 2015), facilitating rapid changes in SWI redox chemistry (*Smith et al.*, 2011). The interannual variability in the duration and severity of cyanobacteria blooms in MB has been attributed to the frequency and duration of these contradictory conditions at times when water temperatures are in a range that promote cyanobacteria dominance (*Isles et al.*, 2017a).

Study Insights into P Loading Dynamics

A sediment and water sampling campaign was carried out for this project to quantify the concentrations and mass of redox-sensitive P and total P across Missisquoi Bay and to refine our conceptual understanding of internal P loading dynamics. Our sampling approach was designed to assess the potential for reducing internal P loading through inactivation treatment of legacy sediment P. UVM led collection and analysis of sediment and water samples in the 2020 and 2021 field seasons.

The mean total P (TP) concentration in the top 10 cm of sediment across all sampling locations was 1.00 mg/g of dry sediment (range: 0.63–1.42 mg/g). Redox-sensitive P varied in concentration from 0.13 mg/g to 0.70 mg/g and was 38% of TP on average. The highest P concentrations were in the deeper waters of the western bay (north of the U.S. – Canada border), along the east side of the bay, and near the southwestern outlet. Concentrations were lower in shallow areas such as the northwestern lobe, along the western shore, and along the west side of the southeast lobe. There were positive correlations between TP and total iron (Fe) concentrations ($r = 0.92$, $n = 110$, $p < 0.0001$) and between redox-sensitive P and Fe concentrations ($r = 0.88$, $n = 110$, $p < 0.0001$) in sediment across all sampling locations.

Density generally decreased toward the deeper central bay where organics likely make up a larger proportion of sediment due to accumulation of autochthonous biomass. Sediment samples from shallow areas near shore had nearly twice the density of those from the middle of the bay. The highest P mass that can potentially contribute to internal loading is found in the overlap of areas with high redox-sensitive P concentration and high bulk density. P flux rates do not directly correspond with P mass. Because lower density sediments generally have higher porosity, water and dissolved P flow more readily through these sediments into the water column. P flux may be especially high in the deeper central bay where some of the highest concentrations of redox sensitive P are found in some of the lowest density sediments.

Redox-sensitive P mass in the top 10 cm of sediment ranged from 10 g/m^2 in the northern bay to 31 g/m^2 in the east/southeast and near the outlet of the bay (interpolation root-mean-square error = 4.6 g/m^2). We estimate there are 76,000–84,000 kg of redox-sensitive P in the top 1 cm and 1,157,000–1,398,000 kg in the top 10 cm of sediment. There are 168,000–192,000 kg of TP in the top 1 cm and 3,390,000–3,791,000 kg in the top 10 cm of sediment. Estimates of P mass are lower if the area is constrained by water depth.

Missisquoi Bay is a polymictic system that experiences brief periods of spatially heterogeneous stratification and anoxia during the ice-free season. The average difference in surface and bottom temperature was 0.37°C during the ~June-October monitoring periods in 2020–2021. This small temperature difference and MB's shallow depth result in a relatively unstable water column even when stratified. Prevailing southerly winds frequently mix MB; there were >600 mixing events in the 2020/2021 field seasons. However, during brief periods of stratification low DO concentrations can develop in the bottom water quite rapidly. Low bottom water DO concentrations (<2.5 mg/L) were measured at UVM's high-frequency buoy (HFB) in 2021 and at Lake Champlain Long-term Monitoring Program stations 50 in 2017 and 53 in 2021 (VTDEC, 2022). In August 2021 DO in the bottom water at the HFB declined from 8.9 mg/L to 2.5 mg/L in the span of about two days (53 hours). Over this period the hypolimnetic oxygen demand was approximately 2.9 mg/L per day. The most widespread low DO encountered was on August 25, 2021, when manual sonde readings just above the SWI were below 1 mg/L in the southeast lobe, 0.48–2.74 mg/L in the southwest and along the western side, increasing to 2.8–6.07 mg/L in the northeast, and 7.36 mg/L in the northwestern lobe.

Episodic, redox-driven release of P was documented on August 25, 2021, when the southern half of the bay had low oxygen and relatively high P and manganese (Mn) concentrations in bottom water; this condition had lasted for a few days, indicating that this was a relatively large-scale internal loading event. Bottom water total dissolved P (TDP) concentrations varied by a factor of 4 across the bay (44–177 µg/L) during the same day, and Mn (70–2,030 µg/L) by a factor of almost 30 across a similar range of depths (2.3–4.4 meters). Spikes in dissolved Mn^{2+} concentrations are reliable indicators of P release, especially in mineral rich sediments like those of Missisquoi Bay (*Isles et al., 2015; Giles et al., 2016*). TDP concentrations in bottom water were strongly correlated with both dissolved Fe [$r = 0.84$, $n = 84$, $p < 0.0001$] and Mn [$r = 0.83$, $n = 84$, $p < 0.0001$] through this sampling period. Conversely, during a fully mixed sampling event on August 13, 2021, bottom water concentrations of TDP (37–70 µg/L) and Mn

(3–11 µg/L) were relatively low and less variable. These results demonstrate that despite the nearly uniform depth of the bay and the ubiquitously high concentration of redox-sensitive P in sediments, conditions that promote internal loading were highly dynamic in space, as MB's hydrodynamics in response to wind promotes variable redox conditions at the SWI.

AEM3D Model Scenario Evaluation

A coupled three-dimensional model of hydrodynamics and biogeochemical processes was used for this study. AEM3D has been used widely in numerous lakes and reservoirs for estimating required external and internal load reductions for achieving water quality goals (*Burger et al., 2008; Trolle et al., 2008; Valipour et al., 2016; Mueller et al., 2019; Rao et al., 2023*). The physical model domain of Missisquoi Bay was discretized with a uniform horizontal grid size of 250 m by 250 m, and a vertical resolution of 0.25 m. AEM3D regulates the sediment phosphate (PO_4) and ammonium releases according to concentrations of DO and temperature in the overlying water layer. The model was calibrated against field data for the time period June 1, 2017 – December 31, 2019 for the variables water temperature, DO, TP, PO_4, total nitrogen, and chlorophyll a (Chl-*a*) in near-surface water and bottom water at different locations within MB using monthly, biweekly, and high-frequency observations from different monitoring programs. The model was validated against the same variables over the period January 1, 2020 – December 31, 2021.

The calibrated and validated model was run for the time period January 1, 2010 – December 31, 2021 using the nearly complete meteorological and riverine inflow datasets available for this period and daily concentrations of total suspended solids and different forms of P and nitrogen (N), which we estimated using the statistical model Weighted Regression on Time, Discharge, and Season, with Kalman filtering (WRTDS-K; *Zhang and Hirsh, 2019*). The model was run in a forecasting mode to evaluate the effectiveness of P inactivation scenarios under differing conditions of future watershed loading for 24 years (January 1, 2022 – December 31, 2045). Five external P loading reduction scenarios were simulated: 0% (baseline) and annual (cumulative) reductions of 1%, 2%, 3%, and 4% in tributary P inputs through 2036. After 2036 the reduction percentage was held constant.

Multiple sediment P inactivation scenarios were evaluated, considering treatment rate (typical or low rate), aerial extent, and recurrence. These treatments are defined in Table 1. Scenario 2 represents a theoretical maximum reduction of 90% in internal P loading, continuous over the entire 2022–2045 forecast period, without regard to treatment rates or timing. A single, typical dose treatment is specified in Scenarios 3A, 3B, and 3C, in the summer of 2026. In Scenario 4, annual low dose treatments are rotated among quadrants, beginning in 2026, with three treatments per quadrant. The total amount of P inactivation chemicals assumed in Scenario 4 (60-75 g of aluminum (Al) per m^2) and Scenario 3C (75 g Al/m^2) are similar; however, bloom suppression is achieved over a longer period of time in Scenario 4 because P binding reactions tend to be more efficient at lower doses.

Table 1 summarizes the predicted effects of P inactivation treatments in the context of assumed watershed loading reductions; it indicates the number of years in the 2026–2045 period (20-years) during which summer bay-wide average Chl-*a* concentrations exceed the 20 µg/L target for Missisquoi Bay. Combinations with 5 or fewer years in 20 with excessive Chl-*a* concentrations are shaded in green, with 6-10 years (30-50%) in yellow, and with 11-20 years (55-100%) in red.

Table 1. Years in 2026–2045 period that summer bay-wide average chlorophyll *a exceeds 20 µg/L*

Sediment P Inactivation Scenarios	**External P Loading Annual Reduction Factors**				
	0%	**1%**	**2%**	**3%**	**4%**
Scenario 1: No in-lake management	16	16	15	12	12
Scenario 2: Constant 90% internal load reduction in contributing area (ideal case)	5	2	0	0	0
Scenario 3A: One full rate treatment of area with most frequent low DO (~1,650 ha)	16		15		11
Scenario 3B: One full rate treatment of area with most/moderately frequent low DO (~3,800 ha)	15		14		11
Scenario 3C: One full rate treatment of all areas with frequent low DO (~5,580 ha)	13		9		6
Scenario 4: Annual low dose treatments by quadrant (1,395 ha per year, 3 rotations)	13		6		5

Management Alternatives

The approved Total Maximum Daily Load (TMDL) for MB (*US EPA*, 2016) mandates a 64.3% reduction by 2036 in P loading from the Vermont portion of the bay's watershed to achieve an in-lake water quality standard of 25 µg/L TP (annual mean). Relative to the TMDL model baseline, the 1%, 2%, 3%, and 4% annual external P load reductions we evaluated equate to cumulative reductions of 23%, 38%, 53%, and 68% in tributary P inputs by 2036. Only the 4% annual reduction scenario would meet the TMDL target. While a 64.3% reduction in external P loading would be a remarkable achievement from a management standpoint, this study confirms earlier modeling data (LimnoTech, 2012; Hanson et al., 2023; *Zia et al.*, 2016; *Zia et al.*, 2022) indicating that such reduction would have a lagged effect in coming decades on high summer P concentrations that fuel cyanobacteria blooms, due to persistent internal P loading. Table 1 demonstrates that even the most aggressive external load reductions (4% annual / 68% cumulative) will be insufficient to meet the Chl-*a* target in most years (12 of 20) if the internal load is not controlled.

Most successful internal P loading control efforts involve one or more of four techniques: dredging, circulation, oxygenation, and/or P inactivation. Any successful approach will have to address nearly all of MB. While dredging could remove P-rich sediment and greatly decrease internal loading, it is exceedingly expensive and technically challenging in such a large waterbody and is only likely to be implemented on a localized basis. Circulation has less potential to achieve desired results from a practical perspective, given the difficulty of maintaining adequate oxygen at the SWI by most circulation methods. Recent experience at Lake Carmi in Franklin, Vermont has illustrated the problem with circulation (*Kirol, 2023*). Oxygenation strategies, whereby more oxygen could be added near the SWI without substantial vertical mixing, could suppress internal P loading but would be challenging to implement efficiently over such a large area and would be expensive in terms of both capital and ongoing operational cost. Chemical inactivation of P has the greatest potential to control internal loading and can counter ongoing external loads to some extent. Therefore, we used model scenarios to define an optimal approach to inactivating legacy P in Missisquoi Bay.

Among the more realistic internal P inactivation scenarios (i.e., Scenarios 3A, 3B, and 4), Scenario 4 dramatically lowered the number of years the Chl-*a* target would be exceeded, from 15 to 6 years in the

2% external reduction scenario (Table 1). The remaining exceedances occur during the ramp up and ramp down periods of this treatment; after the first rotation, there are no exceedances until 2040 (during the treatment ramp down). While we find Scenario 4 advantageous, a variety of variations can be envisioned that could more nearly approach the effectiveness of Scenario 2; however, practical limits on the amount of area treated in any one year and the dose delivered will tend to restrict achievement of maximum P reduction.

Various scenarios for treatment with aluminum compounds were examined and suggest that suppression of internal P loading could be achieved to a degree that much reduces Chl-*a* and the probability of cyanobacteria blooms. In years the Chl-*a* target is exceeded despite sediment P controls, it is likely that there will be fewer cyanobacteria as a consequence of changed nutrient ratios; golden or green algae are more likely to dominate and these groups represent lesser threats to human and ecological health. However, consistent achievement of goals is unlikely without watershed P load reduction. The most efficient approach is to treat portions of MB on a rotating basis; division into quarters with a dose of 20-25 g Al/m^2 every four years appears to be the most advantageous approach, but application over three cycles still allows exceedance of goals without watershed management. The use of P inactivation provides great flexibility in control options and could facilitate adaptive management of MB. Costs, while still substantial, can be spread over a longer time period without compromising results.

Evaluating Alternatives to Control Internal Phosphorus Loading in Missisquoi Bay

Contents

List of Figures

List of Tables

1. Introduction

Missisquoi Bay (MB) of Lake Champlain underwent anthropogenic eutrophication over the latter half of the 20th century (*Levine et al.,* 2012*; Levine et al.,* 2018). This was primarily due to the intensification of agricultural production and associated macronutrient inputs across the landscape of the MB Basin and their consequent increased riverine loading to MB. As a result, there are persistent and relatively severe cyanobacteria blooms that occur in late summer and early fall in MB, degrading surface water quality and decreasing ecosystem services (*Isles et al.,* 2017a). For most of the bloom season, phosphorus (P) is thought to be the dominant limiting nutrient, although co-limitation with nitrogen and light has also been suggested (*Isles et al.*, 2015; *McCarthy et al.*, 2016). Whereas the long-term eutrophication of MB was driven by increased riverine nutrient loads, the build-up of legacy P in the sediments, and subsequent release of immediately bioavailable benthic P to the water column (internal P loading), can drive cyanobacteria bloom initiation, duration, and severity (e.g., *Smith et al.*, 2011; *Pearce et al.*, 2013; *Giles et al.*, 2016; *Isles et al.*, 2017a).

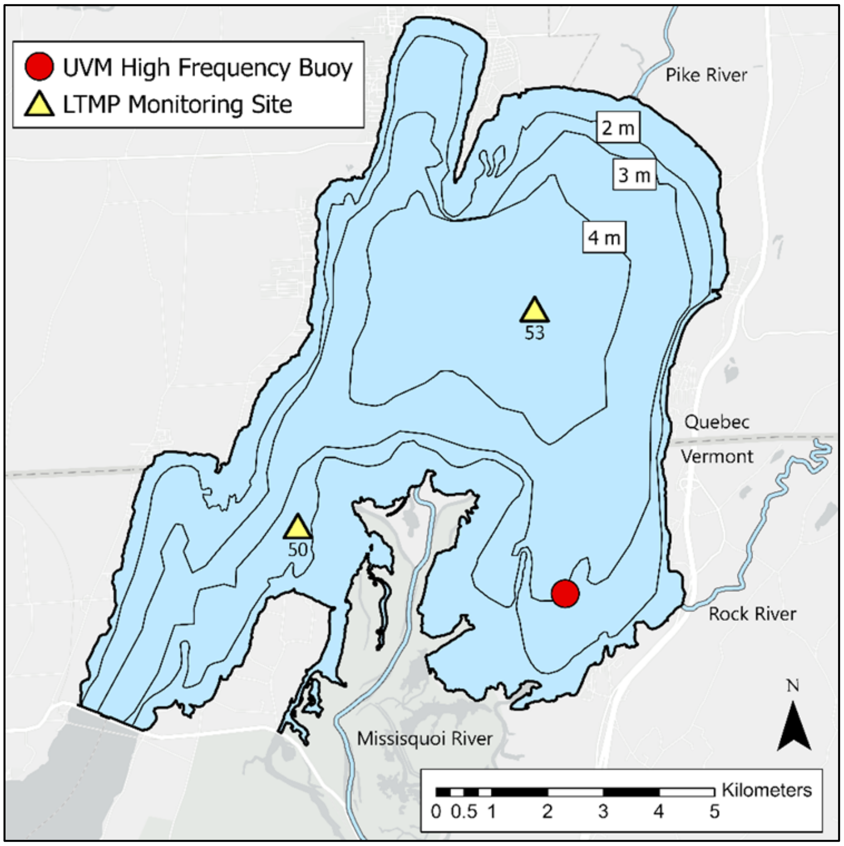

Figure 1. Missisquoi Bay bathymetry map with long-term monitoring locations.

Missisquoi Bay is a shallow system (Figure 1), with a mean depth of 2.8 m and a maximum depth of 4 m (*Levine et al.*, 2012). Due to the shallow bay's particularly high surface area relative to its volume, coupled with its robust inventory of legacy P in surface sediment, nutrient dynamics in MB are strongly impacted by internal P loading, particularly when river inputs are near baseflow. Approximately 25% of the P flux in the bay on an annual basis is estimated to be derived from internal loading (*LimnoTech*, 2012). This number underestimates the impacts of internal P loading in degrading water quality because of the timing and conditions associated with internal P flux (relative to the larger riverine P flux). Much of the internal P loading to MB occurs during summer months, when the majority of water column P is likely derived from internal loading, although this relative contribution fluctuates each year due to variability in weather patterns (*Giles et al.*, 2016; *LimnoTech*, 2012; *Isles et al.*, 2017a,b). Summer internal P loading occurs during periods when bay water residence times are longest due to low riverine inputs, when temperatures are favorable for cyanobacteria growth, and when the water column is stable and stratified, allowing cyanobacteria to outcompete other phytoplankton for this nutrient due to their buoyancy regulation (*Huisman et al.*, 2018).

Conversely, much of the riverine P is delivered to the bay from storm and snowmelt-derived high flow events under conditions not conducive to promoting blooms. Specifically, high flow events deliver P to the bay when the residence time of water (and P) can be the shortest (e.g., days), cyanobacteria buoyancy regulation capabilities are suppressed by mixing of the water column, and relatively cool water conditions of spring/fall are not conducive to bloom development (*Isles et al.*, 2017a).

The hydrodynamic condition that promotes internal P loading is a calm, stable water column. A stable water column with minimal vertical mixing enables reducing conditions to develop at the sediment-water interface (SWI) as dissolved oxygen (DO) in the bottom water is depleted, which leads to release of P from redox-sensitive mineral phases, primarily iron oxyhydroxides in the case of MB (*Schroth et al.*, 2015; *Giles et al.*, 2016). Wind and riverine inputs promote mixing off the water column, input of riverine sediments, and re-oxidation of the SWI, all of which promote accumulation of sediment P (*Giles et al.*, 2016). The interannual variability in the duration and severity of cyanobacteria blooms in MB has been attributed to the frequency and duration of each of these contradictory water column/SWI conditions when water temperatures are in a range that promote cyanobacteria dominance (*Isles et al.*, 2017a). While the only long-term solution to decreasing legacy P in MB will depend on achieving reductions in watershed loading, such reduction would have only limited impact on cyanobacteria blooms in coming decades due to persistent internal P loading.

MB is a particularly dynamic system with limited water flux and connectivity to the rest of Lake Champlain. It has three major riverine inputs, the Missisquoi (~80% of MB Basin), Pike (~10%) and Rock (~5%) Rivers, that all export terrestrial-derived P to MB in both dissolved and particulate forms. The magnitude and reactivity of particulate P loads have been shown to vary extensively in time and by event (*Rosenberg and Schroth*, 2017). These three input points also exert a strong control on the hydrodynamics of MB, particularly under high flow conditions.

Because the system has such a high surface area to volume ratio, MB is particularly sensitive to wind speed and orientation, completely turning over in response to relatively minor wind events (e.g., 4 m/s, *Isles et al.,* 2015), facilitating rapid changes in SWI redox chemistry (*Smith et al.*, 2011). Wind stress and heat fluxes on the surface water, and river discharges interacting with the bay's morphology are the major local forcing mechanisms creating a variable circulation pattern. Four modes of circulation were found to exist in MB (*Manley, T.*, unpublished). First, the "wintertime sluggish" mode, in which water velocities are vertically uniform and very low (< 1 cm/s). Second, the "spring melt", where the three rivers discharge high flow volumes. From May to November when thermally stratified conditions could develop, a third mode, "well-mixed summer", when the water column is well-mixed, or a fourth mode, "two-layer summer", in which stratified conditions are present, will occur. Water residence times vary seasonally ranging from several days during high spring river flows to several months during periods of low summer river flows.

Circulation patterns and residence time affect the fate and transport of biogeochemical constituents within MB. Since 2012, researchers led by Andrew Schroth have deployed sensors in MB to capture high-frequency physical and biochemical dynamics of MB. These data have enhanced our conceptual model of internal loading and cyanobacteria dynamics in MB. These data have been utilized by Clelia Marti to simulate the time- and space-varying physical and biogeochemical processes across seasons in MB (Marti et al., 2019) using the Aquatic Ecosystem Model 3D (AEM3D), which couples the hydrodynamic 3-D Estuary, Lake and Coastal Ocean Model (ELCOM) and the Computational Aquatic Ecosystem Dynamics Model (CAEDYM) (*Romero et al.*, 2004; *Silva et al.*, 2014a). The independent review by Trolle et al. (2012) judged these models to be the superior choice for standing waters of varying scales from large natural systems, such as Lake Erie (*Leon et al., 2005; Leon et al. 2011*) to smaller lakes and reservoirs (*Romero et al., 2004; Missaghi et al., 2013; Weigel et al., 2017*) and widely used for estimating load reductions necessary to support water quality goals (*Burger et al., 2008; Trolle et al., 2012*), studying the design and effectiveness of management methods for controlling algal blooms (*Xing et al., 2014; Preston et al., 2014*), and assessing the response to climate change and nutrient loading projections (Vilhena et al., 2010; van der Linden et al., 2015).

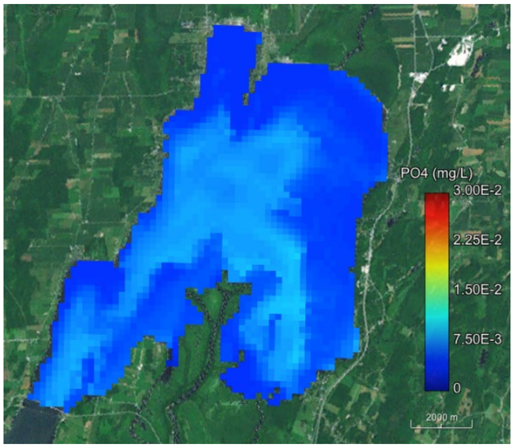

Figure 2. Predicted orthophosphate (PO_4) concentrations in MB 1 m from bottom.

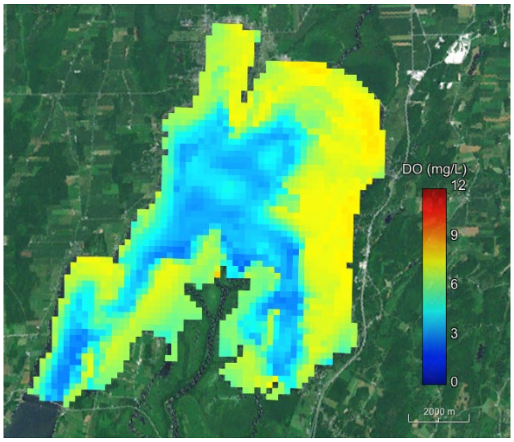

Figure 3. Predicted DO concentrations in MB 1 m from bottom.

Simulation results produced in previous work by Marti using the AEM3D model reveal patterns in the distributions of orthophosphate (PO_4) (Figure 2) and DO (Figure 3) in the bottom water (1 m from bottom) that resemble the sediment grain size map (Figure 4) prepared by P. Manley and T. Manley (unpublished), illustrating transient relationships between small particle size, low DO concentrations, and elevated bottom water PO_4.

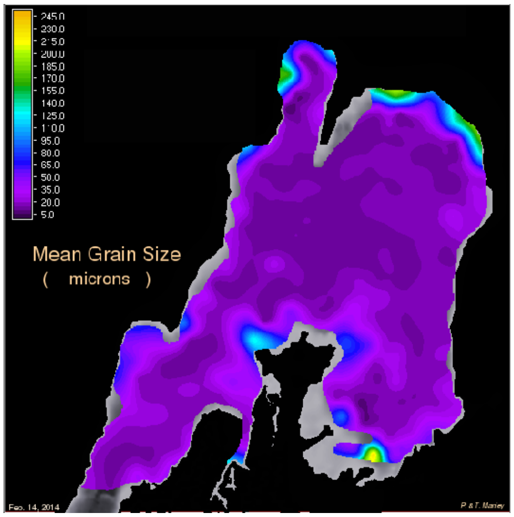

Figure 4. Sediment grain size in MB (P. Manley and T. Manley, unpublished).

The approved Total Maximum Daily Load (TMDL) for MB (*US EPA*, 2016) mandates a 64.3% reduction in P loading from the Vermont portion of the bay's watershed to achieve an in-lake water quality standard of 25 µg/L TP (annual mean). While such a reduction in external loading would be a remarkable achievement from a management standpoint, modeling data (LimnoTech, 2012; Hanson et al., 2023; *Zia et al.*, 2016; *Zia et al.*, 2022) indicate that such reduction would have a lagged effect in the coming decades on high summer P concentrations that fuel cyanobacteria blooms, due to persistent internal P loading. Furthermore, characteristics of ongoing and projected climate change in the Lake Champlain Basin will continue to enhance cyanobacteria bloom occurrence (i.e., warmer, more stratified water promotes cyanobacteria reproduction and the advantages of buoyancy regulation capabilities), which have a synergistic effect with internal P loading to sustain blooms (*Zia et al.*, 2016; *Zia et al.*, 2022). Therefore, mitigating internal loading of legacy P is required in concert with external nutrient loading reduction to achieve water quality and bloom suppression goals and preserve the credibility of management entities with the public.

There is a suite of potential remediation options available to address internal P loading (e.g., *Paerl et al.*, 2018), few of which are likely well-suited to address the unique configuration of MB's hydrodynamic, biogeochemical, and ecological systems. Of the roughly dozen approaches to managing cyanobacteria, many suffer from some constraint that would greatly limit their application to MB. For example, flushing requires a tremendous amount of water and MB already has a short residence time. Bacterial additives have a short and mixed track record with virtually no supporting peer reviewed literature. Most successful internal P loading control efforts involve one or more of four techniques: dredging, circulation, oxygenation, and/or P inactivation. These techniques were the focus of our evaluations to define an optimal approach for mitigating internal loading of legacy P in Missisquoi Bay.

In this study, the project team refined the previously developed conceptual and process-based model of MB's hydrodynamic-biogeochemical system to meet the following objectives:

1.1. Objectives

1. Design and implement a robust sampling campaign to further spatially identify and map P distribution in MB, with particular focus on hot spots of accumulation and release from the sediments.
2. Establish the physical and chemical drivers of P distribution.
3. Assess the capacity of different intervention strategies to control internal P loading and achieve bloom suppression goals.
4. Predict the efficacy and appropriate timing of potential interventions over multiple decades in the context of EPA-mandated watershed nutrient reductions; and
5. Present effective internal P loading reduction strategies through an accessible, visually appealing tool enabling managers to view the simulated results of various management interventions over time.

2. Tasks Completed

The following tasks were accomplished to meet the study objectives.

Convene Project Advisory Committee (Task 1): The project advisory committee (PAC) convened for this project met on four dates: 7/30/2020, 4/9/2021, 3/4/2022, and 6/8/2023. Among its many substantive contributions, the PAC provided input on the Missisquoi Bay sediment sampling campaign, AEM3D model scenarios, and lake management considerations.

Prepare Quality Assurance Project Plan (QAPP) (Task 2): A primary and secondary data QAPP addressing the monitoring phases of the project was approved on September 17, 2020. The approved QAPP was updated on January 31, 2022 to reflect additional sediment sampling and analysis. This QAPP is included as Appendix A.

Map Sediment P (Tasks 3 and 4): Co-Principal Investigator Dr. Andrew Schroth and M.S. student Ashton Kirol completed a two-year sampling campaign throughout Missisquoi Bay, and sediment and water sample analyses, in completion of these tasks. The methods and results of this campaign are described in Section 3.

Analyze Hydrologic and Hydrodynamic Responses (Tasks 5 and 6): Co-Principal Investigator Dr. Clelia Marti led the completion of all modeling tasks. The methods and results of the modeling effort are described in Section 4.

Evaluate Internal P Loading Strategies and Develop Implementation Plan (Tasks 7, 8, and 9): Co-Principal Investigator Dr. Ken Wagner of WRS Inc. led the completion of these evaluations. The findings and recommendations from these evaluations are described in Section 5.

Create Visualization Tools (Tasks 10 and 11): Stone developed an ArcGIS StoryMap presenting the internal P load inactivation strategies considered in Tasks 7 through 9. The AEM3D model includes the interface HydroHub, which we used to prepare video clips of model simulations. These model result videos may be viewed in the ArcGIS StoryMap. Due to software constraints and enormous computing requirements, it was not technically feasible to make the model simulations interactive, as originally planned.

Reporting (Task 12): Stone submitted quarterly progress reports throughout the project term. This final report covers the methods and results of Missisquoi Bay data collection and AEM3D modeling as well as evaluation of management alternatives.

3. Missisquoi Bay Data Collection

3.1. Sediment and Water Sampling Methods

Existing UVM sediment P data were supplemented by collection of sediment cores at predetermined locations to capture the spatial distribution of P accumulation and release in MB. UVM's calibrated AEM3D model was used in developing a sediment sampling plan for the first year (2020) of the sampling campaign. Areas in MB with predicted low DO and associated P release were identified (Figure 5). Sediment cores and bottom water were collected across MB at locations predicted to have higher occurrence of low DO conditions (<3 mg/L) in bottom water.

Considering low DO zones predicted by the model, sampling transects were developed in 2020 in consultation with the PAC (Figure 5). The initial plan included equidistant sampling points along multiple transects (2 North-South, 2 East-West). We did not sample regions of MB that are 1.5 meters or less, because those shallow waters are not generally sources of internal P loading and DO conditions never reach this threshold. The sampling plan was updated in the second year of the campaign based on analysis of the 2021 data and further consultation with the PAC in April 2021.

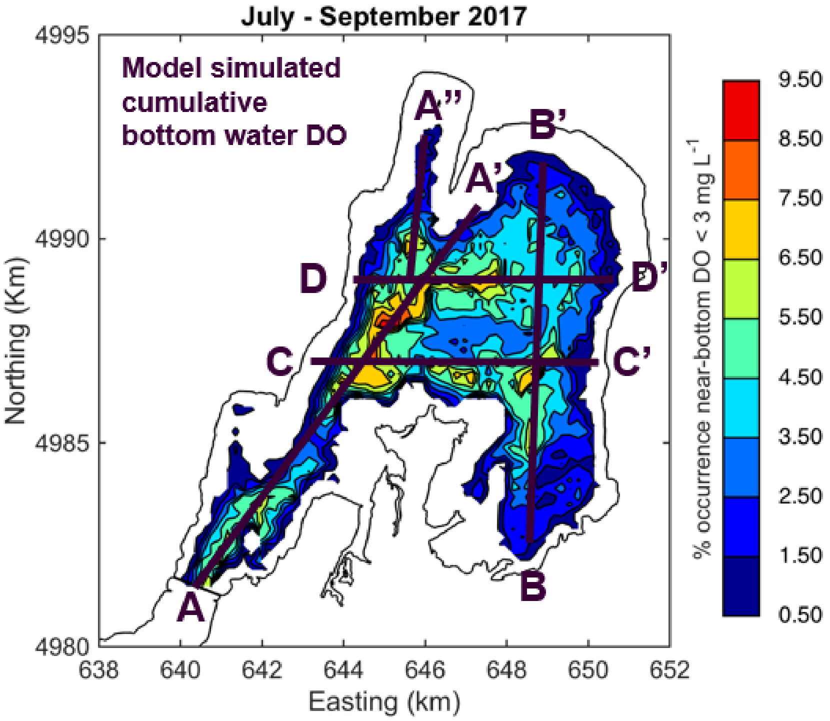

Figure 5. Sediment sampling transects.

UVM collected sediment cores using a gravity corer and polycarbonate core tubes. A minimum of 10% of sediment cores were collected and analyzed in duplicate to quantify precision using calculation of relative percent difference (RPD). Sediment cores were capped and stored in their polycarbonate tubes in a cooler until transported to the shore (or the lab) for sectioning. Once sectioned, polycarbonate tubes were rinsed with lake water, and then repurposed for collection of subsequent sediment core samples. Sediment samples were sectioned as soon as possible on land, frozen, and subsequently freeze dried at the UVM Department of Geology prior to undergoing digestion and extraction procedures.

At the same time and location that each sediment core was collected, a manual cast using a YSI EXO2 sonde was performed to measure temperature, conductivity, pH, dissolved oxygen, turbidity, fluorescent dissolved organic matter (fDOM), and chlorophyll *a*/phycocyanin fluorescence. Data were collected at half meter intervals from the bottom with additional measurements made as close to the SWI and surface as possible. At each depth where sensor data were collected, triplicate measurements were made to quantify precision using relative standard deviation (RSD).

At selected sediment core locations, a 250-mL filtered bottom water sample was collected using an in-line 0.45 micrometer Pall Supor filter attached to acid clean tubing and a peristaltic pump. A minimum of 10% of water samples were collected and analyzed in duplicate to quantify precision using calculation of relative percent difference (RPD). Schroth et al. 2015, Giles et al. 2016, Joung et al. 2017 are all examples of the implementation of these sampling protocols.

The field sampling campaign was performed when boating conditions were safe. Schroth typically assesses this based on NOAA forecasts with particular emphasis on wind speed, wind direction, and potential for thunderstorms. Sampling was not conducted if winds were forecast to be higher than 10 mph. If there was a chance of thunderstorms, the sky and radar were monitored for potential cells, and the team stopped sampling and took shelter on land if a thunderstorm developed in the vicinity of MB.

The team targeted sampling in the period following peak spring runoff (late May/early June), the pre-bloom period, the late summer bloom period in August/early September, and the post bloom fall period (October). Within these time frames, sampling dates were determined by researcher availability and safe boating conditions. These sampling periods were informed by robust contextual information provided by years of monitoring MB that distinguishes these time periods in the context of distinct bloom and P biogeochemical behaviors (e.g. *Giles et al. 2016, Isles et al. 2015, 2017a,b*). Sampling in 2020 was delayed due to the COVID19 state of emergency; therefore, a substantially greater effort was needed during the 2021 field season to obtain the desired samples throughout MB.

Spatial distributions of sediment P observed in 2020 were used to improve the MB AEM3D model parameterization and the simulation of P distributions and dynamics. The refined model was then used in planning a second field campaign in 2021, with input on sampling locations from the PAC. The objectives of the second field campaign were to further ground truth and refine model simulations, characterize temporal variation in sediment chemistry, and fill in areas either not sampled in 2020 or where discrepancies were observed in 2020. Table 2 summarizes the number of samples collected. In 2021, water samples were collected at every location where we collected time series sediment cores to help inform trends in the concentrations of P in sediment over time in response to water column seasonal dynamics.

Table 2. Sediment and water sample numbers.

	Sediment cores	Water samples	Sediment grab samples
Locations	76	47	5
Samples	110	84	6
Core sections	330	NA	NA

Sediment digestions and subsequent digestate and water sample analysis for P and metals concentrations occurred at the University of Vermont's Geology Department and Rubenstein Ecosystem Science Laboratories. Phosphorus and metals concentrations in sediment digestates and extracts were analyzed by the inductively coupled plasma optical emission spectrophotometer (ICP-OES) at the UVM Agriculture and Environmental Testing Laboratory (AETL). Appropriate blanks, replicates and reference materials were run on the ICP-OES following the Schroth lab's existing protocols.

Five grab samples were collected in 2021 from zones spanning the range of observed ascorbate-extractable sediment P concentration to evaluate the efficiency of P reactions with aluminum using an assay method. Grab samples were collected using a petite ponar dredge and were submitted for analysis by the laboratory operated by Dr. Emily Lesher of St. Joseph's College in Standish, ME, following the Lesher lab's existing protocols. The QAPP (Appendix A) was updated on January 31, 2022 to incorporate the assay method. These assay data were used in estimating the amount of aluminum that would need to be applied (as aluminum sulfate or sodium aluminate) to control internal loading of P from sediment.

3.1.1. **Sample handling and custody**

Sediment cores were sectioned at 0-1 cm, 1-4 cm, and 4-10 cm depth intervals following the Schroth lab's longstanding sediment analysis protocols (see Appendix A). Depth splits were placed in sealed plastic bags. Filtered water samples were acidified to 1% HNO_3.

Sediment depth splits and water samples were labelled with unique IDs, project name, sampler identification, and sample date. Samples were transported on ice in coolers to the laboratory. Sediment samples were frozen on arrival at the Rubenstein Ecosystem Science Lab. Table 3 summarizes the preservation conditions by sample type.

Table 3. Sample types collected.

Matrix	Analytical Parameters	Container	Preservation	Hold Time (days)
Sediment	Total P, Al, Ca, Fe, Mn Redox-sensitive P, Al, Ca, Fe, Mn	Polycarbonate core tube	Frozen after sectioning and then freeze dried	Indefinite after freeze drying
Sediment	Dry bulk density	250-mL plastic jar	None	28 days
Sediment	Redox-sensitive P (dithionite)	1-L Ziplock bag	Frozen	Indefinite after freezing
Water	Dissolved P, Al, Ca, Fe, Mn	250-mL plastic bottle	Filtered (0.45 μM Pall Supor); acidified to 1% HNO_3; cool (<4°C)	28 days

3.2. Analytical Methods

After lyophilization, sediment samples were homogenized and then extracted in ascorbate to determine redox-sensitive P and aqua regia to determine TP per Schroth lab's established methods (Appendix A, following *Smith et al.*, 2011 and *Giles et al.*, 2016). Subsequent solutions were analyzed for P concentration on the UVM AETL's ICP-OES. Filtered and acidified water samples were analyzed for Ca, Mn, and Fe using the same approach. The SEAL Autoanalyzer was used for total dissolved P (TDP) analyses. The analysis protocols, summarized in Table 4, are consistent with data requirements needed to assess internal P loading intervention strategies.

Table 4. Analytical methods.

Sample Matrix	Analytical Parameter	Lab	Method	Reference
Sediment	Total P, Al, Ca, Fe, Mn	AETL	Extraction: Aqua regia Analysis: ICP-OES	Smith et al., 2011
Sediment	Redox-sensitive P, Al, Ca, Fe, Mn	AETL	Extraction: Ascorbate Analysis: ICP-OES	Smith et al., 2011
Sediment	Redox-sensitive P (dithionite)	Lesher	Preparation: Aluminum assay Extraction: Ammonium chloride, Bicarbonate-dithionite, and sodium hydroxide Analysis: Molybdate blue method / Hach spectrophotometer	Lesher et al. (QAPP Appendix C)
Sediment	Dry bulk density	AETL	Gravimetry	Grossman and Reinsch, 2002.
Water	Dissolved Al, Ca, Fe, Mn	AETL	ICP-OES	Schroth et al., 2015
Water	Dissolved P	Schroth	Determination of Phosphorus by Semi-Automated Colorimetry (SEAL)	EPA Method 365.1, Revision 2.0

3.3. Sediment and Water Geochemistry

Sediment bound P varied spatially across Missisquoi Bay. The mean TP in the upper 10 cm across all sampling locations was 1.00 mg/g of dry sediment (range: 0.63–1.42 mg/g). Redox-sensitive P varied in concentration from 0.13 mg/g to 0.70 mg/g and was 38% of TP on average. Spatial interpolation shows that the highest concentrations were in the deeper waters of the western bay (north of the U.S. – Canada border), along the east side of the bay, and near the southwestern outlet (Figure 6). Concentrations were lower in shallow areas such as the northwestern lobe, along the western shore, and the west side of the southeast lobe. The RMSE of interpolated P concentrations was 0.10. In Figure 6, the gap in samples through the western channel is due to the presence of very coarse sediment that prevented core retrieval.

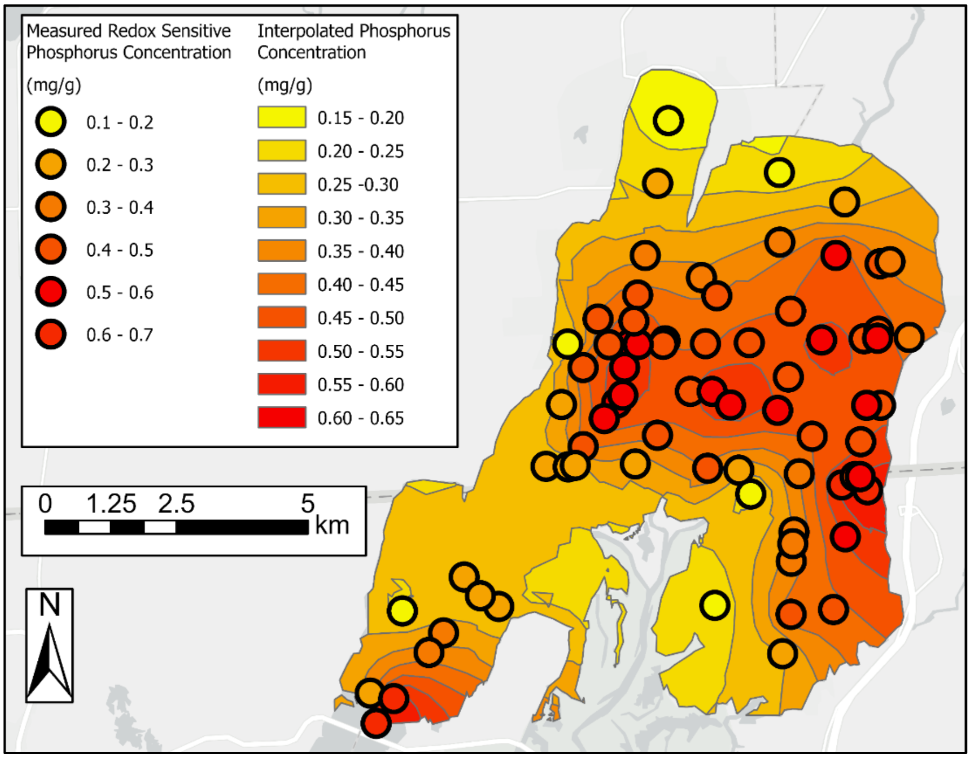

Figure 6. Measured redox-sensitive P concentrations in the upper 10 cm of sediment.

Sediment samples from Missisquoi Bay had a mean Fe:TP ratio of 44.43 (range: 26.27 to 60.41) by mass (Figure 7). There were positive correlations between TP and total Fe concentrations ($r = 0.92$, $n = 110$, $p < 0.0001$) and between redox-sensitive P and Fe concentrations ($r = 0.88$, $n = 110$, $p < 0.0001$) in sediment across all sampling locations.

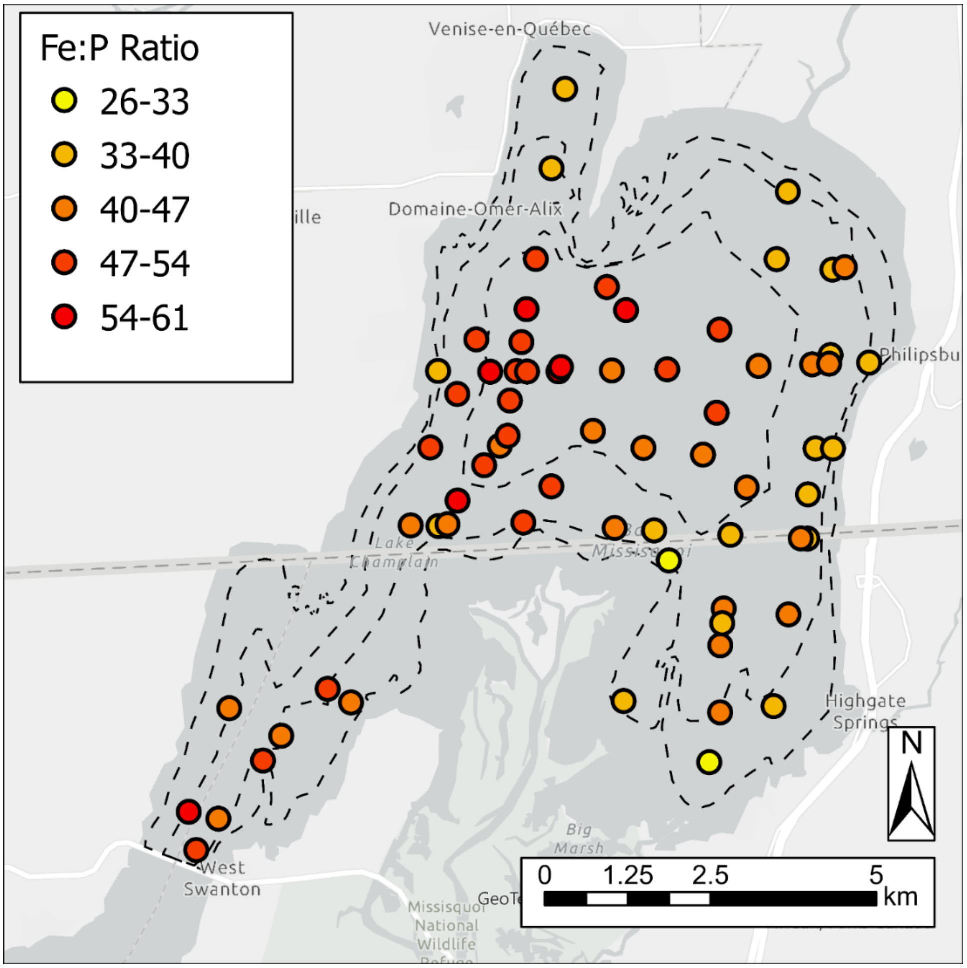

Figure 7. Fe:TP ratio in upper 10 cm of sediment with 2-m, 3-m, and 4-m depth contours.

The mass of available P depends on the bulk density of sediment, which also varies spatially in Missisquoi Bay. Figure 8a presents an interpolated surface illustrating the average bulk density in the upper 10 cm of sediment across MB. Dry sediment bulk density ranged from 0.30 to 0.73 g/cm^3, with an interpolation RMSE of 0.07. Density generally decreased toward the deeper central bay where organics likely make up a larger proportion of sediment due to accumulation of autochthonous biomass. Sediment samples from shallow areas near shore had nearly twice the density of those from the middle of the bay.

The highest P mass that can potentially contribute to internal loading is found in the overlap of areas with high redox-sensitive P concentration and high bulk density. Figure 8b presents an interpolated surface illustrating total redox-sensitive P mass in the upper 10 cm of sediment. Dashed black lines indicate 2-m, 3-m, and 4-m bathymetric contours. Redox-sensitive P mass in the top 10 cm ranged from 10 g/m^2 in the northern bay to 31 g/m^2 in the east/southeast and near the outlet of the bay, with an interpolation RMSE of 4.6 g/m^2. The total redox-sensitive P mass in Missisquoi Bay was calculated for the uppermost 1 cm and 10 cm of sediment from the range of interpolated values and the area of each zone. We estimate there is between 76,000 and 84,000 kg of redox-sensitive P in the top 1 cm of sediment, and as much as 1,398,000 kg in the top 10 cm (Table 5). We estimate there is 168,000–192,000 kg of TP in the top 1 cm of sediment, and as much as 3,791,000 kg in the top 10 cm (Table 6). Estimates of P mass are lower if the area is constrained by water depth. P flux rates do not directly correspond with P mass. Because lower density sediments generally have higher porosity, water and dissolved P flow more readily through these sediments into the water column. P flux may be especially high in the deeper central bay where some of the highest concentrations of redox sensitive P are found in some of the lowest density sediments.

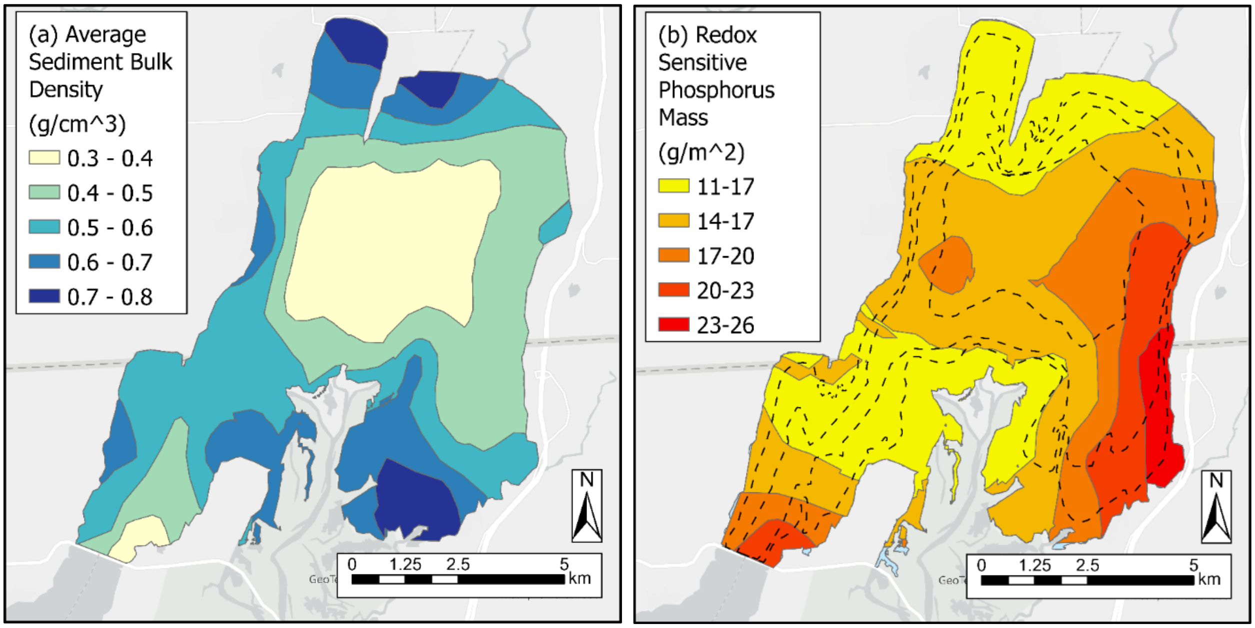

Figure 8. Average bulk density (a) and total redox sensitive P mass (b) in the upper 10 cm of sediment.

Table 5. Missisquoi Bay redox-sensitive sediment P mass by depth interval.

	Redox-sensitive Phosphorus Mass (x1,000 kg)			
Sediment Depth	**Whole Bay (77.5 km^2)**	**> 2-m water depth (58.6 km^2)**	**> 3-m water depth (39.7 km^2)**	**> 4-m water depth (15.9 km^2)**
0-1 cm	76 - 84	56 – 62	37 - 41	14 - 15
0-10 cm	1,157 - 1,398	869 - 1,045	601 - 720	237 - 285

Table 6. Missisquoi Bay sediment TP mass by depth interval.

	Total Phosphorus Mass (x1,000 kg)			
Sediment Depth	**Whole Bay (77.5 km^2)**	**> 2-m water depth (58.6 km^2)**	**> 3-m water depth (39.7 km^2)**	**> 4-m water depth (15.9 km^2)**
0-1 cm	168 - 192	120 - 138	79 - 91	28 - 33
0-10 cm	3,390 – 3,791	2,410 – 2,704	1,561 – 1,760	561 – 640

Surface water TP concentrations at the two Lake Champlain Long-term Water Quality and Biological

Monitoring Program (LTMP) stations in Missisquoi Bay—stations 50 and 53 (formerly 51)—averaged 48 µg/L between 2017 and 2020 (*VTDEC, 2022*). Note that the LTMP is a partnership among LCBP, SUNY Plattsburgh, NYDEC, VTDEC, and the EPA. TP concentrations were typically elevated in the spring, and then dropped to 20-40 µg/L in May and June. TP concentrations increased in the summer and peaked in late August through early October (60-90 µg/L). TP concentrations were often nearly the same between stations 50 and 53, but sometimes varied by 10 to 20 µg/L on the same sampling day. The largest difference between the two stations was 23.4 µg/L, on September 3, 2021.

3.4. Water Column Dynamics

Missisquoi Bay is a polymictic system that experiences brief periods of spatially heterogeneous stratification and anoxia during the ice-free season. Over the study period, bottom water temperature measured using the sonde profiler at UVM's high-frequency buoy (HFB) in the southeast lobe reached a maximum of 26.29 to 28.85°C (Figure 9). The average difference in surface and bottom temperature was 0.37°C, while the maximum difference was 7.83°C. This small temperature difference and MB's shallow depth results in a relatively unstable water column. In 2018-2021, Missisquoi Bay had a maximum and average Schmidt stability of 13 J/m^2 and 1 J/m^2, respectively (Table 7). During the study period in 2020 and 2021 there were over 600 mixing events (Figure 10b), defined by changes in water temperature indicating transitions from thermal stratification to well mixed conditions.

Table 7. Annual maximum and average water column Schmidt stability for Missisquoi Bay.

	Missisquoi Bay Schmidt Stability (J/m^2)	
Year	**Maximum**	**Mean**
2018	11	0.9
2019	11	0.9
2020	13	0.8
2021	12	1.4

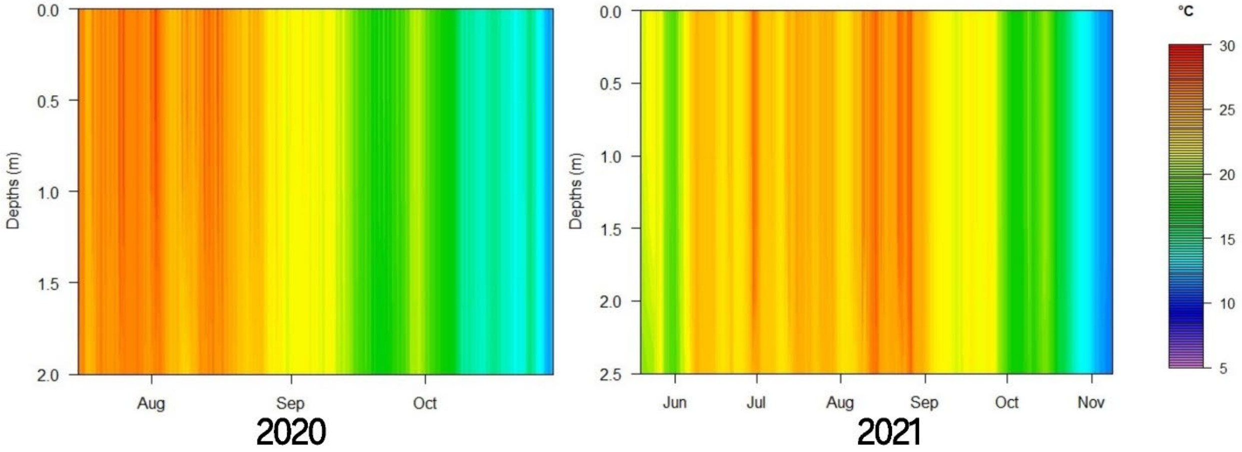

Figure 9. Thermal profiles at the HFB in Missisquoi Bay, 2020-2021.

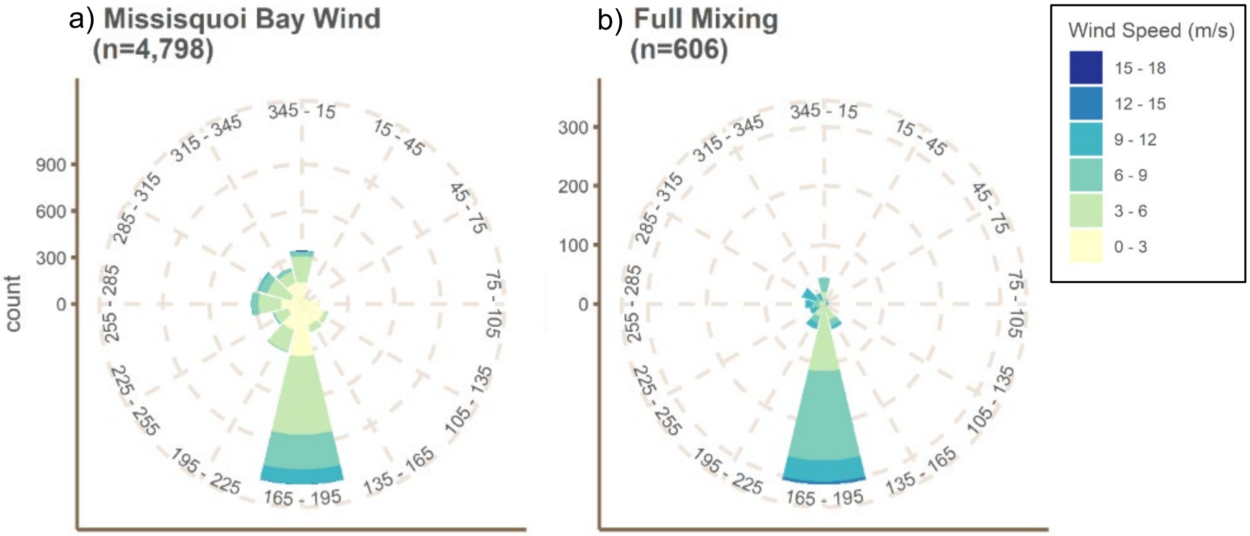

Figure 10. Windspeed and direction and water column mixing, 2020-2021.

3.5. Dissolved Oxygen

Bottom water DO concentrations change rapidly during brief periods of stratification. The minimum bottom water DO concentration at the HFB ranged from 5.8 mg/L in 2020 to 0.24 mg/L in 2021 (Figure 11a). Gaps in the time series data in Figure 11a correspond to downtime of the profiler. Sampling at LTMP stations 50 and 53 in Missisquoi Bay shows similar results (*VTDEC, 2022*). The bottom water at these stations sometimes had low DO (e.g., 2.17 mg/L at station 50 in 2017, 2.38 mg/L at station 53 in 2021), but the hypolimnion was never fully anoxic. It is important to note that redox gradients at the SWI have been demonstrated to be very steep in previous research (i.e., *Schroth et al., 2015; Smith et al., 2011*), so these data underestimate exposure of bottom water and near surface sediment to reducing (P mobilizing) conditions.

We sampled across areas of the bay on several days when conditions favored stratification. Spatial interpolations of bottom water DO concentrations along with bottom water TP and Mn concentrations are shown for low oxygen events observed on August 10, 2021 (Figure 11b) and August 25, 2021 (Figure 11c). The most widespread low DO we encountered was on August 25, 2021, the same day as the lowest DO readings at the HFB. Manual sonde readings of DO just above the SWI were below 1 mg/L in the southeast lobe of the bay. Bottom water DO was also low (0.48–2.74 mg/L) in the southwest and western side. DO increased to the northeast (2.8–6.07 mg/L) and in the northwestern lobe (7.36 mg/L). Sampling on August 10, 2021 (Figure 11b) also captured a difference in bottom water DO concentration across the bay, but no anoxia. Bottom water DO south of the HFB was 2.65 mg/L. Moving north, bottom water DO in the rest of the southeast lobe ranged from 5.63 to 6.96 mg/L. Other samples in MB on this date were even higher (7.52–9.77 mg/L).

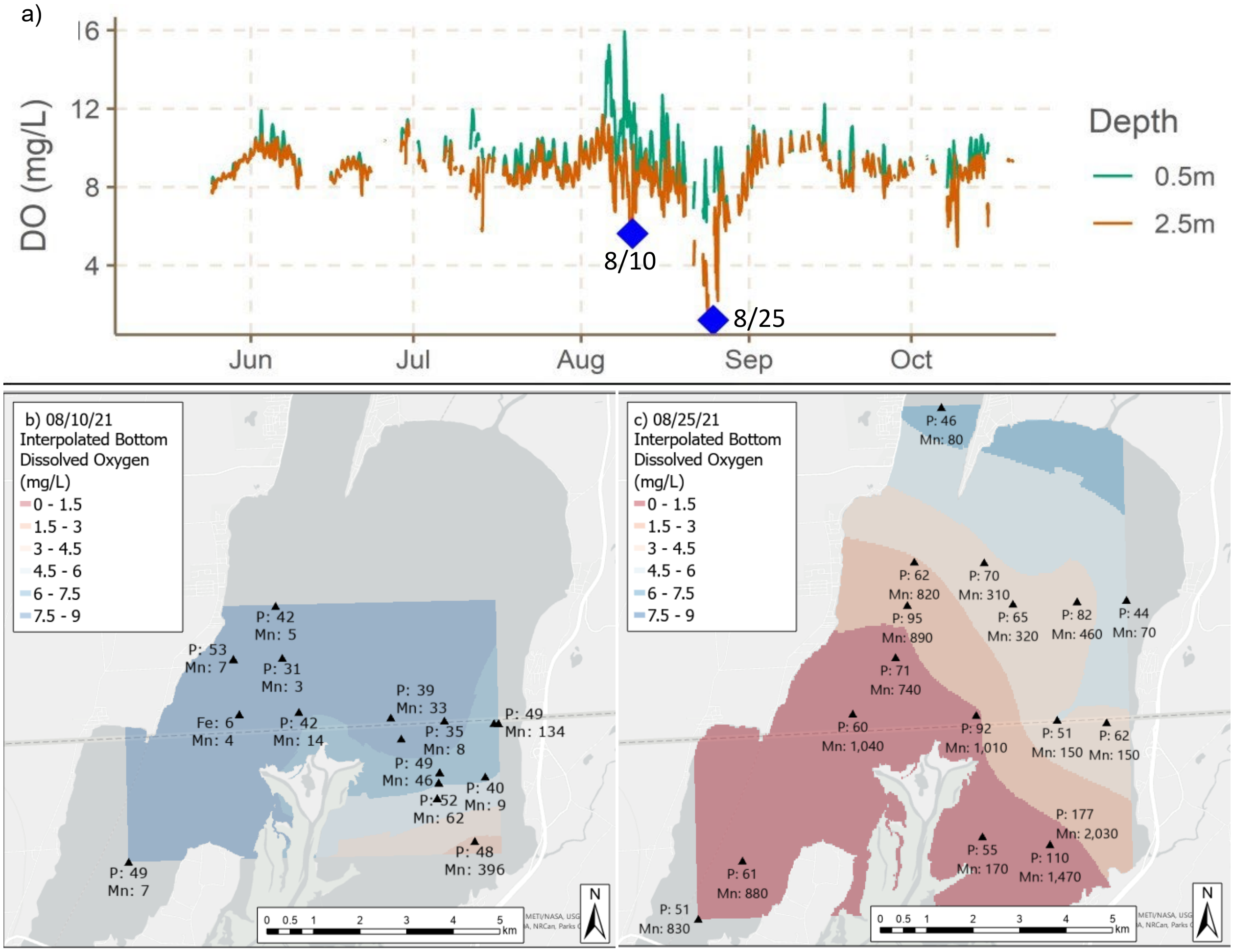

Figure 11. 2021 time series of surface and bottom DO at the HFB (a); concentrations of DO (mg/L), TDP (µg/L), and Mn (µg/L) on August 10 (b) and August 25, 2021 (c).

Oxygen demand was relatively high during brief periods of stratification. For example, between August 19 and August 21, over a 53-hour period, the dissolved oxygen concentration at the HFB declined from 8.9 mg/L to 2.5 mg/L, equaling a hypolimnetic oxygen demand (HOD) of 2.9 mg/L per day. Given the previously discussed steep oxygen gradients around the SWI, the near surface sediment may very well have been anoxic on these occasions. In general, these data suggest that, particularly in summer when bottom water is relatively warm, low level thermal stratification triggered by calm local winds can cause rapid consumption of bottom water DO with the potential to trigger episodic redox-driven release of P.

3.6. Phosphorus Response to Dissolved Oxygen

Our sampling showed that both legacy sediment P and anoxic conditions that promote internal P loading vary spatially across Missisquoi Bay. The overlap of these areas likely contributes disproportionately to internal P loading. Bottom water samples collected from locations with high P mass during two low DO events in 2021 showed elevated concentrations of TDP and Mn. On August 10, 2021, when there was one location with low DO (2.65 mg/L), the TDP concentration at this location was similar to the rest of the bay, but the Mn concentration was 8 times higher than at nearby locations (Figure 11b). On August 25, 2021, when much of the bay had low bottom water DO, TDP concentrations over 60 µg/L were measured at several locations, and the maximum TDP concentration was 177 µg/L (Figure 11c). Locations that were well mixed and oxygenated had an average TDP concentration of 45 µg/L. Concentrations of Mn (70–2,030 µg/L) were up to 29 times higher at locations with low bottom water DO compared with locations with fully mixed conditions. Through this sampling period, dissolved P in bottom water samples was strongly correlated with both dissolved Fe [$r = 0.84$, $n = 84$, $p < 0.0001$] and Mn [$r = 0.83$, $n = 84$, $p < 0.0001$], further indications of spatially and temporally heterogeneous redox-driven internal loading of P.

3.7. Heterogeneous Legacy P Distribution and Loading Dynamics

High-frequency, in-situ monitoring confirmed the highly transient nature of low-level thermal stratification (often less than 1°C), low DO conditions at the SWI, and associated internal P loading in Missisquoi Bay, which is consistent with our previous findings (*Smith et al. 2011, Isles et al. 2015, Giles et al. 2017*). However, our spatial sampling campaigns revealed spatially heterogeneous internal P loading that was not captured at the HFB or in our previous work. Indeed, bottom water TDP concentrations varied by a factor of 4 across the bay (44–177 µg/L) during the same day, and Mn (70–2,030 µg/L) by a factor of 29 across a similar range of depths (2.3–4.4 meters). This demonstrates that despite the nearly uniform depth of the bay and ubiquitously relatively high concentration of redox-sensitive P in sediments, conditions that promote internal loading were highly dynamic in space, as the bay's hydrodynamics in response to wind promotes variable redox conditions at the SWI. For example, on August 25, 2021 the entire southern half of the bay had low oxygen bottom water, and relatively high bottom water P and Mn (Figure 11c), and this condition had lasted for a few days, indicating that this was a relatively large-scale internal loading event, at least in the portion of the bay with the smallest fetch for a southwestern wind. Conversely, on August 10, 2021, low oxygen conditions and high bottom water P and Mn concentrations were only present in the southeast lobe of the bay, indicating this event was localized in the most sheltered portion of the bay, presumably due to wind forced mixing in the rest of the bay.

Wind data and frequency of turnover (Figure 10) suggest that there is a very subtle threshold for wind driven mixing to occur in MB given its shallow depth and large surface area. This is likely why we did not observe chemical evidence of internal loading events in the northern portion of the bay, given its large fetch under the predominant southwestern wind orientation of the summer, even under the relatively hot and calm conditions under which the August 25, 2021 spatial sampling event occurred. Similarly, bottom water TDP (37–70 µg/L) and Mn (3–11 µg/L) concentrations were relatively low and less variable on August 13, 2021, which represents a fully mixed condition (Figure 12). As such, our analysis suggests that in systems like Missisquoi Bay (high surface area, high sediment surface area to volume ratio, similar shallow depth), small differences in the physical characteristics and hydrodynamic response of different regions to the prevailing summer wind direction can control the extent to which any given region of the lake may contribute to internal P loading budgets. The relative contribution of these regions to internal P loading will vary as wind driven forcing of hydrodynamics changes in response to the weather. Because of this, wind driven forcing is important to consider with targeted treatment plans. As a whole, insights gleaned from these high-frequency, in-situ sensing and comprehensive geochemical spatial monitoring datasets provide extremely useful information toward optimizing a management plan for suppressing internal loading of phosphorus in Missisquoi Bay, as discussed in subsequent sections of the report.

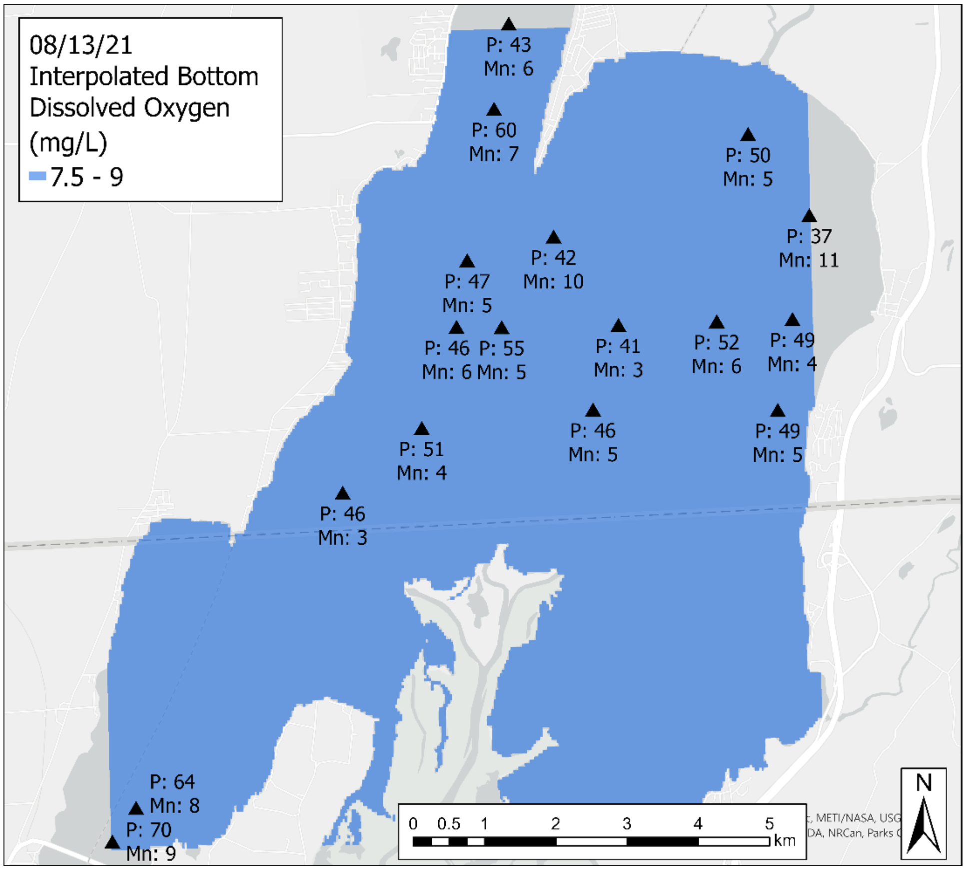

Figure 12. Bottom water TDP and Mn concentrations (µg/L) under fully mixed conditions

4. Model Development and Application

4.1. AEM3D Model Description

A coupled three-dimensional (3D) model of hydrodynamics and biogeochemical processes was used for this study. This model is based on the ELCOM-CAEDYM, originally developed by the Centre for Water Research at the University of Western Australia (*Hodges et al., 2000; Romero et al., 2004*), and recently updated by Hydronumerics (AEM3D, https://www.hydronumerics.com.au). The hydrodynamics component in AEM3D predicts velocity, temperature, salinity, and tracer distributions in standing waters that are subjected to external forcing from the atmosphere, river surface inflows and outflows, groundwater flows, and built structures. It solves the unsteady, viscous Navier-Stokes equations for incompressible flow with an option of using the hydrostatic assumption for pressure (Hodges et al., 2000). Simulated processes include explicit algorithms for baroclinic and barotropic responses, rotational effects, tidal forcing, wind stresses, surface thermal forcing, inflows, outflows, ice formation dynamics, internal mixing, and transport of salt, heat, and passive scalars. The hydrodynamic algorithms in AEM3D are based on the Euler-Lagrange method for advection of momentum with a conjugate-gradient solution for the free surface. Passive and active scalars (i.e., tracers, salinity, and temperature) are advected using a conservative "ULTIMATE QUICKEST" scheme. AEM3D has been optimized for computational efficiency and has typical real time to simulation time ratios of O (100 to 1000):1 depending on the grid resolution and domain size. Calibration of the hydrodynamics component of AEM3D requires few parameter tests because the algorithms are intentionally generic process models and coefficients are process-based, not site-dependent. The values (or at least the appropriate range) of most of the coefficients can be specified from literature values.

The water quality component in AEM3D is dynamically coupled to the hydrodynamics component to simulate the fate and transport of physical, chemical, and biological state variables (*Romero et al., 2004; Vilhena et al., 2010; Weigel et al., 2017*). It consists of a series of mathematical equations representing biogeochemical processes that influence water quality including primary and secondary production, nutrient and metal cycling, oxygen dynamics, movement of the sediment, and sediment-water interactions.

AEM3D simulates state variables at the chemical and biological species level (e.g., organic and inorganic nitrogen, carbon and phosphorus species, and phytoplankton species) and provides aggregate measures to compare with typical observed variables (e.g., total suspended solids (TSS), total nitrogen (TN), TP, and chlorophyll *a* (Chl-a)). Higher trophic levels are included in AEM3D and the utility of the model in this regard has been demonstrated with simulations of the microbial loop and secondary production associated with zooplankton grazing (e.g., *Bruce et al., 2006*). The water quality component requires specification of several parameters used to simulate the biogeochemical processes, but they are also constrained within ranges found in literature.

Technical specifications of AEM3D may be found in the Science and User Manuals (*Hodges and Dallimore, 2018*) and are available at: http://www.hydronumerics.com.au/#software. The manual does not list any hardware requirements as it may be run on most modern personal computers.

The configuration of AEM3D is flexible so that the user can select to model the processes of interest, or within the limitations set by the availability of data and parameters. The model allows the user to define a range of outputs and extract model results at selected spatial and temporal scales.

AEM3D has been used widely in numerous lakes and reservoirs for estimating required external and internal nutrient load reductions for achieving water quality goals (*Burger et al., 2008; Trolle et al., 2008; Valipour et al., 2016; Mueller et al., 2019; Rao et al., 2023*).

4.2. AEM3D Model Development

Bathymetric data of Missisquoi Bay were available from a survey completed in 2014 (Manley,T.; *pers. communication*). The physical model domain of Missisquoi Bay was discretized with a uniform horizontal grid size of 250 m by 250 m, and a vertical resolution of 0.25 m. A time step of 200 s was used to satisfy the Courant-Friedrichs-Lewy criteria for numerical stability. The model included the three major tributaries to the bay: the Missisquoi River, Rock River and Pike River, and an open boundary to Lake Champlain at the Route 78 causeway location. Figure 13 is a map with sampling locations relevant for this study. For the type and details of the data collected see Appendix B, Table A1.

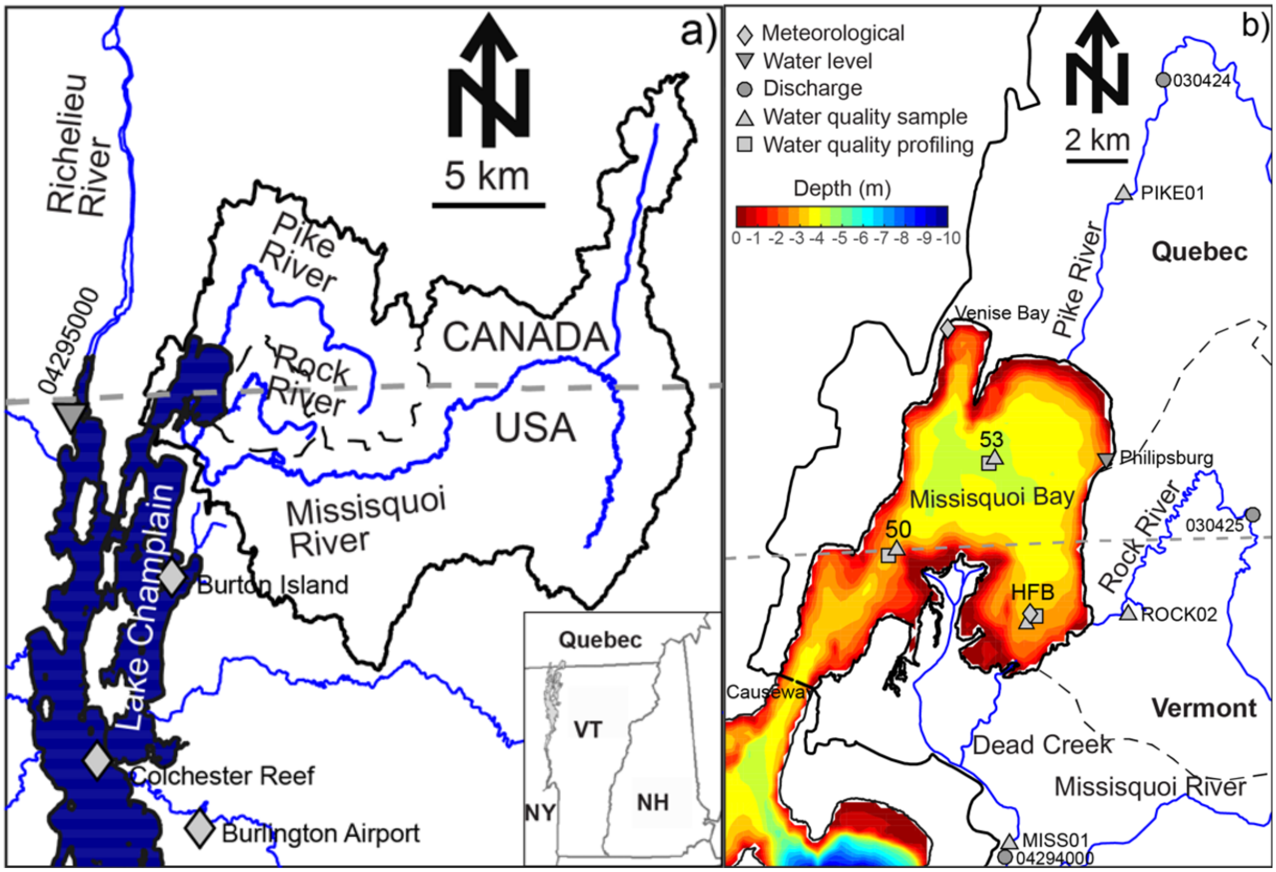

Figure 13. Map of sampling locations relevant for this study: a) MB and major tributaries and b) bathymetry (Manley, T., unpublished).

AEM3D was configured to simulate atmospheric exchange, inflow dynamics, turbulent mixing dynamics, Coriolis forcing, ice formation dynamics (*Oveisy et al., 2021*), one uniform size class of suspended solids, nitrogen and phosphorus in both particulate and dissolved organic and inorganic forms [to include particulate organic nitrogen (PON), dissolved organic nitrogen (DON), ammonium (NH_4), nitrate (NO_3), particulate organic phosphorus (POP), dissolved organic phosphorus (DOP), orthophosphate (PO_4)], dissolved oxygen, particulate organic carbon (POC), and dissolved organic carbon (DOC), as well as two dominant phytoplankton groups: cyanobacteria and diatoms, simulated as chlorophyll *a*, with a constant carbon to Chl-*a* ratio. Nutrient and oxygen fluxes between the sediment and water were simulated using a simple static model based on empirical relationships between the sediment and water (*Bocainov et al., 2016*). AEM3D regulates the sediment phosphate and ammonium releases according to concentrations of dissolved oxygen and temperature in the overlying water layer.

4.3. Model Performance and Uncertainty

Model performance was assessed as follows:

1. Descriptive visualization was used to compare simulated time series and contour plots against observed data and assess whether the model reproduces the observed characteristics over the correct temporal and spatial scales.
2. Statistical performance tests such as regression testing, correlation coefficients, least squares differences, and more complex tests (see *Bennett et al., 2013*) were used as required. The most appropriate performance measures were selected after a review of the available validation data. The performance indicators accommodated the combination of potential spatial and/or temporal (i.e., phase) inaccuracies within the model that may be tolerable but weaken single point and time comparisons against data.

The biogeochemical process algorithms in AEM3D contain numerous rate coefficients that depend on the species in the water and certain site-specific characteristics (e.g., bottom sediment organic content). However, given a particular species group, these coefficients may be viewed as generic, and this has been shown in various publications for pathogens, phytoplankton, and up to zooplankton (e.g., *Bruce et al. 2006*).

The accuracy of simulations hinges on the availability of adequate boundary condition validation data at strategically placed locations.

The water quality component of AEM3D requires calibration as a result of different species assemblages (e.g., phytoplankton), inadequate mathematical representation of some biogeochemical processes, and state variables or constituents not explicitly included in the model. Having a sound physical basis for the model, both as a result of measurements and because of the physical basis of the model, provides a good foundation upon which to undertake calibration of the ecological component of the model. Wherever possible, ecological theory (e.g., stoichiometry, allometric scaling, etc.), careful consideration of relevant state variables, and literature were used to minimize dependence on calibration of the ecological model.

The performance of each iteration of the model undertaken during the calibration exercise was assessed using the performance criteria identified above. Batches of multiple situations within a range of parameters and/or configurations were automated. Further calibration and validation were undertaken against the new field data collected.

4.4. Model Application

4.4.1. Model calibration and validation

Datasets originating from a range of sources were used to generate the initial and forcing boundary conditions for the model (see Appendix B, Table A1). The model was calibrated against field data for the time period June 1, 2017 – December 31, 2019 for the variables water temperature, DO, TP, PO_4, TN, and Chl-*a* in near-surface water and bottom water at different locations within MB using monthly, biweekly, and high-frequency observations from different monitoring programs (see Appendix B, Table A2). Parameters relevant to the hydrodynamic processes were not adjusted and minimal adjustment of biogeochemical parameters was performed using literature values or direct estimates within default literature ranges (Appendix B, Table A3). The final model parameters from the calibration were then fixed for model validation over the period January 1, 2020 – December 31, 2021.

Model performance was assessed by comparing model outputs to measured data using a skill index, mean absolute error (MAE), and root mean square error (RMSE) following Willmott (1982) (Table 8). These metrics suggest that the model was generally able to satisfactorily reproduce the magnitude and dynamics of field measurements at the LTMP's Missisquoi Bay stations and at UVM's HFB. The values were comparable to or better than those from other modelling studies (*Leon et al., 2011; Bocaniov et al., 2016; Muller et al., 2019; Robertson et al. 2022, Rao et al., 2023*), providing confidence that AEM3D simulations could be used to evaluate P load reduction scenarios.

Table 8. Statistical comparisons between model simulations and monitoring data.

		Station					
Parameter	**Statistics**	**LTMP 53**		**LTMP 50**		**UVM HFB**	
Water temperature (°C)	Skill index	0.98^{S}	0.98^{B}	0.98^{S}	0.98^{B}	1.00^{S}	0.99^{B}
	MAE	1.00^{S}	0.98^{B}	0.95^{S}	0.87^{B}	0.60^{S}	0.67^{B}
	RMSE	1.22^{S}	1.17^{B}	1.15^{S}	1.04^{B}	0.78^{S}	0.86^{B}
Dissolved oxygen (mg L^{-1})	Skill index	0.73^{S}	0.71^{B}	0.77^{S}	0.62^{B}	0.67^{S}	0.72^{B}
	MAE	0.79^{S}	1.16^{B}	0.84^{S}	1.31^{B}	1.13^{S}	1.23^{B}
	RMSE	0.93^{S}	1.64^{B}	1.01^{S}	1.79^{B}	1.60^{S}	1.74^{B}
Total nitrogen (mg L^{-1})	Skill index	0.58^{E}		0.47^{E}		0.36^{S}	0.33^{B}
	MAE	0.16^{E}		0.15^{E}		0.24^{S}	0.19^{B}
	RMSE	0.19^{E}		0.18^{E}		0.38^{S}	0.30^{B}
Total phosphorus (mg L^{-1})	Skill index	0.47^{E}		0.49^{E}		0.46^{S}	0.39^{B}
	MAE	0.01^{E}		0.01^{E}		0.02^{S}	0.02^{B}
	RMSE	0.02^{E}		0.01^{E}		0.03^{S}	0.03^{B}
Phosphate (mg L^{-1})	Skill index	-		-		0.36^{S}	0.43^{B}
	MAE	-		-		0.01^{S}	0.01^{B}
	RMSE	-		-		0.01^{S}	0.01^{B}
Chlorophyll *a* (µg L^{-1})	Skill index	0.54^{E}		0.48^{E}		Not computed	
	MAE	11.65^{E}		14.01^{E}		Not computed	
	RMSE	14.77^{E}		17.89^{E}		Not computed	

Notes: Skill index is dimensionless while MAE and RMSE have the units of the respective parameters. ^{S} indicates 1 m below surface, ^{B} 0.5 m above bottom, and ^{E} mean in the photic zone.

Visual comparisons of simulated water temperature, DO, TN, TP, PO_4, and Chl-*a* are shown in Appendix B, Figures A1-A6. The model was able to simulate brief periods of hypoxia and anoxia in the lower water column (Appendix B, Figure A2) that could result in increased internal loading of dissolved nutrients (Appendix B, Figure A7). The extent of low DO conditions near the bottom can thus contribute to a disproportionately high amount of P (Appendix B, Figure A8).

4.4.2. **Scenarios**

During the third Project Advisory Committee meeting (April 22, 2022), the project team discussed phosphorus load reduction scenarios and how these scenarios could be represented in the AEM3D model. Following further discussions, the project team prepared a draft plan with proposed loading scenarios and assumptions. We submitted this on May 16, 2022 for consideration by a VTDEC group convened by Sarah Coleman. After some back and forth, the plan described in this section was agreed to.

The calibrated and validated model was run for the time period January 1, 2010 – December 31, 2021 (hereafter the "baseline period") using the nearly complete meteorological and riverine inflow datasets available for this period (Appendix B, Table A1) and daily concentrations of total suspended solids and different forms of P and N, which we estimated using the statistical model Weighted Regression on Time, Discharge, and Season, with Kalman filtering (WRTDS-K; *Zhang and Hirsh, 2019*). The model was run in a forecasting mode to evaluate the effectiveness of P inactivation scenarios under differing conditions of future watershed loading for 24 years (January 1, 2022 – December 31, 2045). Visual comparisons of simulated water temperature, DO, TN, TP and Chl-*a* are shown in Appendix B, Figures A9-A13. Forcing boundary conditions (i.e., meteorological, inflows, and concentrations) were randomly selected from the baseline period (2010-2021) on a yearly basis to generate the forcing boundary conditions for the forecast period. The year 2011 (Irene and major spring storms) was not included. Figure 14 shows the riverine water flux and P loading computed using WRTDS-K for the baseline period and forecast period, reflecting the year-to-year variability in water flux and P concentrations.

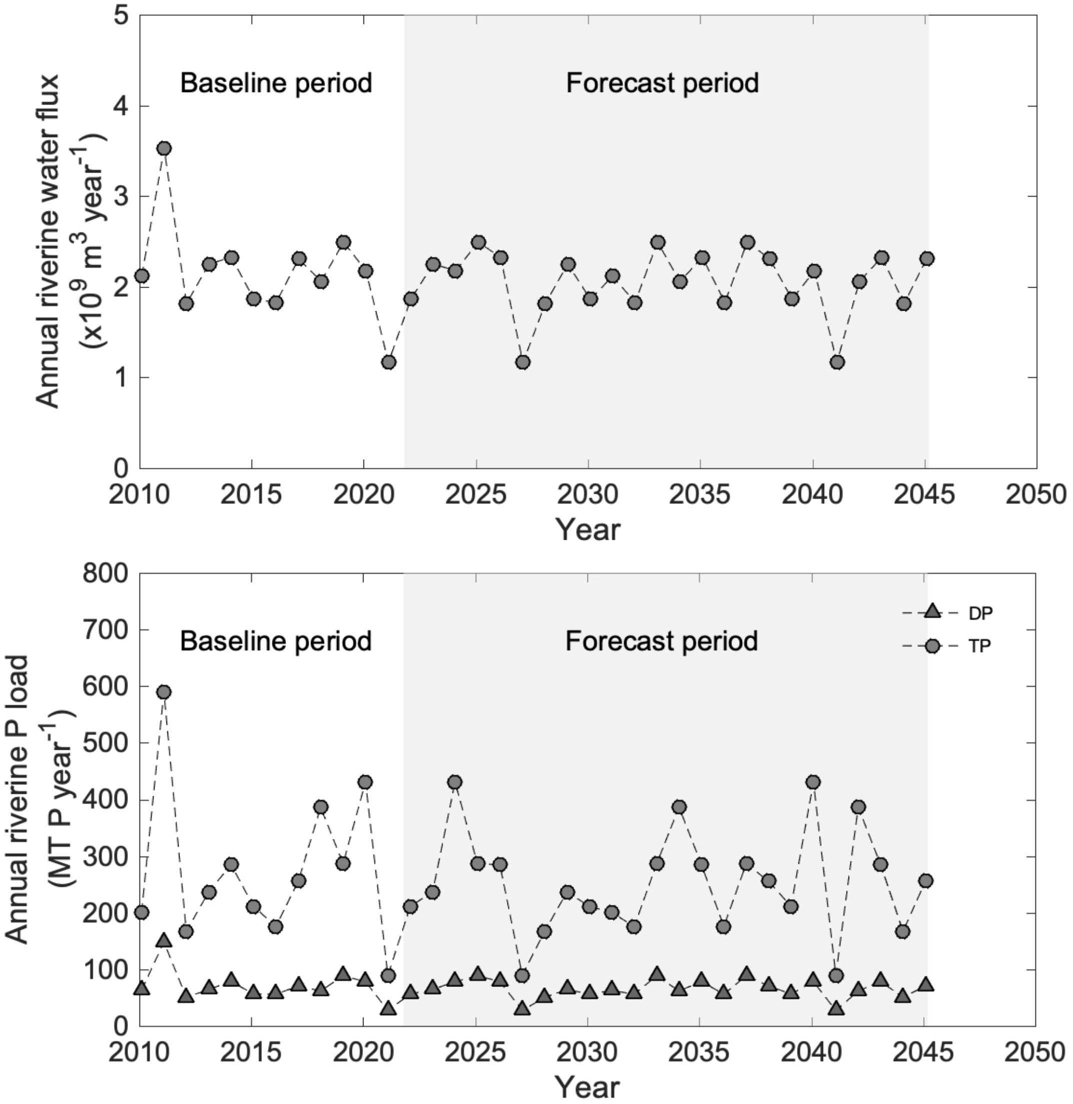

Figure 14. Riverine water flux (top panel) and P loading (bottom panel) for the baseline and forecast periods.

4.4.2.1. External P loading scenarios and assumptions

- External P loading reductions were simulated by applying reduction factors to estimated daily tributary P loads. Five external P loading reduction scenarios were simulated: 0% (baseline) and annual (cumulative) reductions of 1%, 2%, 3%, and 4% following a series of simplifying assumptions: P load reduction factors were applied to the riverine P inputs in equal proportion on every day of the forecast period (regardless of flow rate, season, or P concentration). All three rivers were treated identically. For example, in a year in which a 20% external P load reduction was assumed for Missisquoi Bay, each daily total and dissolved P loading value for the Missisquoi, Pike, and Rock Rivers was reduced by 20% from their corresponding baseline period daily values.

- P load reduction factors were applied equally to the various forms of P.

- In the 2016-2021 period, P reduction estimates provided by VTDEC for the Vermont portion of the Missisquoi River Basin (Table 9) were assumed to be applicable to the entire Missisquoi Bay watershed. Further, these “tracked” reductions were assumed to be imbedded or incorporated in the empirically derived annual P loading estimates for the 2016-2021 period, regardless of the magnitudes of these loading estimates (in most years, annual P loading in the 2016-2021 period exceeded the annual average for the 2001-2010 TMDL baseline period).

Table 9. P loading reduction estimates for the Vermont portion of the Missisquoi River Basin.

	2016	**2017**	**2018**	**2019**	**2020**	**2021**
P reduction (kg)	3,103.5	4,417.8	5,522.6	7,179.8	8,275.1	10,713.2
P reduction (%)	2.3%	3.2%	4.1%	5.3%	6.1%	7.9%

- In accordance with VTDEC’s input, linearly increasing P loading reductions in the period 2022-2036 were assumed. Since the WRTDS-K derived loading estimates for 2021 were assumed to represent an ~8% P loading reduction (Table 10), the P loading reductions in 2022 for the 1%, 2%, 3%, and 4% reduction scenarios were stepped to 9%, 10%, 11%, and 12%, respectively (Table 10). In the forecast period, the baseline period data years were recycled and randomly selected (Figure 14) prior to applying the corresponding percent loading reductions from Table 10. Figure 15 illustrates these scenarios given the randomized selection used in this study. As in Table 10, P loading reductions are stepped up in 2022 in Figure 15. The forecast period is represented by the shaded area.

- A wide range of watershed loading conditions (i.e., 0 - 4% annual P reduction scenarios) that bound the TMDL-mandated loading reductions were simulated rather than trying to exactly reproduce a TMDL-compliant loading scenario. Under some scenarios, the target loading capacity of Missisquoi Bay (81 MT/year, including Quebec) may still be exceeded beyond 2036.

- No further external P loading reductions beyond 2036 were assumed, although the forecast period extended to 2045.

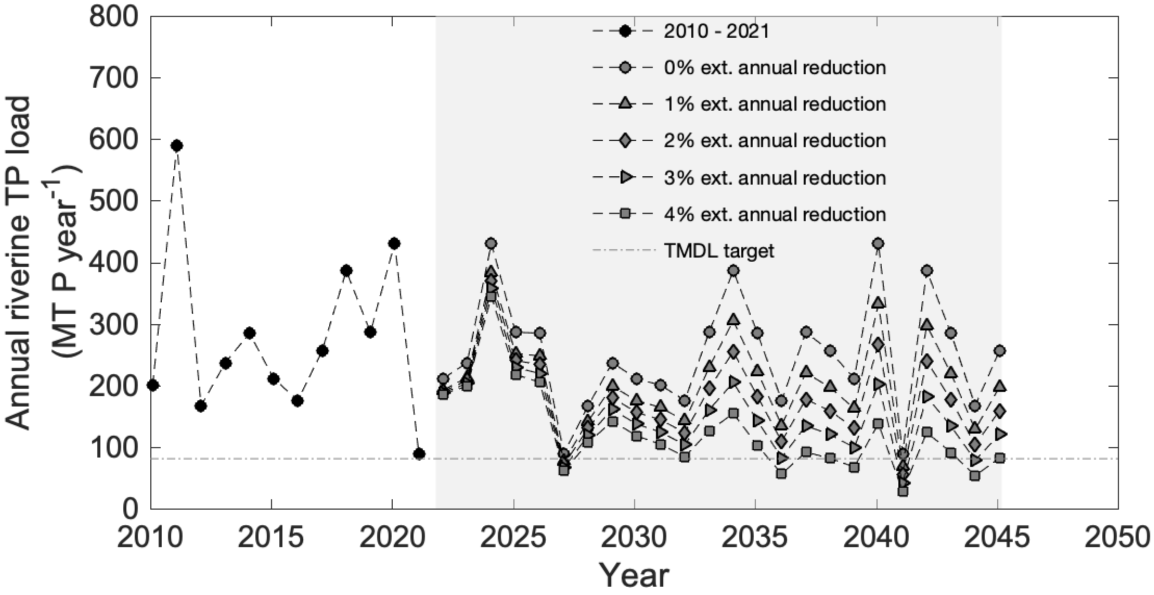

Figure 15. Linear reductions in TP loading to MB, 2022–2036.

- Since AEM3D does not track sediment P stores over time, the model cannot simulate changes in internal loading as a function of external load reductions. Given the short duration (24 years) of the forecast period, as well as the slow ramp up in external load reduction factors shown in Table 10, the impact of this model limitation is minor, even considering the 4% annual reduction scenarios. However, the inability of AEM3D to track sediment P stores suggests it may not be appropriate to use this model in substantially longer simulations.

Table 10. External P loading model scenarios with stepped reductions in 2022.

	External P loading Reduction Factors (%)				
Year	**0% Annual Reduction**	**1% Annual Reduction**	**2% Annual Reduction**	**3% Annual Reduction**	**4% Annual Reduction**
2010 - 2021	NA	NA	NA	NA	NA
2022	0%	9%	10%	11%	12%
2023	0%	10%	12%	14%	16%
2024	0%	11%	14%	17%	20%
2025	0%	12%	16%	20%	24%
2026	0%	13%	18%	23%	28%
2027	0%	14%	20%	26%	32%
2028	0%	15%	22%	29%	36%
2029	0%	16%	24%	32%	40%
2030	0%	17%	26%	35%	44%
2031	0%	18%	28%	38%	48%
2032	0%	19%	30%	41%	52%

Year	External P loading Reduction Factors (%)				
	0% Annual Reduction	1% Annual Reduction	2% Annual Reduction	3% Annual Reduction	4% Annual Reduction
2033	0%	20%	32%	44%	56%
2034	0%	21%	34%	47%	60%
2035	0%	22%	36%	50%	64%
2036	0%	23%	38%	53%	68%
2037	0%	23%	38%	53%	68%
2038	0%	23%	38%	53%	68%
2039	0%	23%	38%	53%	68%
2040	0%	23%	38%	53%	68%
2041	0%	23%	38%	53%	68%
2042	0%	23%	38%	53%	68%
2043	0%	23%	38%	53%	68%
2044	0%	23%	38%	53%	68%
2045	0%	23%	38%	53%	68%

4.4.2.2. Internal P Loading Scenarios and Assumptions

To simulate reductions in internal P loading due to management interventions, the rate coefficient for the maximum potential P release from the sediment was adjusted in the model. Four scenarios were implemented, as follows:

Scenario 1: No in-lake management. Uncontrolled internal P loading continues indefinitely.

Scenario 2: 90% internal load reduction in contributing area. The area of the bay potentially releasing significant dissolved P from sediment was assumed to equal the entire area with depths greater than 1.5 m, ~6,000 ha (Figure 16). This contributing area includes the deeper portions of Missisquoi Bay subject to transient low DO conditions at the SWI (Appendix B, Figure A8) and associated P release through reductive dissolution of iron and manganese compounds in the sediment. Shallower areas are less likely to become stratified, precluding release of P through reductive dissolution of Fe-P and Mn-P forms. It is also technically infeasible to treat shallower areas. For the duration of the forecast period (2022–2045), maximum potential P release from the sediments was reduced by 90% throughout this P contributing area. This reduction was instantaneous and continuous, starting January 1, 2022 and continuing through December 31, 2045.

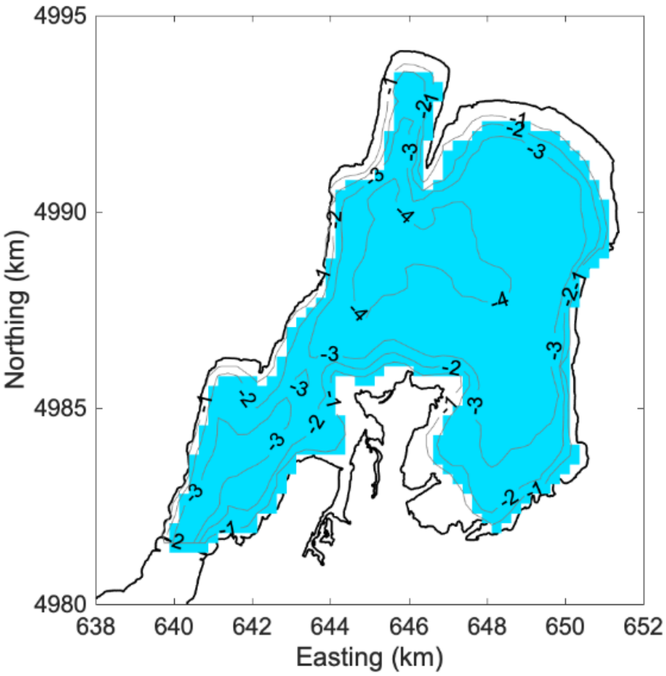

Figure 16. Treatment area of MB potentially releasing significant dissolved P from sediment.

This scenario is an ideal case, theoretically possible only with repeated and timely chemical inactivation of sediment P throughout the contributing area. In this scenario, the manner of P inactivation treatment is not presumed. For example, this result could be achieved by aluminum application at typical rates throughout the Bay, with retreatment when breakthrough sediment P flux is first detected. Alternately, it could be achieved with more frequent, lower rate P inactivation treatments.

Scenario 3: Target areas of frequent low DO. The central bowl of Missisquoi Bay has depths > 3.6 m and generally finer textured, lower density sediment with higher organic matter. This approximately 1,650 ha area is believed to have the most frequently depressed bottom water DO concentrations and to thus contribute a disproportionately high amount of P. Treatment of this area should be most efficient. A single aluminum product application at a typical (75 g Al/m^2) dose was simulated over this priority area. This application occurred in 2026 and should provide effective control (~90% reduction) of P flux from the treated area for approximately 8 years. However, treatment of only 1,650 ha of the approximately 5,580 ha P contributing area may be insufficient to reach water quality goals. Therefore, the treatment area could be expanded to include areas with less frequent low DO conditions, allowing assessment of the tradeoff between area treated and percent load reduction. Three extents (scenarios 3A, 3B, 3C), with varying durations of predicted low DO conditions were simulated (Figure 17):

Scenario 3A: Target area of most frequent low DO (~1,650 ha)

Scenario 3B: Target area of most/moderately frequent low DO (~3,800 ha); inclusive of 3A

Scenario 3C: Target all areas of frequent low DO (~5,580 ha); inclusive of 3A and 3B

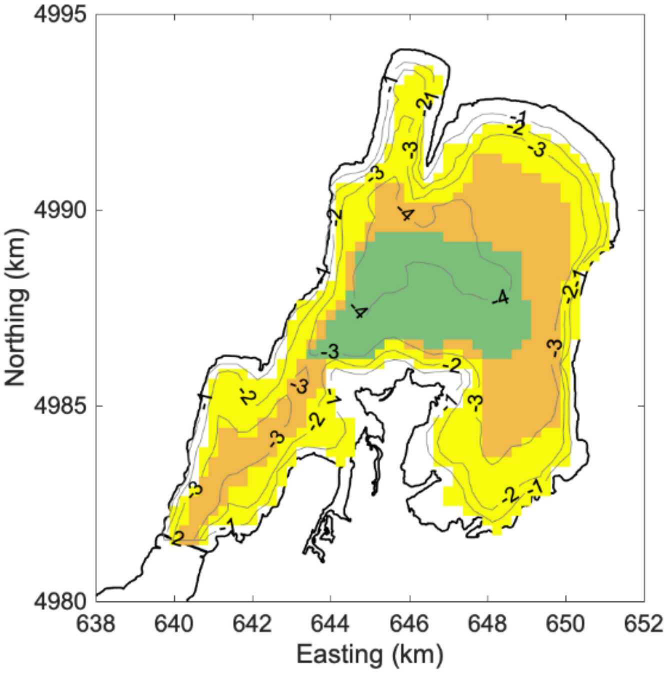

Figure 17. Target areas of MB with most frequent low DO concentrations (Scenario 3A=green: 3B=green+orange, 3C=green+orange+yellow).

Scenario 4: Annual low dose treatments by quadrant. A low rate (20-25 g/m^2) aluminum product treatment of the entire 5,580 ha area believed to contribute substantial P via fluxes from the sediment was simulated, with one quarter (1,395 ha) of the contributing area treated each year. A 20-25 g Al/m^2 dose should be adequate to treat the average P in the upper 2 cm of sediment (with Al applied at about a 10 Al:1 P ratio). This should provide about four years of internal P load reduction at about the 90% level. In the first treatment year (2026) internal P flux was reduced by 90% across 1395 ha. An additional 1395 ha was treated in the second, third, and fourth years, with no diminishment of effectiveness. The 4-year treatment cycle was repeated twice more, starting again in 2030 and 2034. Note that the final treatment (3rd treatment of Area 4) occurred in 2037 (Figure 18). Table 11 presents assumed reductions in P flux corresponding with this schedule of low dose treatments. In each treatment year (Table 11), the partial treatment was

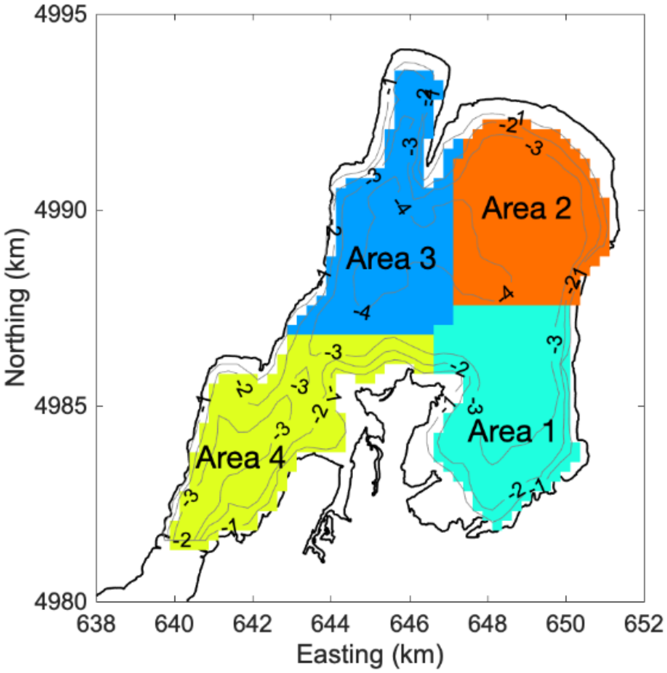

Figure 18. Four treatment quadrants

assumed to occur instantaneously on June 1. In fact, considering the large areas involved, it would likely require ~3 months to accomplish a partial treatment (the June 1 date is roughly the midpoint of a typical treatment period).

Table 11. P flux reductions assumed for Scenario 4, annual low-dose treatments of partial areas

	P flux reduction factors (%)				
Year	**Area 1**	**Area 2**	**Area 3**	**Area 4**	**Bay average**
2016-2021	0%	0%	0%	0%	0%
2022	0%	0%	0%	0%	0%
2023	0%	0%	0%	0%	0%
2024	0%	0%	0%	0%	0%
2025	0%	0%	0%	0%	0%
2026	90%	0%	0%	0%	22.5%
2027	90%	90%	0%	0%	45.0%
2028	90%	90%	90%	0%	67.5%
2029	90%	90%	90%	90%	90%
2030	90%	90%	90%	90%	90%
2031	90%	90%	90%	90%	90%
2032	90%	90%	90%	90%	90%
2033	90%	90%	90%	90%	90%
2034	90%	90%	90%	90%	90%
2035	90%	90%	90%	90%	90%
2036	90%	90%	90%	90%	90%
2037	90%	90%	90%	90%	90%
2038	50%	90%	90%	90%	80.0%
2039	0%	50%	90%	90%	57.5%
2040	0%	0%	50%	90%	35.0%
2041	0%	0%	0%	50%	12.5%
2042	0%	0%	0%	0%	0%
2043	0%	0%	0%	0%	0%
2044	0%	0%	0%	0%	0%
2045	0%	0%	0%	0%	0%

4.4.2.3. External and Internal P Loading Scenarios

The forecast model was used to evaluate the combined external and internal P load reductions scenarios that would reduce the long-term TP and Chl-*a* concentrations. Table 12 presents the combinations of external and internal P loading reduction scenarios simulated (22 in total). The corresponding results are presented below.

Table 12. Combined external and internal P load reduction scenarios.

P Inactivation Scenario	External P Loading Annual Reduction Factors				
	0%	1%	2%	3%	4%
Scenario 1: No in-lake management	X	X	X	X	X
Scenario 2: Constant 90% internal load reduction in contributing area (ideal case)	X	X	X	X	X
Scenario 3A: One full rate treatment of area with most frequent low DO (~1,650 ha)	X		X		X
Scenario 3B: One full rate treatment of area with most/moderately frequent low DO (~3,800 ha)	X		X		X
Scenario 3C: One full rate treatment of all areas with frequent low DO (~5,580 ha)	X		X		X
Scenario 4: Annual low dose treatments by quadrant (1,395 ha per year, 3 rotations)	X		X		X

Scenario 1: *No in-lake management*

The summer (June - September) bay-wide average water column TP and Chl-*a* concentrations are shown in Figure 19. As expected, in-lake TP concentrations decline in response to increasing reductions in external loads. However, even with an annual 4% external load reduction the in-lake TMDL P concentration target (annual average TP = 0.025 mg/L) was only achieved in the year 2045. It is noteworthy that other years with relatively low external P loading, such as 2038, 2043, and 2044, also showed progress toward achievement of the target. This suggests that the interannual variability of external loads significantly influences TP concentrations in MB, and a substantial annual reduction in external loads will be necessary to consistently meet the TMDL P target. Despite reductions in summer bay-wide average water column TP concentrations in response to increasing external load reductions, there were only marginal reductions in Chl-*a* concentrations in any given year. This observation suggests that the availability of nutrients from internal loading continues to support phytoplankton growth.

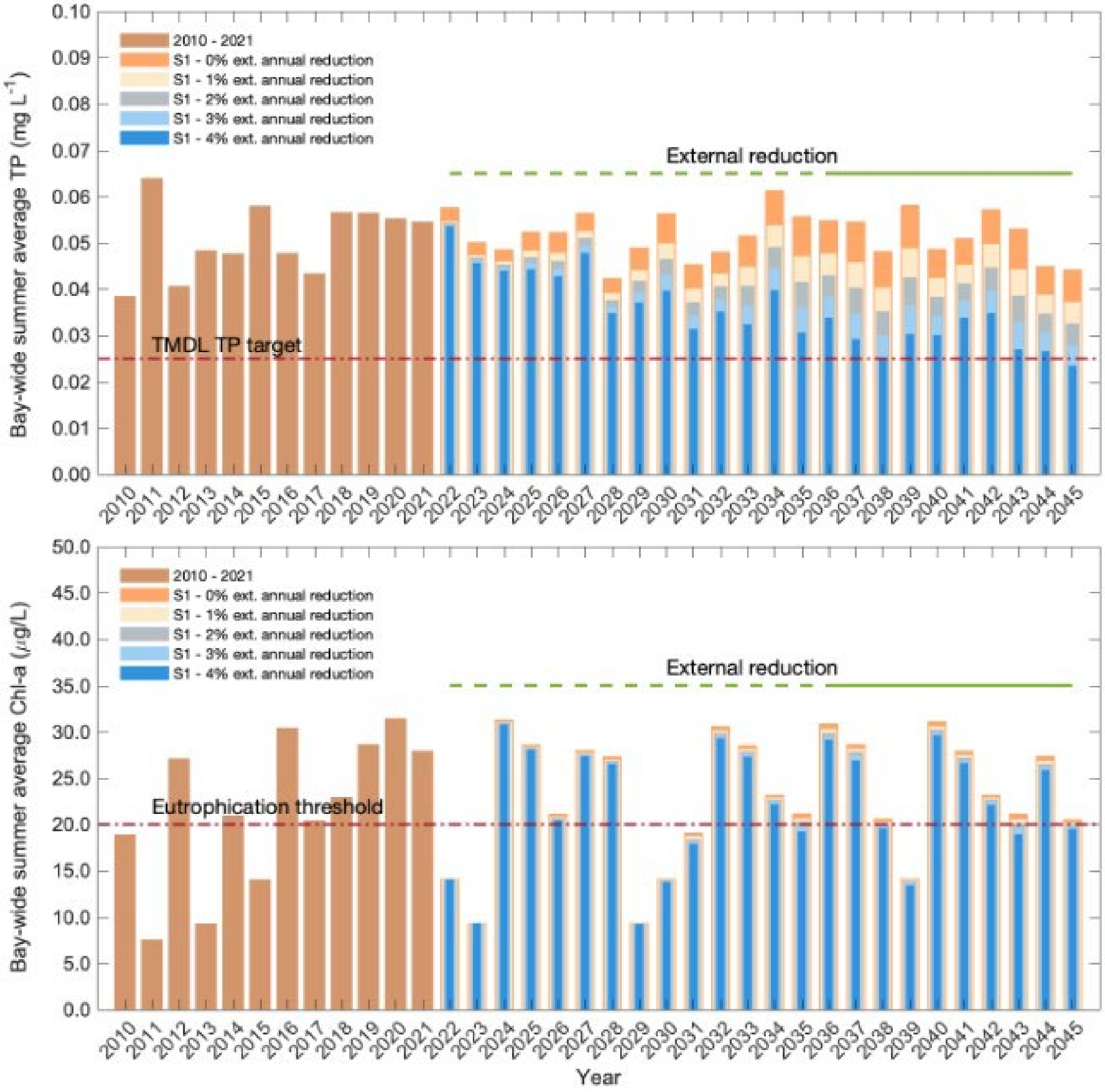

Figure 19.Summer bay-wide average water column TP (top panel) and Chl-a (bottom panel) concentrations for Scenario 1.

Scenario 2: *Constant 90% internal P load reduction in contributing area (ideal case)*

The summer (June–September) bay-wide average water column TP and Chl-*a* concentrations are shown in Figure 20. Internal load reduction in the contributing area resulted in greater reductions in TP concentration as compared with Scenario 1 (no-in-lake management). In 2022, the initial drop in TP concentration of approximately 25% was due solely to reduction of the internal load. Assuming no external load reduction (0%), there was a 27% reduction in summer average TP concentrations across all years (2022 - 2045) relative to Scenario 1. However, this reduction alone did not achieve the TMDL P concentration target. The combination of internal and external load reductions had a profound effect on the timing of achieving the TMDL P target. Except for the 1% annual external P load reduction, all scenarios that included both internal and external load reductions achieved the TMDL target earlier than in Scenario 1 with a 4% annual external reduction. Specifically, Scenario 2 with a 4% annual external reduction consistently achieved the target from year 2031 onwards, followed by Scenario 2 with a 3% annual external reduction from year 2035 onwards.

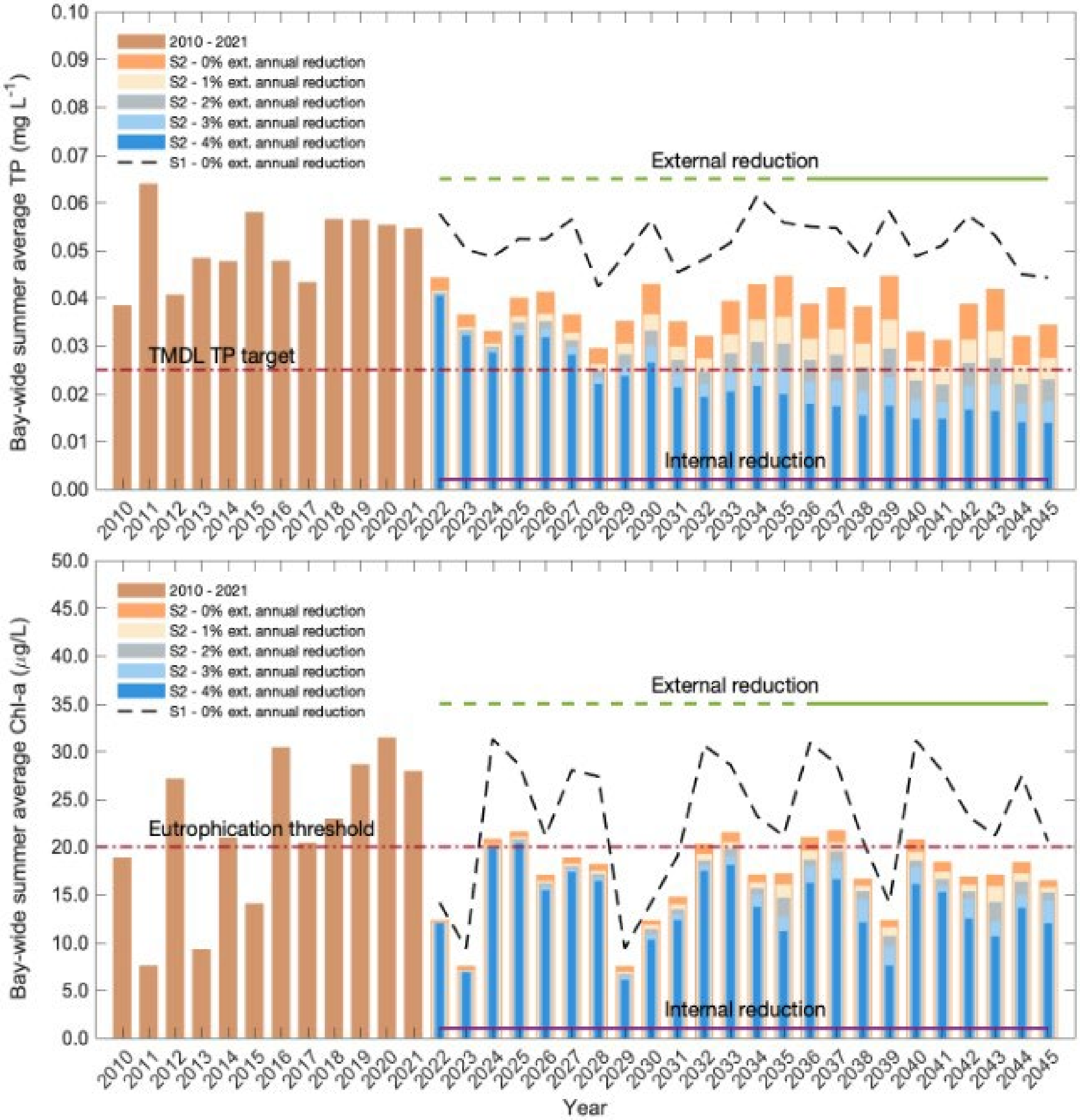

Figure 20. Summer bay-wide average water column TP (top panel) and Chl-a (bottom panel) concentrations for Scenario 2.

Substantial reductions in Chl-*a* concentrations were observed in response to internal load reductions alone. On average, with 0% external annual P reduction, there was a 23% Chl-*a* concentration reduction across all years (2022–2045) as compared to the no in-lake management scenario. Chl-*a* concentrations fell below the eutrophication threshold 70% of the time. At a relatively modest 2% annual external load reduction, the Chl-a target was achieved every year between 2026 and 2045.

The degree of external annual P reduction appeared to influence Chl-*a* concentrations from about 2031 onwards, as shown by increasing differences in Chl-*a* concentrations among the different scenarios through the forecast period. This suggests that cumulative external load reductions do result in reduced sediment P feedback into the water column, even if the effect takes longer and is weaker than we would prefer.

Scenario 3: *One full rate treatment of areas with low DO concentration*

The summer (June–September) bay-wide average water column TP and Chl-*a* concentrations are shown in Figure 21 and 22. The effects of internal load reduction alone can only be observed in the 9-year period following treatment (2026–2034). Treating only Area A resulted in a 5% reduction in TP concentration. Treating Area A and Area B resulted in a 14% average reduction in TP concentration over a 9-year period following treatment, and treating Areas A, B, and C resulted in a 25% average reduction in TP concentration. The in-lake P target was not met in any scenario except for Scenario 3C with 4% annual external load reduction, and then not consistently. After 2035, TP concentration trends and values follow those in Scenario 1.

Chl-*a* concentrations decreased in response to increases in treatment area extents. Scenario 3C with 2% and 4% external annual reductions met or nearly met the eutrophication target during a 9-year period following treatment (2026–2034). Scenarios 3A and 3B demonstrate that Chl-a concentrations were not adequately reduced by treatment of these substantially smaller areas. After 2035, Chl-*a* concentration trends and values follow those of Scenario 1.

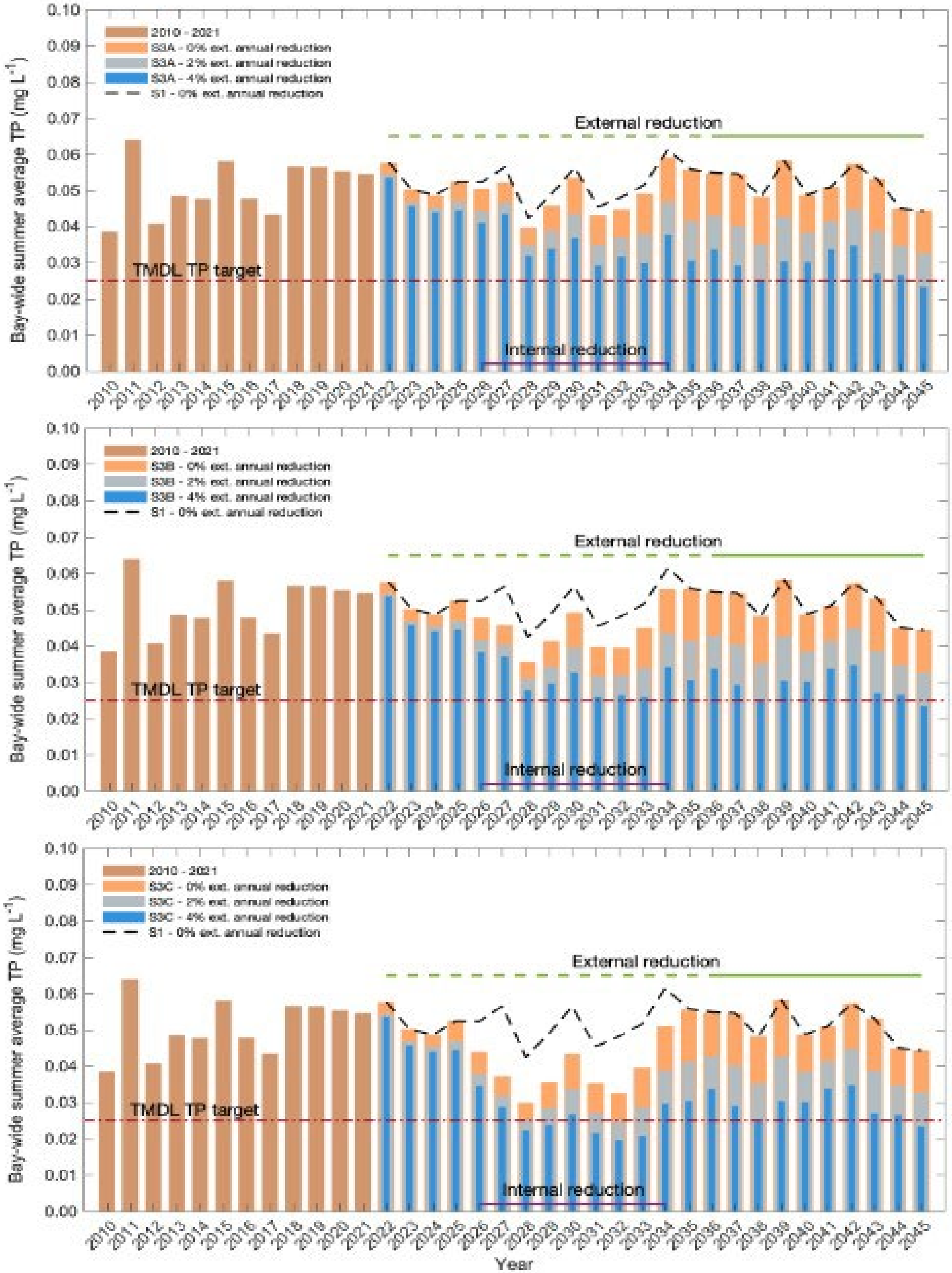

Figure 21. Summer bay-wide average water column TP concentrations for Scenario 3A (top panel), 3B (middle panel), and 3C (bottom panel).

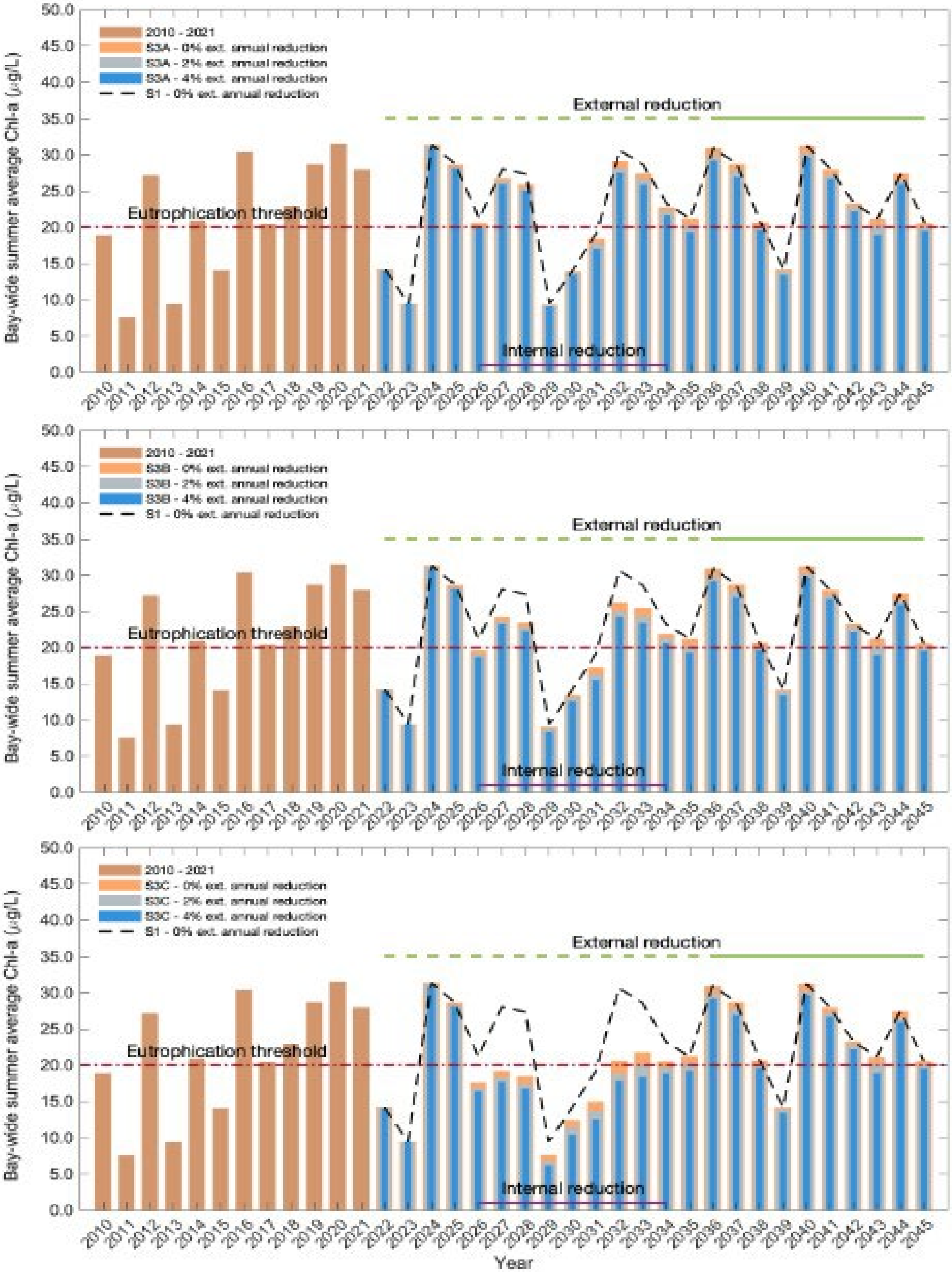

Figure 22. Summer bay-wide average water column Chl-a concentrations for Scenario 3A (top panel), 3B (middle panel), and 3C (bottom panel).

Scenario 4: *Annual low dose treatments by quadrant (1,395 ha per year, 3 rotations)*

The summer (June–September) bay-wide average water column TP and Chl-*a* concentrations are shown in Figure 23. The initial drop in TP concentrations of approximately 6% in 2026 is attributable to internal load reduction in Area 1 alone. On average, a 19% reduction in TP concentration was observed across the treatment period (2026–2041) compared to the no in-lake management scenario with 0% external annual reduction. However, this reduction did not meet the in-lake P target. With increasing external load reductions, TP concentrations decreased further during the treatment period to an average of 39% and 53% for the 2% and 4% external annual reductions, respectively. With 4% external annual reduction, the TMDL P target was initially achieved in 2028, when three of the four quadrants had received one treatment. Control appeared quite good through 2040 with either 2% or 4% external annual load reduction. Subsequently, TP concentration trends and values followed those of Scenario 1.

Chl-*a* concentrations decreased in response to the schedule of P inactivation treatments. With 2% and 4% annual reductions in external P loading, the Chl-*a* eutrophication target was achieved consistently from 2028 through 2039. Even assuming no reductions in external nutrient loading, the Chl-*a* target was achieved or nearly achieved every year from 2028 through 2039, compared with only four years without P inactivation treatments.

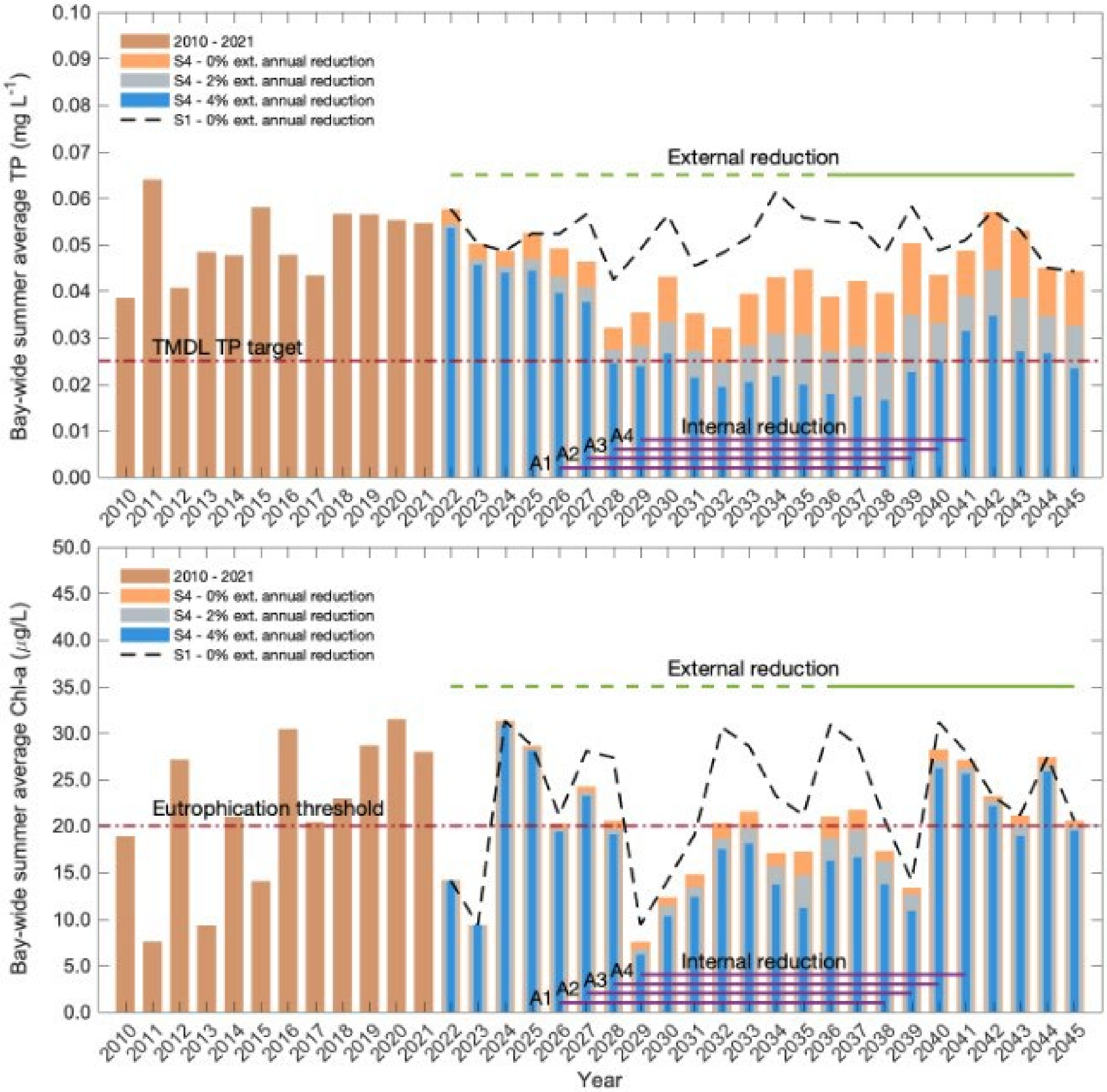

Figure 23. Summer bay-wide average water column TP (top panel) and Chl-a (bottom panel) concentrations for Scenario 4.

5. Management Options Review for Missisquoi Bay

5.1. Background

Missisquoi Bay is the northernmost bay of Lake Champlain and covers 7,850 ha (just under 20,000 acres) in Vermont, USA, and Quebec, Canada (Figure 24). The Vermont Route 78 causeway is generally taken as the southern boundary of Missisquoi Bay, south of which water flows into the Inland Sea portion of Lake Champlain. Missisquoi Bay is shallow (Figure 25) with a maximum depth of 4.3 m (14 feet), but with about 30% of the basin having a depth near 3.6 m (12 feet) in a central bowl. While pronounced or prolonged stratification does not occur in Missisquoi Bay, the project team found that 71% of the bottom is subject to temporary depletion of dissolved oxygen and associated release of redox-sensitive P from the sediment.

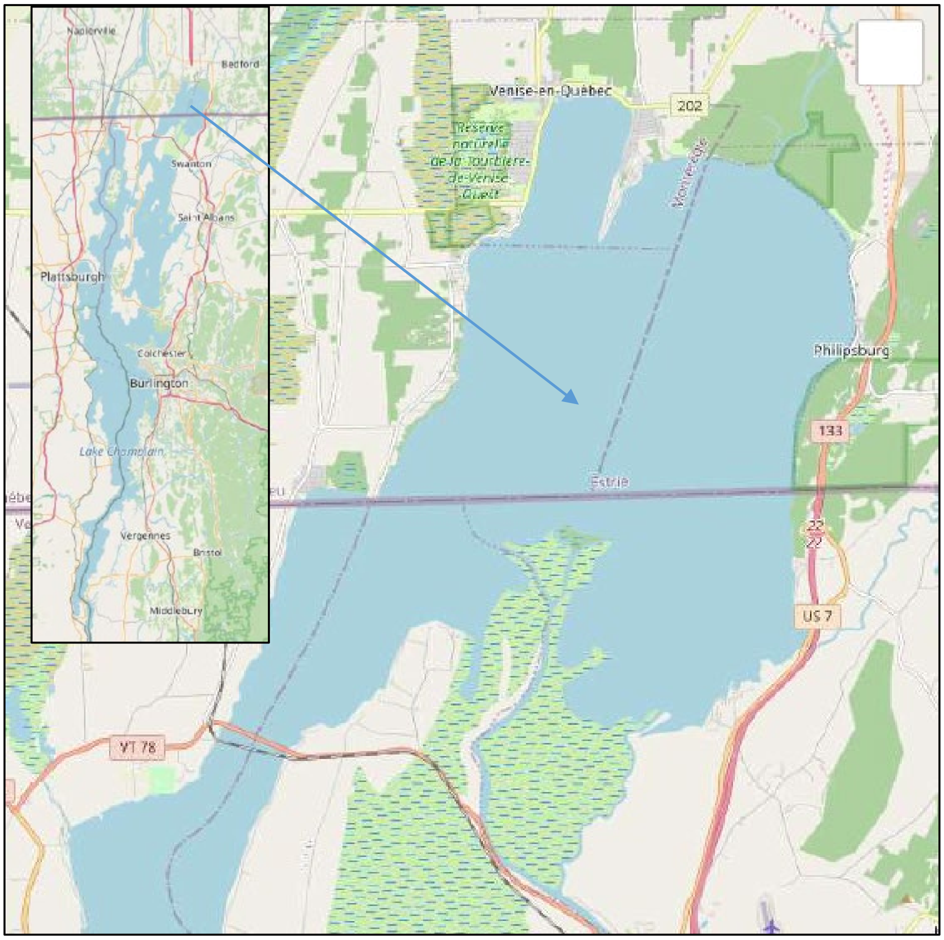

Figure 24. Missisquoi Bay within Lake Champlain.

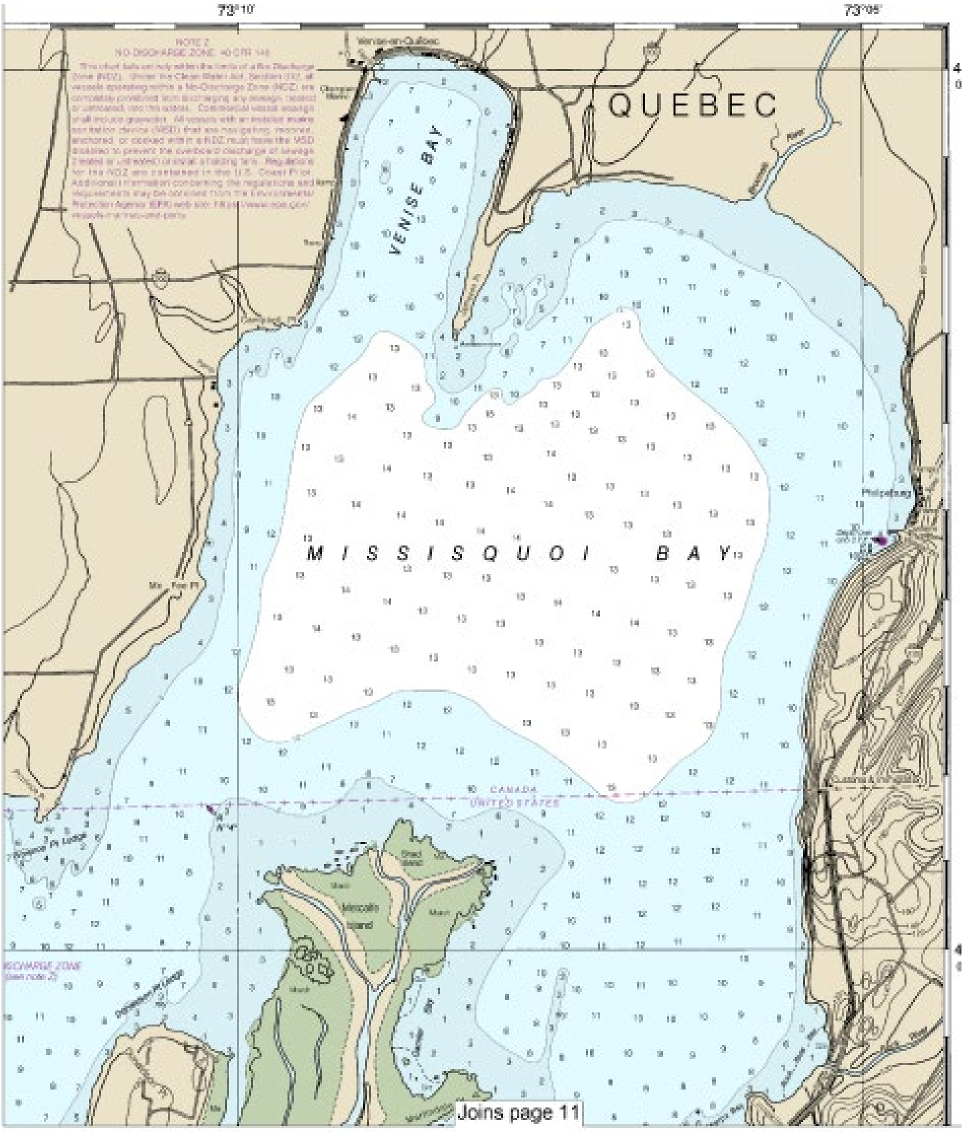

Figure 25. Missisquoi Bay water depths in feet.

Data from 2001–2010 collected by VTDEC and reported by LimnoTech (2012) indicated that average summer TP concentrations in Missisquoi Bay ranged from about 40 to 60 µg/L; P concentrations remain high today. The internal P load is estimated to average 20% of the annual total load but 43% of the summer load, with substantial inter-annual variability governed by variability in summer weather. With most of the internal load occurring during the warmer summer and early autumn months, the low N:P ratio of that load, and accompanying nutrients like iron, production by cyanobacteria will be favored (*Randall et al., 2019; Molot et al., 2021*), a long-term and increasing problem in Missisquoi Bay. While a major decrease in external loading appears necessary (*USEPA, 2016; Celikkol et al., 2021*), the internal load has increased to the point where it must be addressed to achieve desired conditions. Modeling by both LimnoTech and this project team indicates that target levels for P and chlorophyll *a* cannot be reached without reduction in internal P loading.

Multiple forms of P are found in sediment with varying availability for recycling. Of primary concern is the redox-sensitive P fraction, usually bound to iron but sometimes manganese and subject to release under low oxygen conditions, especially when oxygen has been depleted. A sediment core sample from the middle of Missisquoi Bay (N 45.0367; W -73.130) revealed that redox-sensitive P ranged from about 0.3 to 0.7 mg P per g of dry sediment in the upper 10 cm (*Ostrofsky et al., 2020*). Redox-sensitive P peaked at 4 cm depth. Below 4 cm, redox-sensitive P declined with depth, reaching about 0.18 mg/g at 19 cm, corresponding to a date of about 1930, and leveling off at about 0.13 mg/g at a depth of 27 cm, representing a date of about 1860.

Sediment interaction with the overlying water is greatest at the surface of the sediment and declines with sediment depth, although many sediment constituents, including redox-sensitive P, can migrate upward. A depth of 10 cm is generally recognized as an appropriate sediment depth for consideration of internal P loading over a period of years, although the quantity of P released from sediment exposed to anoxia over any given summer will be only a portion of that total. Research on Missisquoi Bay sediment suggests that the increase in summer P concentration in the overlying water column can be explained by the release of redox-sensitive P in less than the upper 2 cm of sediment (*Smith et al., 2011; Giles et al., 2016*). However, the upward migration of P in the sediment over time suggests that addressing a greater depth of sediment is necessary for long-term internal P load control.

Sediment core sampling of Missisquoi Bay by the project team in 2020–2021 provided an indication of the distribution of redox-sensitive P in the upper 10 cm of the sediment (Figure 6). Values ranged from 0.1 to 0.7 mg P per g of dry sediment using an ascorbate extraction. Values <0.05 mg/g are considered low, while values >0.2 mg/g are considered high and values >0.5 mg/g are viewed as very high for bicarbonate-dithionite (BD) extraction results A comparison done elsewhere (*Zhang and Lanning, 2018*) suggests that ascorbate and BD extraction results are comparable. However, direct comparison tests for Missisquoi Bay samples revealed that ascorbate extraction yielded as much as twice as much redox P as BD extraction. This methodological discrepancy does not detract from the importance of internal P loading but underscores the difficulty in getting an accurate assessment. By either extraction approach, the redox-sensitive P in the upper sediment of the bay is quite high. Only about 10% of all 10-cm sediment cores had <0.2 mg P/g and about 40% had >0.5 mg P/g by ascorbate extraction, confirming the need to consider sediment to 10 cm as a viable P contributor to internal loading in much of the bay.

While the concentration of redox-sensitive P is a useful indicator, the actual mass of available P in the sediment depends on the bulk density of the sediment. The distribution of sediment density in Missisquoi Bay (Figure 8a) follows a predictable pattern, with greater bulk density near the periphery of the bay where sand content will be higher and lower density in the deeper, central area where organic matter and finer sediments will accumulate. Bulk density is a function of both the solids content of the sediment (the part that is not water) and the specific gravity of the dry sediment. Values ranged from 0.3 to 0.8 g/cm^3, indicating moderate to high solids content relative to most lakes.

The product of redox-sensitive P and bulk sediment density for the upper 10 cm of each sediment core provides a mass of P that can be released over time if exposed to anoxic conditions (Figure 8b). Values tend to be highest on the east side of the bay but are substantial in virtually all areas. Some of this P mass lies outside the zone of expected anoxic conditions and will not likely be released by redox reactions. Even where oxygen is depleted, only a small fraction of the redox-sensitive P in the upper 10 cm will be released in any summer (<20%), based on experience elsewhere. With only intermittent low oxygen conditions at the SWI, a release rate as low as 5% might be expected. Considering the target water column TP concentration of 25 µg/L and the relatively shallow (no more than 4.3 m) water depth (LimnoTech, 2012), sediment with a redox-sensitive P mass in excess of 2 g/m^2 could release enough P to exceed the target P concentration over a summer. In other words, release of just 5% of a P mass of 2 g/m^2 into an overlying water column of 4.3 m is enough to raise the P concentration by 23 µg/L over whatever background P concentration exists. Redox-sensitive P mass in the upper 10 cm of Missisquoi Bay routinely exceeds 11 g/m^2. Even the lower dithionite extraction results signal a highly elevated mass of potentially released P in Missisquoi Bay.

Considerable field work coupled with process-based modeling has defined the area of Missisquoi Bay subject to transient anoxia at the SWI. Subtle differences in depth across most of the bay coupled with complex hydrodynamics that are highly sensitive to changes in wind speed and direction lead to these transient episodes of anoxia. Superimposing that area on the map of redox-sensitive P mass provides an approximation of the release area of concern in the bay (Figure 26). While the interpolation of areas and concentrations creates some uncertainty, the total affected area is about 5,580 ha (slightly less than 14,000 acres), or about 71% of the total bay area. Five levels of redox-sensitive P mass are defined, with a low value greater than 11 g/m^2 and a high end of almost 26 g/m^2. The highest P mass is found on the east side of the bay; however, all areas subject to anoxia have ample redox-sensitive sediment P that could be released.

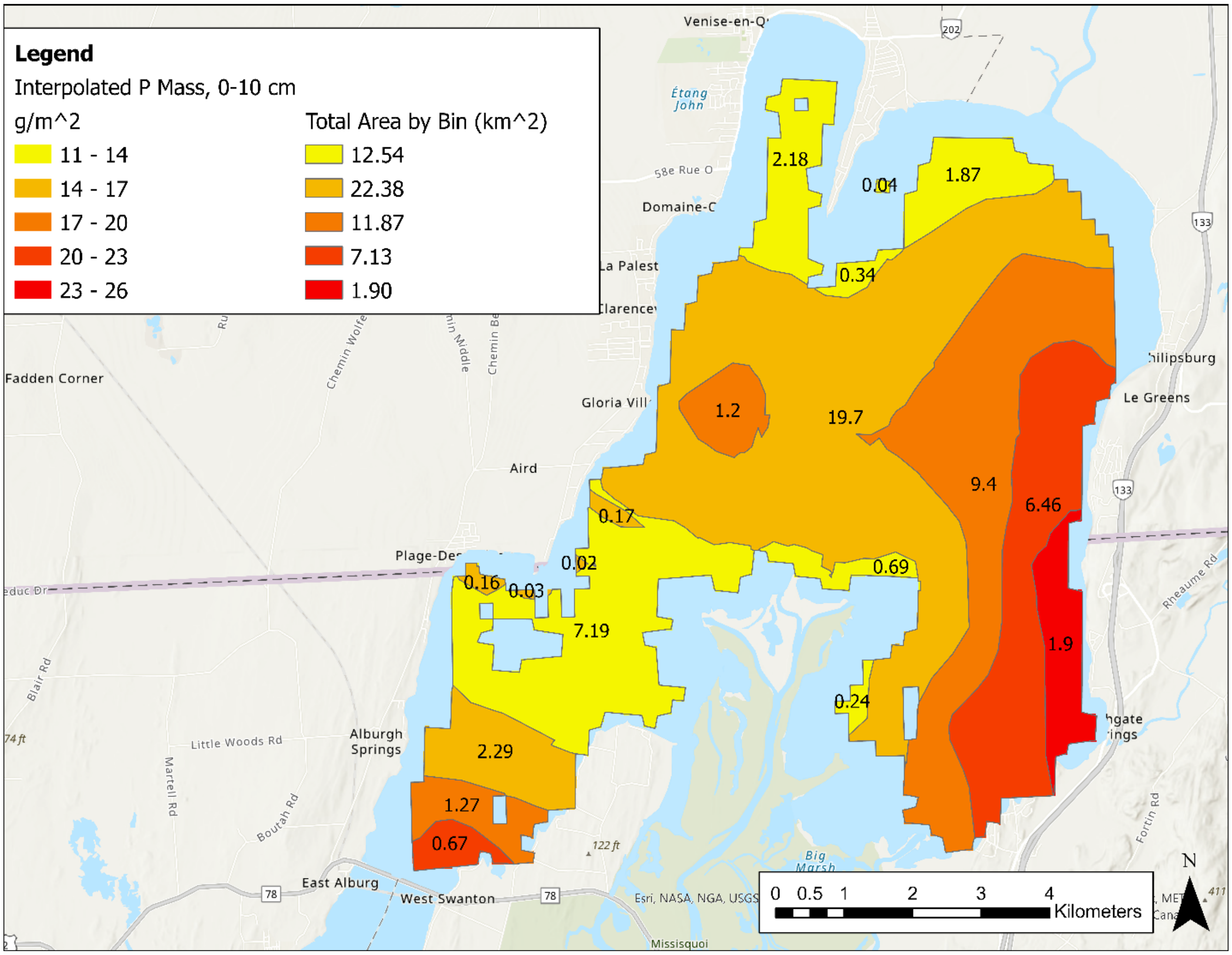

Figure 26. Redox-sensitive P mass (0-10 cm) in areas subject to anoxia.

The total mass of redox-sensitive P in the upper 10 cm of the sediment within Missisquoi Bay that could be subject to anoxia is about 923,000 kg or 923 metric tons. The mass balance analysis (*LimnoTech,* *2012*) indicated that on average about 245 metric tons of total P moved into Missisquoi Bay annually between 2001 and 2010, so the redox-sensitive P reserves in just the top 10 cm of sediment subject to possible release represent almost four times the annual total P load. The annual P load from internal sources was estimated (*LimnoTech, 2015*) at about 50 metric tons, suggesting that the upper 10 cm in the area potentially exposed to anoxia harbors over 18 years of available P reserves. As relatively little of that P leaves the bay and more sediment P is deposited each year, those reserves are increasing. If only 5% of the redox-sensitive P in the upper 10 cm of sediment potentially exposed to anoxia was released each year, the annual internal load would be 46 metric tons, close to the LimnoTech estimate.

Only the upper couple of centimeters of sediment are likely to interact directly with the water column in Missisquoi Bay. However, that thin interface stores enough redox-sensitive P to promote algae blooms. If the redox-sensitive P was distributed evenly in the upper 10 cm, the upper 2 cm of sediment in the potentially anoxic area would contain 92 metric tons, almost twice the estimated annual flux of P out of the sediment. The P mass in the upper 1 cm of sediment exposed to anoxia could be enough to account for estimated internal loading and related cyanobacteria blooms under this assumption (*Smith et al., 2011; Giles et al., 2016*).

The vertical P distribution is not even, however, and there is vertical P flux occurring within the sediment. The project team sectioned sediment cores collected for this study in 2020-2021 into the upper 1 cm, 1-4 cm, and 4-10 cm intervals (Figures 27–29). Redox-sensitive P in the upper 1 cm of sediment ranges from 0.7 to 1.5 g/m^2 with a weighted (by area) average of 1.0 g/m^2. Redox-sensitive P in the 1-4 cm slice of cores ranged from 3 to 8.5 g/m^2, with a weighted average of 4.66 g/m^2 for the 3-cm slice, equivalent to a per centimeter value of 1.55 g/m^2, which is higher than for the upper 1 cm. Redox-sensitive P in the 4-10 cm core sections ranged from 4 to 16 g/m^2, with a weighted average of 10.42 g/m^2 for the 6-cm slice and a per centimeter value of 1.74 g/m^2, higher yet than the 0-1 cm or 1-4 cm slices. This analysis suggests that the upper 1 cm of sediment harbors 56 metric tons of redox-sensitive P, enough to account for the sediment P release estimated by LimnoTech (*2012*). It also suggests that redox-sensitive P reserves increase with depth through at least 10 cm of sediment. Within the 10 cm limit cored in this study, this result is consistent with the results from the core sample tested by Ostrofsky et al. (*2020*). Ostrofsky et al. found redox-sensitive P was lower at the surface of the sediment, peaked at about 4 cm, but did not experience a substantial decline until deeper than 10 cm.

Whether the decrease in redox-sensitive P closer to the sediment surface represents movement of P into the water column from the uppermost sediment layer or a decrease in P deposition in more recent years is not known. Nevertheless, the amount of available P in the upper 10 cm is high enough to cause eutrophication problems indefinitely if not addressed by management.

The actual release of redox-sensitive P from the sediment will depend on redox potential, which is a function of chemistry surrounding oxygen availability. Free dissolved oxygen in the water slightly above the sediment is used as an indicator of redox potential at the SWI. During prolonged anoxia, after free oxygen is reduced (to H_2O), a cascading series of reactions takes place in which nitrate is converted to N_2, manganese and iron oxides are reduced to dissolved manganese and ferrous iron ions, followed by reduction of sulfate to hydrogen sulfide and carbon dioxide to methane. P complexed with iron and manganese oxides is liberated upon their dissolution. This is the reason spikes in dissolved Mn^{2+} and Fe^{2+} concentrations are reliable indicators of P release, especially in mineral rich sediments like those of Missisquoi Bay (*Isles et al., 2015; Giles et al., 2016*).

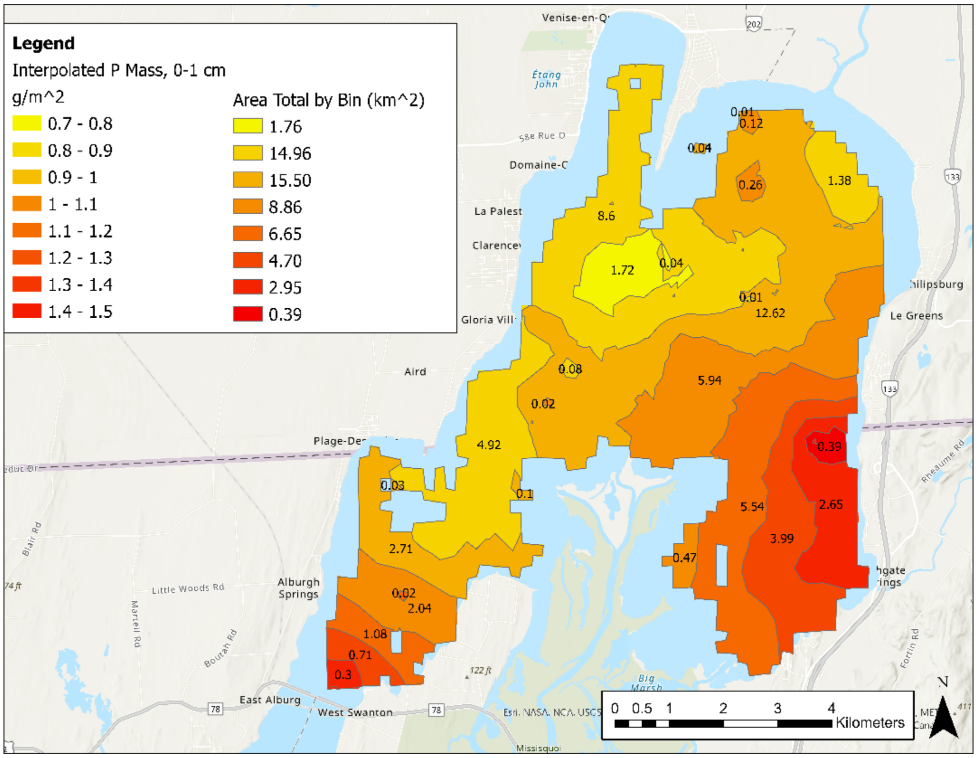

Figure 27. Redox-sensitive P mass in 0-1 cm core sections of Missisquoi Bay sediment.

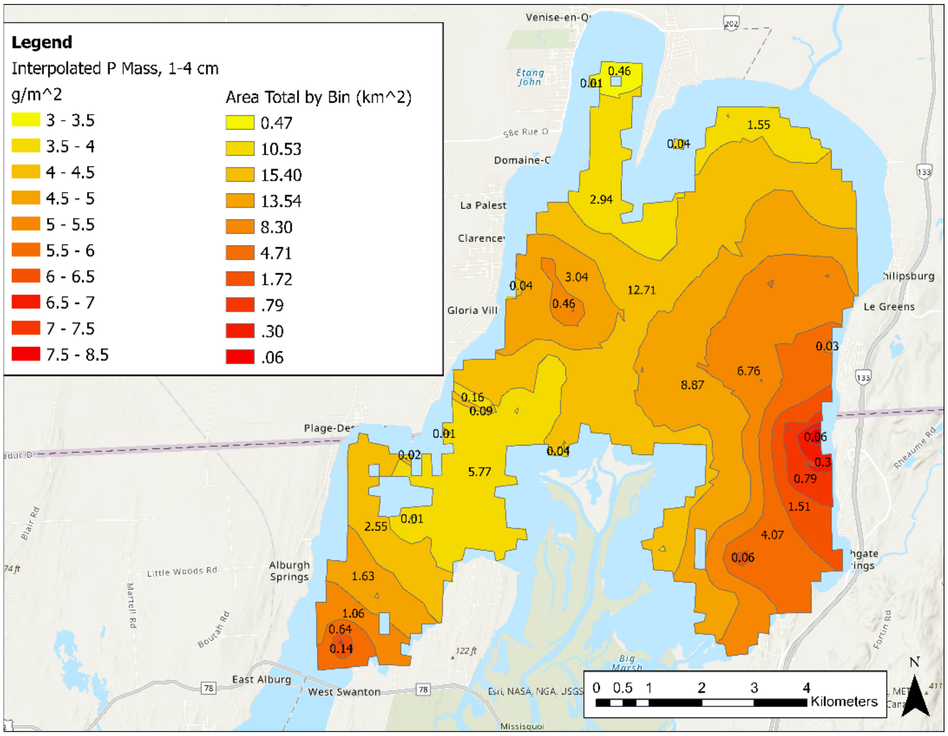

Figure 28. Redox-sensitive P mass in 1-4 cm core sections of Missisquoi Bay sediment.

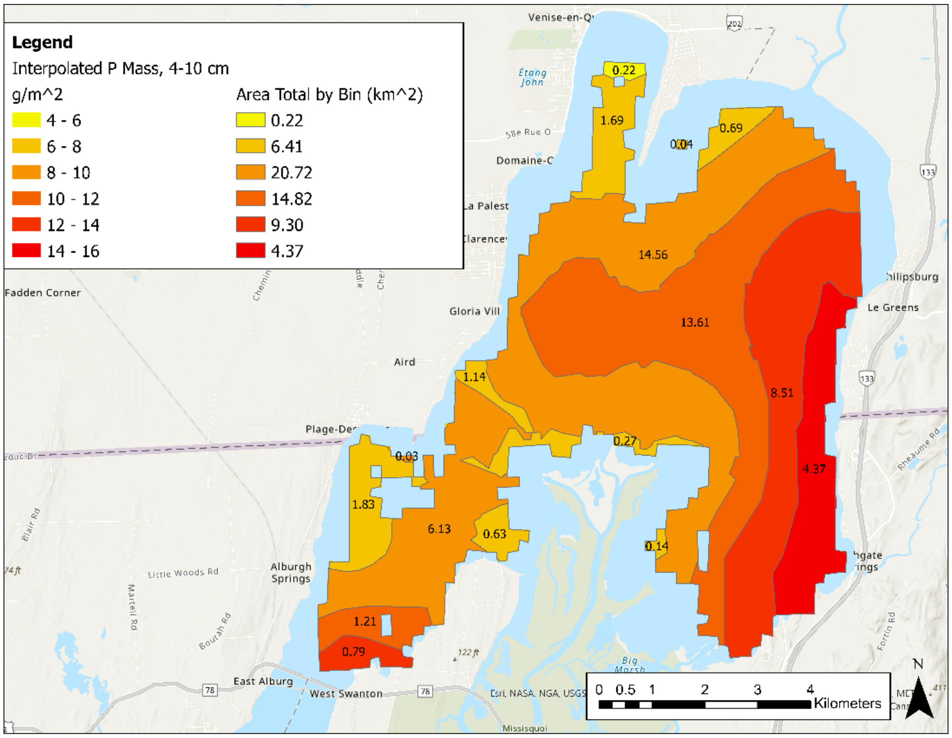

Figure 29. Redox-sensitive P mass in 4-10 cm core sections of Missisquoi Bay sediment.

Further, when oxygen is depleted the demand for oxygen may continue to rise even though the dissolved oxygen concentration cannot decline below 0 mg/L. The release rate of redox-sensitive P is therefore not constant. Some time may be required after anoxia occurs for redox-mediated P release to initiate, and the rate of release may increase with increasing duration or fluctuation of exposure to low oxygen. Areas subject to oxygen depletion more often or for longer periods may therefore contribute disproportionately, and consideration of the variation in oxygen concentrations over space in Missisquoi Bay is warranted.

The frequency and duration of anoxic conditions in the bottom water near the SWI are mainly functions of sediment oxygen demand and vertical water mixing. Mixing depends on water depth, temperature, and wind. Co-PI Marti used the calibrated Missisquoi Bay AEM3D model to simulate continuous DO concentrations in bottom water for the period 2017–2020. The duration of predicted anoxic conditions at the SWI, based on water column oxygen <3 mg/L slightly above the sediment, was highest in 2020 and lowest in 2017. The percentage of time that anoxic conditions persist ranged from 0.5% to 9.5% in July through September, based on model runs representing 2017 through 2020.

It is assumed that oxygen below the established threshold in the water column will translate into anoxia at the SWI, a reasonable assumption based on monitoring here and elsewhere, but there can be variation between oxygen concentration and redox potential that induces some uncertainty into such modeling. It would not be surprising to find anoxia at the SWI more often than low oxygen is detected above it, but the presence of oxygen will limit direct transfer of released P into the water column, as the iron or manganese from which P was released would be expected to re-precipitate and adsorb some available water column dissolved P (*Smith et al., 2011; Joung et al., 2017*). However, algae growing at the SWI could take up P released by redox reactions before it reaches the water column. Many cyanobacteria utilize this growth mode and then produce gas pockets in cells that allow filaments and colonies to rise in the water column, bringing excess P with them.

The cyanobacteria *Dolichospermum* and *Microcystis* that are known to dominate cyanobacteria blooms in Missisquoi Bay (*LimnoTech, 2012*) initiate growth at the SWI from resting stages in the surficial sediment and take up available P in surplus amounts before forming gas pockets in their cells and rising in the water column. These cyanobacteria will have ready access to redox-sensitive P before it even enters the water column. Anoxia above the SWI is not necessary, only in the upper centimeter or so of the P-rich sediment. With shallow depth, adequate light penetrates to the lake bottom to support such growth, at least before blooms become dense and restrict light penetration. This mode of bloom formation makes the internal P load even more important. Indeed, such vertical migration of cyanobacteria was observed in high-frequency sensor time series during summer in Missisquoi Bay (*Isles, 2016*).

Blooms that form from synchronous rise of cyanobacteria from the sediment surface are often short-lived in deep lakes, with mainly the nutrient reserves brought from the bottom of the waterbody to support growth. However, the average summer P concentration in the upper water column of Missisquoi Bay is sufficient to sustain algal growth for quite some time, suggesting that blooms could last for weeks or even a couple of months without additional nutrient loading from lake sediments or the watershed. The initial bloom will alter other aspects of water quality, possibly leading to a succession of cyanobacterial types, each best adapted to ambient conditions. The observed sequence of *Dolichospermum* giving way to *Microcystis* in Missisquoi Bay is a very common manifestation of this process.

5.2. Management Options

If the primary goal is to minimize cyanobacteria blooms, one can consider both directly attacking the cyanobacteria and preventing the blooms from developing. Direct approaches could involve algaecides that kill algae/cyanobacteria, flushing with extra added water that washes the bloom downstream, or circulation that disrupts the buoyancy mechanisms of at least some cyanobacteria. All are valid methods in some aquatic systems, but resumption of blooms can be expected when the action ceases. Additionally, other algae, including some cyanobacteria, may thrive; some species are resistant to common algaecides and some grow very well when the water is circulated regularly. While cyanobacteria may be reduced, overall algal abundance may remain high. Opportune timing of direct algal controls may thwart a bloom before it becomes intense, but this strategy requires frequent monitoring and highly responsive action.

In the case of Missisquoi Bay, use of algaecides would be a monumental undertaking, given the large area that might need to be treated. Copper and peroxide are the two main active ingredients in most algaecides, and while both can be used at low concentrations to control cyanobacteria in New England waters, there are still risks to non-target organisms that may make permitting for repeated additions over a large area difficult. Even if treatment was permitted, label restrictions on virtually all algaecides prohibit treating more than half the waterbody in a two-week period. Adding the essential tracking of the algae community over such a large area, this approach is not likely workable for Missisquoi Bay.

Likewise, the extensive network of pipes or tubes and extremely high number of diffusers that would be needed to guarantee adequate circulation over the whole area of the bay would represent an installation and operational challenge that would likely be considered unworkable in Missisquoi Bay. The amount of water needed to flush the bay at least once every three weeks is simply not available. Direct control of algae in Missiquoi Bay does not seem appropriate as a long-term management approach. Limiting the supply of nutrients to algae to minimize blooms in Missisquoi Bay is a much better strategy.

Algae require a variety of nutrients. While P and N are most studied, a wide range of elements are needed in finite quantities. For cyanobacteria, many of which can utilize dissolved nitrogen gas and do not need nitrate or ammonium in the water as an N source, P is more likely to control productivity. However, other nutrients can also limit cyanobacteria, most notably iron (Fe). Molot and colleagues (*2021*) have documented how internal recycling of Fe-P is a strong promoter of cyanobacteria blooms, with Fe and P dissociating and becoming available to algae when oxygen is depleted at the SWI. As redox-induced internal loading involves low ratios of N to P, cyanobacteria are further favored. While external loading of nutrients is the ultimate source of most sediment P reserves within a waterbody, the process of internal P loading from anoxic sediment is becoming recognized as a major driver of cyanobacteria blooms (*Steinman and Spears, 2020*). Control of internally loaded P is therefore likely to be essential to minimize cyanobacteria blooms.

The USEPA approved a TMDL in 2016 that calls for a 64.3% reduction in external (watershed) P loading to Missisquoi Bay from the Vermont portion of the watershed. An assumption was made that external load reduction would result in a shift from the sediment of Missisquoi Bay being a sink for P to a source and that P reserves would be gradually diminished. Simulations run for a 70-year period by LimnoTech (*2012*) suggested that with a 75% external P load reduction the water column P concentration would drop to near 20 µg/L within a decade but would not decline much further.

A follow up analysis (*LimnoTech, 2015*) indicated that following mandated external P load reduction the decline in internal P loading would be very gradual, allowing redox-sensitive P to maintain water column P concentrations near the limit for support of algal blooms for the full 70-year simulation. The P concentration in surficial sediment started at about 0.9 mg/g, consistent with current findings, and declined very slowly, in a linear manner, to about 0.7 mg/g 70 years later, nowhere near the threshold of about 0.2 mg/g below which the influence of internal P loading could be expected to diminish appreciably. This is consistent with the large mass of redox-sensitive P at sediment depths of at least 10 cm and upward migration of that P within the sediment as P from near the sediment surface moves into the water column. Exhausting the sediment P reserves will be a very slow process, well beyond the time frame of the implementation of the TMDL, even given extraordinary reductions in external loads.

Among the multiple defined basins within Lake Champlain, Missisquoi Bay and St. Albans Bay are recognized as the only basins with significant internal P loading (*USEPA, 2016*). The difficulty of addressing these internal loads was acknowledged in the TMDL. For Missisquoi Bay, the challenges associated with its large area and multinational jurisdiction were noted. If external load reductions did reduce the average summer P concentration to 20 µg/L, cyanobacteria blooms should be lessened to some degree. However, an overall external load reduction on the order of two thirds of current loading will be very difficult to achieve and will certainly not be accomplished quickly, especially with most of the target load contributed by nonpoint sources. Further, the mechanism described previously of initial benthic growth of cyanobacteria followed by synchronous rise into the water column will remain viable indefinitely. It seems very unlikely that impairments associated with cyanobacteria will be mitigated in Missisquoi Bay without directly addressing the internal P load.

While watershed management is encouraged to limit P entering a waterbody, once the P has reached the waterbody and accumulated in the sediment, an additional approach is needed. An applicable analogy is a leaky boat. Leaks should be patched to limit water accumulation in the boat but patching those leaks will not address the accumulated water, necessitating some amount of bailing. If the leaks are small, bailing out the boat will restore utility for some time. Patching the leaks is still desirable, but the boat can be used in the meantime. If the leaks are large, repair will be needed before the boat can be used. Available data for Missisquoi Bay suggest large external loads (boat leaks) that need to be addressed. However, the pattern of cyanobacteria blooms is indicative of support by internal P loading (water already in the boat), and it is likely that both watershed and in-lake actions will be needed to provide long-term relief from cyanobacteria blooms. Addressing the internal load is more likely to provide immediate relief from cyanobacteria blooms than watershed management and the duration of benefits could be years, although not indefinitely.

There are four proven ways to address internal P loading that leads to cyanobacteria blooms:

1. Dredging – removal of sediment that demands oxygen and supplies P
2. Selective withdrawal – discharge of water with higher concentrations of P, leading to eventual exhaustion of P reserves
3. Oxygenation – provision of oxygen to the SWI to minimize release of P from redox reactions
4. P inactivation – binding of P to reduce release from sediment and availability to algae

5.2.1. **Dredging**

Dredging is true lake restoration, removing accumulated sediment and setting the lake back in time. While dredging does not affect ongoing watershed inputs, it can control internal loading and minimize oxygen demand. Dredging removes sediment and the associated algal resting stages, along with a host of other contaminants that have accumulated since the waterbody was formed. It will remove minimally mobile benthic organisms such as mussels from the dredged area and change the bottom features in ways that will affect waterbody ecology for many years to come, but most of those changes may be considered to be positive (e.g., coarser sediment, lower oxygen demand, less P recycling).

Planning a dredging project is fairly involved, with an appropriate dredging feasibility study of Missisquoi Bay likely costing more than $200,000. The quantity and quality of sediment must be known, and the field and lab work would be costly. Engineering and permits add considerably to the cost. More sampling would be needed, but data from a core sample from Missisquoi Bay (*Ostrofsky et al., 2020*) suggest that the concentration of most forms of P (and especially redox-sensitive P) declines with depth and levels off at about 0.13 mg/g at depths >27 cm. The rate of decline in redox-sensitive P is lower below about 19 cm. The P concentrations in the upper 10 cm are quite high, but removal of only the upper 20-30 cm (<1 foot) of sediment would reduce redox-sensitive P availability by 70-75% based on the limited available data.

Once a dredging project is planned, actual dredging is very expensive, with a cost range of $40 to $100 per m^3 of sediment removed offered for initial consideration. There is no easy way to lower the water level enough to dredge under “dry” conditions, so hydraulic dredging (Figure 30) would be necessary. Hydraulic dredging entails pumping a slurry of sediment and water to a containment area where the sediment is dewatered by settling and the water is returned to the waterbody.

If there is any sediment contamination or if land for the containment area is not readily available, the cost can rise sharply. If the sediment is clean and there is nearby land to be reclaimed (i.e., sand and gravel pits), disposal costs can be minimized, and the cost might be near the low end of the estimated range. Yet to remove just 0.25 m of sediment from the roughly 5,580 ha area affected by anoxia and phosphorus release from sediment would cost at least $558 million and could cost $1.4 billion. While attractive on a technical level, this may not be an economically viable approach. Dredging small areas might be considered where important co-benefits are realized.

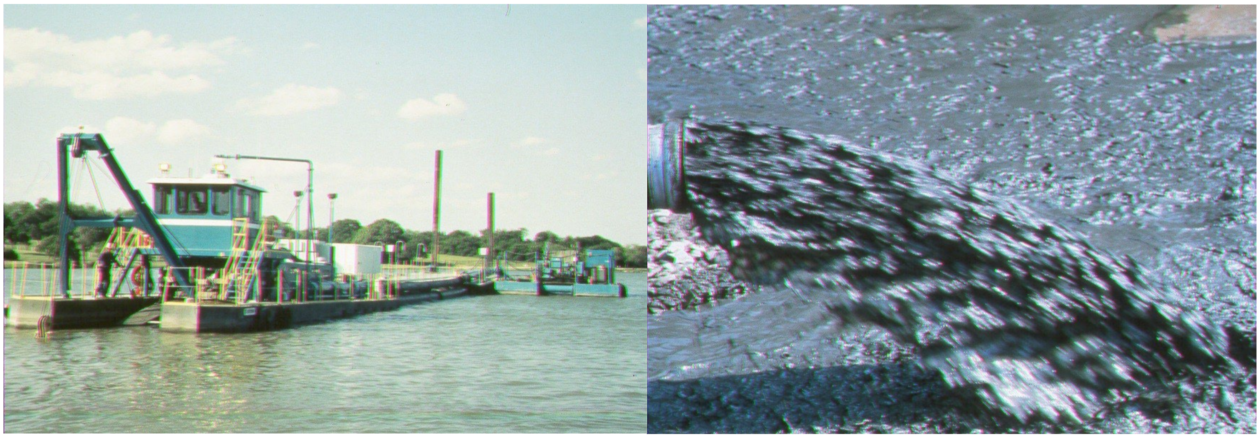

Figure 30. Hydraulic dredging operation.

5.2.2. Selective withdrawal

The normal application of selective withdrawal is to passively discharge deep water instead of shallow water during the summer (Figure 31), causing the discharge of high P water and leaving less P in the waterbody. An alternative approach is to draw a lake down shortly after stratification ends, removing high P water and letting lower P water replace it as the lake refills. Neither of these approaches is practical for Missisquoi Bay, as any water from the bay flows to the main body of Lake Champlain. Additionally, where this approach has yielded reduced P in a waterbody it has taken more than 20 years and not achieved a low enough concentration to prevent all blooms (*ME DEP, 2001; Godfrey et al., 2003; Sosiak, 2022*). Selective withdrawal does not appear to be a viable technique for P or algae control in Missisquoi Bay.

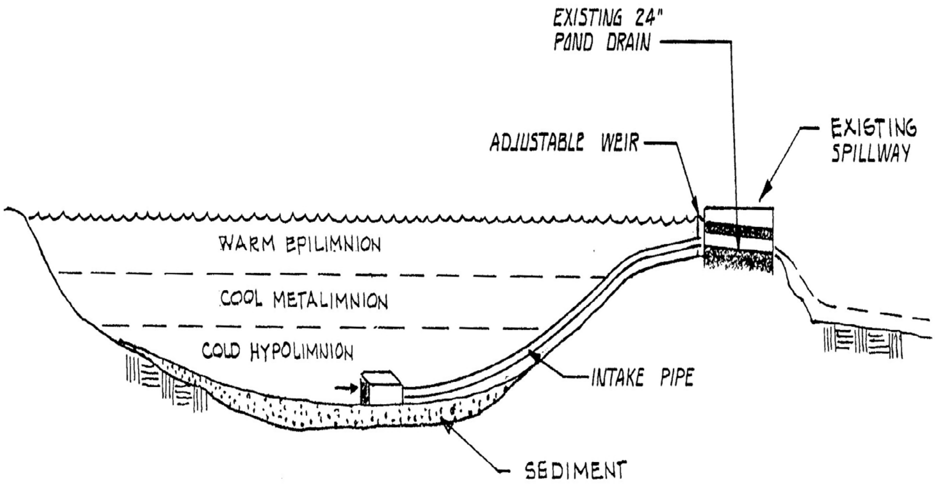

Figure 31. Schematic of a selective withdrawal system.

5.2.3. **Oxygenation**

Low dissolved oxygen is a fairly common phenomenon at the bottom of lakes as a natural result of decomposition of organic matter accumulated over many years. Even slight thermal gradients limit water mixing and the downward movement of oxygen from upper waters. Many strategies are used to promote oxygenation of lakes, several of which rely on inducing water circulation to transport oxygen to the bottom of the lake.

Artificial circulation has already been mentioned as an approach for keeping the water mixed and disrupting the water column features that best support most cyanobacteria. Circulation can also enhance oxygenation of water near the SWI. Water can be circulated by pumping or air driven means to mix the water column and distribute oxygen throughout the waterbody, without any engineered addition of oxygen (Figure 32). Oxygen can also be added in a controlled fashion to increase oxygen in bottom waters without mixing the waterbody; this is called non-destratifying oxygenation (Figure 33). A review of oxygenation and circulation by Wagner (*2015*) covers the theory and practice of these approaches to water quality management.

Artificial circulation has a long track record with some notable successes. However, it does have a tendency to maximize the availability of whatever nutrients are in the water and it is rare to eliminate all internal loading with a circulation system. As discussed previously, mixing may disrupt many forms of buoyant cyanobacteria but other algae, including some cyanobacteria, are not adversely impacted by circulation. A well-designed circulation system may reduce the average P concentration, but the increased availability of P due to complete mixing may offset that advantage. That was the experience at nearby Lake Carmi, where an aeration system reduced thermal stability but did not eliminate low oxygen and P release from sediment (*Kirol, 2023*); chlorophyll *a* concentrations and the duration of cyanobacteria blooms actually increased. Circulation should only be undertaken with sufficient safeguards to ensure that the target zone remains thoroughly mixed, and it may still require additional P reduction to achieve water quality goals.

Diffused Air Circulation

Downdraft Pump

Updraft Pump

Figure 32. Methods for artificial circulation.

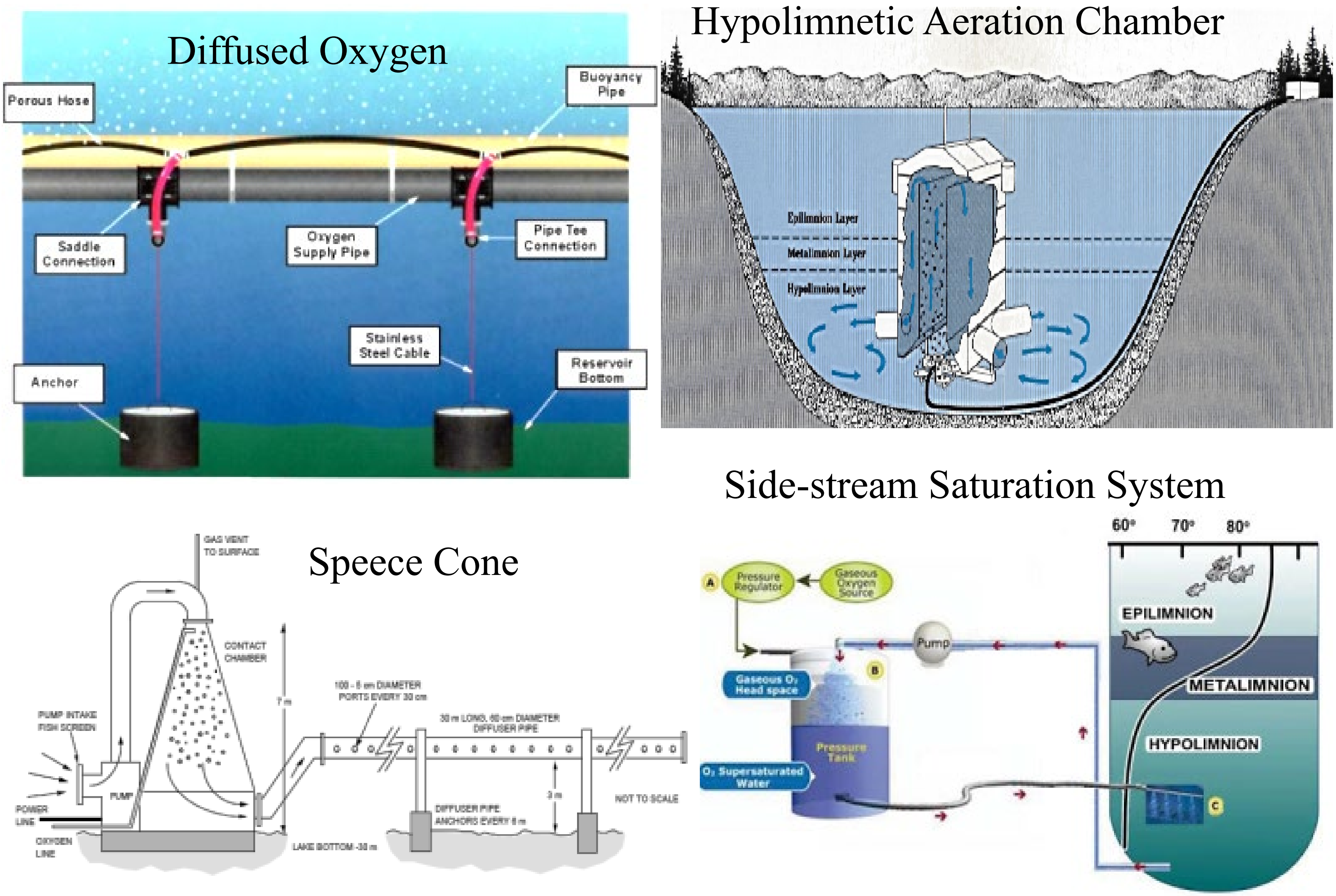

Figure 33. Methods for non-destratifying oxygenation.

As noted previously for consideration of artificial circulation for direct control of cyanobacteria, the extensive network of piping and diffusers that would be necessary to properly circulate all the water in shallow Missisquoi Bay represents a difficult challenge. The horizontal movement of water is rarely more than ten times the vertical distance water is moved, so with such a short vertical run (maximum depth of 4.3 m) a great many diffusers or pump ports would be needed to move enough water to make a difference. Whether water is moved by air bubbles (diffused air from a compressor) or by upward or downward water pumping, getting adequate areal coverage would be problematic in Missisquoi Bay. Powerful circulation may cause sediment resuspension while inadequate circulation will not solve the problem.

SolarBee (updraft) circulators were installed in St. Albans Bay of Lake Champlain as a test in 2007 but did not adequately control cyanobacteria (*VTANR, 2008*). The review of 14 updraft circulation systems by Wagner (*2015*) found that two met algae reduction targets, five showed some improvement but did not meet stated goals, and seven provided no improvement. Simply not enough water was circulated in most cases and the theory of long-distance circulation of water brought to the surface did not hold up in practice. Downdraft circulation, in which surface water is pushed to the bottom of a target zone, has a higher probability of success than updraft circulation, especially if the algae can be moved into a dark zone. However, none of Missisquoi Bay is deep enough to provide light limitation without a severe algae bloom and downdraft circulation is rarely used where the water is <9 m (30 feet) deep because sediment resuspension becomes problematic.

Circulation induced by compressed air has been applied for decades. There are multiple types of diffusers available. While the details can make a difference to performance, most relate to efficiency and maintenance needs. Air driven circulation achieved algae reduction goals about 57% of the time in cases reviewed by Wagner (*2015*) and provided partial success in 29% of reviewed cases. A minimum airflow recommendation of 1.3 cubic feet per minute (cfm) per acre has been developed for adequate circulation. However, efficiency is lost in shallow areas with decreased vertical run for bubbles and airflow of 2 cfm per acre or more may be needed for complete circulation. Of greater cost concern is the increased number of diffuser locations needed in shallow water, as horizontal mixing is proportional to vertical bubble rise distance. The network of air delivery hoses and diffusers necessary to thoroughly mix Missisquoi Bay would be extensive; no system of that size has been installed.

The cost of a destratifying oxygenation system tends to be between $1000 and $3000 per acre, with shallower systems requiring more mixing points (usually diffusers) and greater cost. Even if an economy of scale could keep the cost to $2000/ac, the capital cost would be on the order of $30 million. Operational costs could range from $100-200/ac/yr, suggesting an annual operational cost of $140,000–$280,000. Given the limitation of shallowness on applicability, effectiveness, and cost, destratifying oxygenation does not appear to be a viable approach for internal P load control in Missisquoi Bay.

Oxygenation without complete circulation is a matter of providing enough oxygen to the needed volume of water when it is needed to counter oxygen demand. Oxygenation can be accomplished by releasing tiny bubbles of pure oxygen or enriched air that are absorbed before the bubbles can rise enough to cause mixing or escape into the atmosphere. Alternatively, oxygenation can be performed in a chamber within the lake or on shore, with placement of that water in the target zone, preferably close to the sediment. Wagner (*2015*) reviewed the options and their performance in reservoirs.

Diffused oxygen systems are less expensive than chambered oxygenators but require a vertical run (water depth) of about 6 m (20 feet) to be effective. That depth simply does not exist in Missisquoi Bay.

Oxygenation within an in-lake chamber offers less of an onshore footprint, but a source of oxygen and a pump are required, and maintaining submerged components is problematic. Further, many submerged systems need a stable, hard platform, which does not exist where the soft sediment is deep. Such a system could be considered for Missisquoi Bay but would require a large capital expense.

Using floating chambers may be possible in Missisquoi Bay. Floating chambers were the original type of application of diffused oxygen systems. These systems use compressed air to move and oxygenate water in a central chamber and return flow downward through an outside concentric chamber. Such systems can be effective but are not efficient, as air contains only 21% oxygen, transfer is rarely >3% per vertical meter, and the tallest chambers are <10 m. With a maximum depth of only 4.3 m in Missisquoi Bay, oxygen transfer efficiency by this method would be very low, requiring many such units to adequately oxygenate the target zone at great capital and operating cost as well as navigational impediment.

An offshoot of the chambered approach is the LayerAir system, which pulls in oxygenated surface water and mixes it with lower oxygen deep water, creating a thermally stable and oxygenated mid-depth layer that acts as a barrier to vertical transport of available P. However, with no more than 4.3 m of depth to work with, this approach is not well suited to Missisquoi Bay.

The onshore chamber approach is often called a side-stream supersaturation system (SSS) or oxygen saturation technology (OST), as water pumped up from the bottom of the waterbody is oxygenated in a chamber to a supersaturated condition then placed back in the bottom of the waterbody. The extra oxygen, possibly 5 to 10 times the concentration the water would have naturally held at the ambient temperature, can enable enough oxygen to reach the targeted zone of the lake while moving less water. Lateral movement of dissolved oxygen is much greater than vertical movement if there is any thermal gradient at all, aiding horizontal distribution of the oxygen.

Commercial SSS/OST technologies have become available but there is still more to be learned about optimal application. Oxygenation by this approach has great potential to improve habitat as well as reduce internal loading but the technique is not yet mature. A large system was installed in Thunderbird Reservoir in Oklahoma and, after several years of adjustment, greatly improved oxygen conditions and reduced cyanobacteria blooms (*Wagner, 2015*). A number of smaller systems are currently in use with varying degrees of success. As the bottom can be blanketed with higher oxygen water, anoxia and related P release from the sediment should be prevented. Given strong lateral movement of oxygen along a concentration gradient, the piping system would not have to be nearly as extensive as for circulation systems. SSS/OST would likely be the best choice for Missisquoi Bay if an oxygenation approach is desired.

There is an economy of scale for oxygenation systems, with lower cost per unit of area addressed for larger projects, but that would not likely make such a large project financially attractive. Because an SSS/OST system would only need to be operated intermittently in Missisquoi Bay, operational costs could be lower. A sophisticated monitoring network would be needed to inform operational decisions. An automated system is possible but generating an operational cost estimate is challenging. Capital costs would be on the order of $45 million to cover the entire area subject to low oxygen, and this could not be scaled back to address only areas subject to more frequent and prolonged anoxia with reliable effectiveness. Operational cost would depend on how much oxygen was delivered over what period of time. Based on other projects (*Wagner, 2015*), an annual budget of about $2.5-3 million is suggested.

A fundamental problem with oxygenation is that while it can prevent the low oxygen conditions that lead to the release of redox-sensitive P from sediment, provision of oxygen can be expected to accelerate decomposition of organic matter and mineralization of organic P, increasing release of available P from this store. If there are adequate P binders (e.g., iron, calcium, or aluminum) present in the water, the P released by decomposition may be quickly inactivated in the presence of oxygen and there should still be a major net reduction in available P in the water column, but enough P may still be available to support algae blooms. Operated successfully, an SST/OST system should substantially reduce internal P loading from sediment in Missisquoi Bay. However, development of anoxia can be rapid (<4 days) when a SSS/OST system shuts down, and continuous maintenance of a system large enough to handle Missisquoi Bay would be very difficult.

While oxygenation strategies offer some potential to control internal P loading, flexibility of operation, and additional benefits of increased oxygen to enhance habitat, the cost and logistics of making this a reliable approach for Missisquoi Bay are not favorable.

5.2.4. **Phosphorus inactivation**

P inactivation involves the binding of phosphorus by added compounds that make it unavailable for uptake by algae. P inactivation can be used three ways: to treat incoming water high in phosphorus, to strip phosphorus from the water column in a waterbody, or to bind P in surficial sediments and make reserves less susceptible to release under anoxia. All three modes are applicable to Missisquoi Bay but the focus here is on inactivation of surficial sediment P. As watershed management proceeds, some consideration of the use of dosing stations to improve incoming water quality might be warranted, but that is beyond the scope of this project.

Aluminum has been the phosphorus binder of choice in New England for the last 30 years. Aluminum sulfate can be applied by itself where alkalinity is high, but in most cases sodium aluminate is applied with the aluminum sulfate to minimize depression of pH and increased toxicity during application. Polyaluminum chloride (PAC) is effective and may be preferred for inflow and water column treatments, as it is a less harsh chemical, has less impact on pH, and is easy to apply, but it is more expensive than alum or aluminate per unit of aluminum applied. There is another binder that has been used in recent years called Phoslock, which is bentonite clay impregnated with lanthanum. It has been effective in many European and Canadian treatments, but the cost is higher than for a comparable aluminum dose. Calcium has been used in some high pH systems where it will precipitate, but is not applicable in most of New England where the pH is lower.

Treatment is normally done by barge with a liquid slurry (Figure 34). The dose necessary to inactivate all possible available P in sediment is a matter of both the redox-sensitive P concentration and other sediment constituents that may compete with redox-sensitive P for binding sites on the applied binder compounds. This is an area of current study that has some degree of uncertainty attached to it. Phoslock tends to be more specific for P, requiring a lower product to P ratio by mass, but has so far still been more expensive than aluminum. The aluminum to phosphorus ratio (Al:P) necessary for effective inactivation varies inversely with P concentration (*James and Bischoff, 2015*). Usually, a dose of aluminum that is 10 to 20 times the target concentration of P is applied. For sediment P concentrations like those encountered in Missisquoi Bay, an Al:P ratio no greater than 10 would be likely.


Aluminum application

Phoslock application

Aluminum product delivery and storage

Inlet dosing station

Figure 34. Methods of phosphorus inactivation.

A lab assay has been developed to allow direct measurement of P binding by Al additions. For a selected subset of Missisquoi Bay sediments those assays suggest there is a typical response curve with diminishing returns on P inactivation as more aluminum is added (Figure 35). Although there are other considerations that include the area to be treated and the relative importance of the internal P load, a common inactivation target is to reduce the redox-sensitive (BD-extractable) P concentration to <50 mg/kg. That level is achieved at an aluminum dose of 75 g/m^2 for four of five tested samples, with the fifth having a seemingly anomalous result at the 75 g/m^2 aluminum dose.

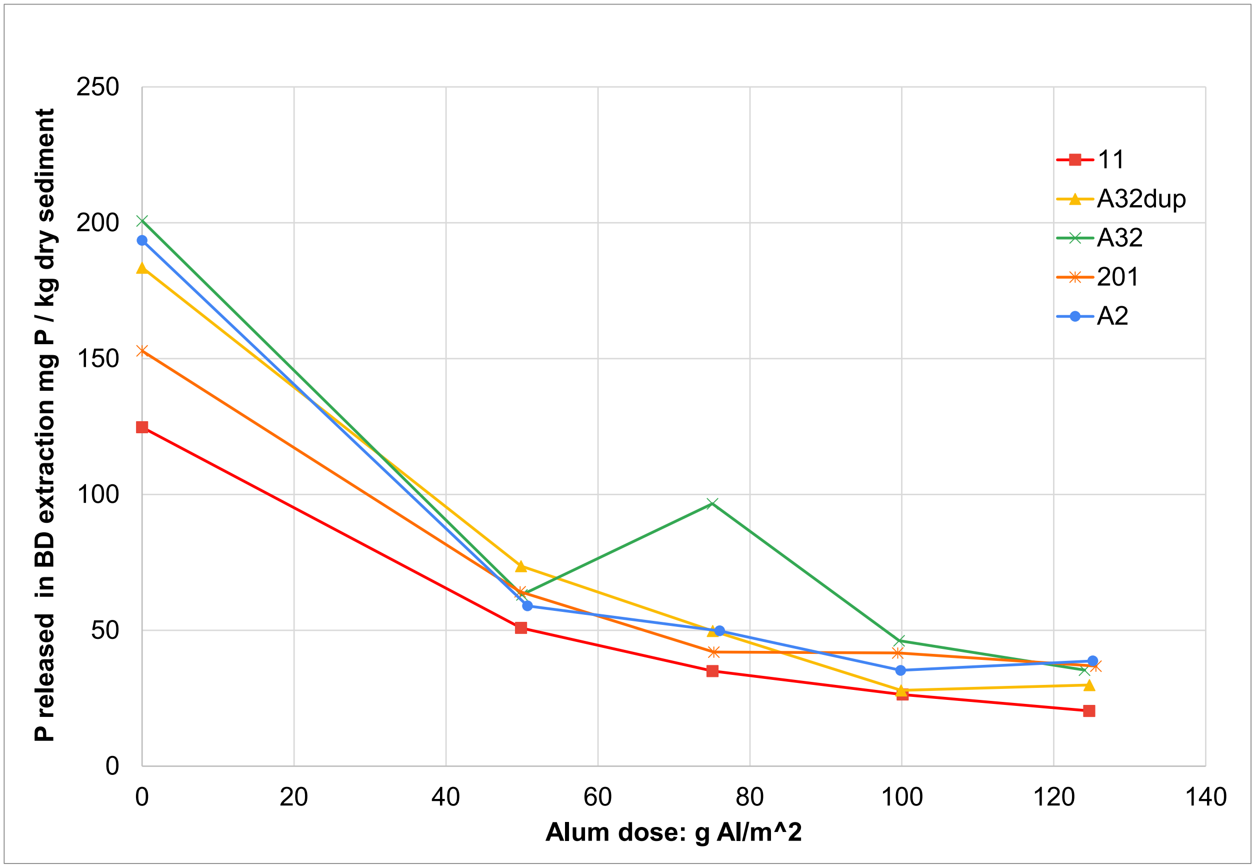

Figure 35. Phosphorus inactivation assay results for Missiquoi Bay sediment.

Successful aluminum treatment is a function of supplying an adequate dose to the appropriate treatment area. For sediment P inactivation, it is generally acknowledged that the targeted treatment area should be the area of sediment that can experience anoxia, which facilitates the release of redox-sensitive phosphorus. This zone is delineated by making oxygen measurements as close to the sediment as possible. Sediment P inactivation by treatments targeting the surficial sediment can be a sequential, additive process. It is only necessary to inactivate the P in the upper 1-2 cm of most sediment to get immediate and acceptable results, but it is necessary to inactivate P in deeper sediment to maintain those results, as redox-sensitive P from deeper in the sediment will migrate upward over a period of years.

Treatment zones are usually too deep (>4-5 m) for wind action to have much impact on surficial sediment after treatment, but the process has been found to be effective in shallower areas as well. It is a common misconception that the floc that forms and settles during an inactivation treatment is lying on top of the sediment and can be redistributed. After a few weeks it congeals with the surficial sediment (the target zone is usually not deeper than the upper 10 cm of sediment) and there is little movement caused by wind. In lakes with any major depth and slope, soft sediment may focus into deeper water, but Missisquoi Bay does not fit that profile. Even if wind and waves manage to resuspend some inactivated material, the suspended sediment P remains inactivated. The concern has always been that sediment not inactivated by treatment might be exposed. Experience in New England lakes does not suggest that this is a significant issue and a published paper on treatment of Grand Lake St. Marys in Ohio (a large treatment of a shallow lake) did not find significant aluminum outside the application area (*Welch et al., 2017*).

P inactivation treatment has also been found to produce rapid benefits in lakes despite ongoing high external loading, with longer lasting results than might be expected given the types of P sources (*Brattebo et al. 2017*). Much of the external P load arrives in forms not readily useable by algae and must be acted upon by in-lake processes before that P is accessible. Additionally, the N:P ratio from many external loading sources is much higher than for internal loading and does not favor cyanobacteria in the way that internal P loading does.

P inactivation has gained popularity in recent years, owing to substantial successes in treatments of many waterbodies (*Huser et al., 2016; Wagner, 2017*). The process is very flexible, allowing treatment of sediment, the water column, or inflows as often as necessary at a cost lower than for competing approaches. The duration of benefits depends on external P loading rates and the upward migration of P from deeper sediment that was not inactivated. For surficial sediment inactivation, application of aluminum products has provided improvement for at least 6 years in shallow, unstratified lakes and for 21 years, on average, in stratified lakes (*Huser et al., 2016*). Missisquoi Bay would more closely represent the unstratified lake situation, but a longer duration of benefits is possible with adequate treatment. Cyanobacteria blooms have been reduced or eliminated in nearly all P inactivation treatments, and those with lesser success invariably result from inadequate dosing or very high ongoing external inputs. A distinct advantage of P inactivation is that rapid and impressive results can be achieved with even a partial dose, as the most available P is right at the sediment surface and inactivation of that P will stop redox-related internal P loading until P from below the inactivation zone migrates upward. If sediment P is the dominant source of P for cyanobacteria, especially those initiating their growth cycle at the SWI, blooms will be prevented. It is more effective to add a lower dose over a larger area than to apply a higher dose to a smaller area. The higher dose maximizes longevity, but the lower dose will be, at least temporarily, effective wherever applied. The target depth of sediment to be treated depends on the distribution of P over depth; 10 cm is a typical maximum target depth. Based on the recent data developed by the project team, cyanobacteria are likely to be controlled in Missisquoi Bay with treatment of as little as the upper 1 cm of sediment, although the duration of control might only be a couple of years.

The size of the target area in Missisquoi Bay is the main impediment to P inactivation. Treatment of more than 40 ha (100 acres) in a day by a barge is unusual, although multiple barges could be employed. It would take many months to complete a full dose treatment in Missisquoi Bay. Spring is the preferred time for treatment, providing benefits in the ensuing summer, but complete treatment at full dose could not easily be done in a season. Treating just part of the contributing sediment area is possible, but untreated areas can be expected to continue to support cyanobacteria and the degree of control, while likely incremental, may not be linear. If less than the entire contributing sediment area is treated, the target zone should be based on the probability of exposure to low oxygen, with those areas experiencing more anoxia at the SWI given higher priority. However, even the shallower areas can contribute P to a significant degree (*Tammeorg et al., 2020*) and the recommendation to apply a lower dose over a larger area is appropriate.

While subdividing the aluminum dose over time and space appears necessary and appropriate for internal P loading control in Missisquoi Bay, options for treating at the full dose were examined for costs and logistics with the help of SOLitude Lake Management. If the entire 5,580 ha (14,000 ac) area in Missisquoi Bay considered to release P in response to low oxygen was treated at a dose of 165 g Al/m^2 (10 X weighted average redox-sensitive P in 0-10 cm sediment depth over whole affected area), the cost would be on the order of $100 million and it would likely take more than two years to perform the treatment. If that same area was treated at a dose of 75 g Al/m^2 (the dose suggested by lab assays, Figure 35), the cost would be expected to be no more than $60 million but it would require more than a year to complete the treatment.

Modeling scenarios were developed under which smaller areas than the whole 5,580 ha contributory zone would be treated to determine how much benefit could be achieved (Scenario 3). For the minimum 1,319 ha (3,300 ac) area with the highest frequency of low oxygen at the SWI, the cost of a 75 g/m^2 treatment would be $12.4 million and treatment would take about 3 months. For an intermediate 3,381 ha (8,450 ac) area with moderate exposure to low oxygen, the cost would be $31.5 million and treatment would require 220 days. Unfortunately, neither of these scenarios achieved the target P or chlorophyll *a* concentrations in model runs, translating into a major expense for relatively little gain. As already stated, better results are expected with a lower dose treatment over a much larger area. The cost would be more over an extended time period but would be less for each round of treatment.

Inactivation of the upper 1-2 cm may provide benefits for only several years, given upward migration of redox-sensitive P from below. Yet the improvement would be immediate and if enough area was treated achievement of at least the chlorophyll *a* target appears possible based on the modeling, even without substantial reductions from the watershed. Achieving adequate control of external loading is expected to require more than a decade, but cyanobacteria blooms could be prevented in the interim with sequential, lower dose treatments with aluminum to the entire 5,580 ha target area. Even with a lower dose, it is not possible to treat the whole area in a season and the cost is substantial, but the area could be divided into four roughly equal areas and treated on a rotating basis, one quarter each year, to get internal loading under control and keep it under control while the watershed work progresses.

Working with a dose of 20 g/m^2 and four areas of 1,500 ha (3,750 ac), each treated once every four years for three cycles (Scenario 4), the annual cost would vary between about $4 million and $5 million with a total 12-year cost of about $52.3 million (Table 13). Each treatment could be completed in about 42 days, making late spring treatment feasible to enhance conditions each summer. The quarters could be split along the international border for permitting simplicity and could be treated in whatever order was most expedient, as long as all four quarters are treated before the first one is retreated.

A permutation of this approach would be to treat the target area in halves (3,000 ha per year), probably still divided at the international border, with two years of treatment and then two years off. Treating half the target zone would require 80 days and over the 12-year program would produce slight savings over treating the target zone in quarters; the total cost is estimated at just under $50 million. Since it would take four years to reach a level of full benefit with the quarter approach, starting by treating each half of the target area in years 1 and 2 would accelerate benefits, after which treatment by quarters could proceed starting in year 5. Monitoring would inform both treatment frequency and dose as the program proceeds.

Table 13. Cost of sequential aluminum treatments at 20 g/m^2 over 1,500 ha per year.

Year	Chemical Cost ($)	Application Cost ($)	Total Cost ($)*	Days of Application
2026	2,400,000	1,500,000	3,900,000	42
2027	2,448,000	1,530,000	3,978,000	42
2028	2,496,960	1,560,600	4,057,560	42
2029	2,546,899	1,591,812	4,138,711	42
2030	2,597,837	1,623,648	4,221,485	42
2031	2,649,794	1,656,121	4,305,915	42
2032	2,702,790	1,689,244	4,392,033	42
2033	2,756,846	1,723,029	4,479,874	42
2034	2,811,983	1,757,489	4,569,472	42
2035	2,868,222	1,792,639	4,660,861	42
2036	2,925,587	1,828,492	4,754,078	42
2037	2,984,098	1,865,061	4,849,160	42
Total	32,189,015	20,118,135	52,307,150	504

*assumes 2% increase in chemical & application costs per year

5.2.5. **Additional P inactivation considerations**

If an alternative P binder is preferred, the use of the product Phoslock could be considered. This lanthanum impregnated bentonite clay is reported to have a higher specificity for P and the added clay may reduce the expression of oxygen demand by organic sediment to some degree. It has less potential for toxicity during application than aluminum, but since it is not a coagulant, it will not remove particulates and associated P from the water column. Phoslock also tends to be more expensive than aluminum. Both aluminum and Phoslock have been used sequentially in European treatments (*Lurling et al., 2020; Cavalcante et al., 2021*) in a process called “floc and lock”, whereby the aluminum is used for initial water column stripping and sediment binding and the Phoslock provides a seal that minimizes P release for an extended time period.

There are additional products on or coming to the market for the purpose of inactivating P. These include EutroSorb, a product from SePRO with proprietary ingredients that has enjoyed some success in storm water treatment situations. Any product that permanently binds P would be of potential use, but for a project of this magnitude the emphasis should be on reliability.

Impacts to aquatic systems from P inactivation can be positive or negative. The primary expected positive result will be reduced frequency and severity of cyanobacteria blooms due to reduced internal P loading. The negative impacts relate mainly to potential toxicity during treatment (mainly for aluminum) and smothering of minimally mobile benthic fauna with the added material. The possible negative impacts are temporary, and some are avoidable.

Treatment with aluminum compounds can alter water quality in several ways. Changes in pH are of greatest concern to aluminum toxicity and can be managed during treatment to maintain a pH between 6 and 8 standard units. This is now standard practice and there has been no obvious toxicity in any New England treatment in over two decades as a result.

For higher dose treatments, simultaneous application of aluminum sulfate (alum) and sodium aluminate (aluminate) is typically performed, usually at a volumetric ratio close to 2:1 (alum to aluminate). This balances the effect of each chemical on pH and keeps it in the normal target range of 6.0 to 8.0 standard units. If the pH is high or low at the start of treatment, that ratio can be altered to drive the pH into the desired range. This is largely a concern in lakes with low alkalinity, which makes them prone to substantial shifts in pH with addition of aluminum products, or lakes with algae blooms at the time of treatment where pH has been elevated by photosynthetic activity. Alkalinity in Missisquoi Bay is around 40 ppm, so lower doses of aluminum in any product form are not likely to shift the pH by much. As long as the pH is <8.0 standard units at the start of treatment, use of alum alone in Missisquoi Bay at the suggested dose of 20 g/m^2 should not unduly shift the pH. The use of alum vs aluminate does not greatly affect the cost of treatment; the cost of alum is less than that of aluminate but the aluminum content of aluminate is higher. Application of the extra alum volume needed to reach the target dose increases labor costs, offsetting lower unit cost for alum over aluminate.

The USEPA has developed a software tool for calculating how much aluminum can be applied at one time without causing toxicity. It incorporates information for pH, hardness, and dissolved organic carbon and provides estimates for acute and chronic thresholds. It does not consider all toxicity factors and appears very conservative; calculated limits are routinely below levels applied in past treatments that have not produced any observed toxicity. VTDEC has been discussing how best to apply this tool and has thus far taken an equally conservative approach. This could reduce the dose that could be delivered at any one time, but with such a large area to treat this should not be a major cost factor unless the instantaneous dose becomes too small to be effectively delivered by the available equipment. A larger area could be treated each day with a lower dose, with repeated treatment until the target dose is reached.

Aluminum compounds contain other elements that will increase conductivity in the receiving waterbody, including sulfates from aluminum sulfate, sodium in sodium aluminate, and chloride in polyaluminum chloride. The conductivity change induced by an aluminum treatment is usually <50 µS/cm and diminishes over successive flushings of the waterbody. No biotic impacts have been detected from any treatment as a consequence of conductivity change.

An aluminum treatment will coagulate and clear the water column of many particulates. Total suspended solids will be reduced, and clarity will increase during an aluminum treatment. Where the particulates are resuspended sediment, the effect may be temporary, as wind can stir up more sediment, but the congealing effect of aluminum on particles can limit resuspension by wind to some degree. Where the particulates are algae, there should be a sustained reduction, as algal biomass production is depressed by lower P availability. Aluminum treatments do not sterilize a waterbody, however. P is reduced but not eliminated and the N to P ratio is increased, which favors algae other than nitrogen-fixing cyanobacteria. These algae groups tend to be more edible, potentially leading to continued overall system productivity without greater standing crops of algae.

The floc that forms in the water column will settle in a matter of hours and form an initial coating on the bottom. In treatments with large doses the floc can be several inches thick and benthic invertebrates can be smothered. Studies on Cape Cod did not find any such mortality for mussels (*Nedeau, 2011*), but chironomids and oligochaete worms that often inhabit the low oxygen sediments can be smothered. Yet even where benthic invertebrates are impacted, recovery has occurred within a few years and the new assemblage has been considered an improvement (*Smeltzer et al., 1999*).

The settling of the floc sometimes removes zooplankton from the water column. Recovery could take from a season to a year, leaving planktivorous fish with fewer food resources. The combination of fewer zooplankton and benthic invertebrates can create some food stress on fish that depend on those resources. Reduced growth of planktivorous/benthivorous fish was observed after aluminum treatment of a Vermont lake (*Smeltzer et al., 1999*) for three years after treatment with gradual recovery of growth rate.

No negative impact on aquatic plants by P inactivation treatments has been detected. If water clarity is improved, there may be an expansion of submerged aquatic plant growth.

Permitting any environmental project of this magnitude can be complicated and protracted. International jurisdiction dictates that two completely separate permitting efforts will be needed, one in Vermont and one in Quebec. Multiple processes are likely to be involved in each case, with water quality impacts, biotic impacts, and other sensitive resource considerations needing to be addressed. Vermont is changing the way it permits P inactivation, with an apparent shift to treating aluminum application under discharge permitting regulations and using the new USEPA aluminum toxicity estimation tool in a Vermont protocol intended to be protective of biotic resources. There will undoubtedly be issues to resolve with this new approach, although other states have successfully implemented similar approaches. In addition, determining the acceptability and permit processes for P inactivation in Quebec is outside the scope of this project. If P inactivation is to be implemented, emphasis should be placed on determining permitting needs.

5.3. Management Conclusion and Cost Comparison

While removal of high P sediment from Missisquoi Bay would likely be the most effective way to address internal loading, and oxygenation could provide additional habitat benefits in surficial sediments, P inactivation provides the lowest cost and most flexible internal load control method. P inactivation can be performed with limited and mostly temporary risk to aquatic biological resources. The Missisquoi Bay AEM3D model results indicate that the entire area subject to possible low oxygen (5,580 ha) should be treated to achieve the desired chlorophyll *a* concentration target and minimize cyanobacteria blooms. Yet benefits should accrue rapidly with sequential treatment of smaller target areas and treatment of half to a quarter of the target zone each year with a dose near 20 g/m^2 could greatly improve conditions while watershed management proceeds. A flexible 12-year treatment program has been derived that, along with a 4% reduction in external P loading annually, is expected to meet both P and chlorophyll *a* targets.

Cost is a potentially large impediment to rehabilitation of Missisquoi Bay. The relative costs of the potentially effective options (Table 14) suggest that no solution will be inexpensive. Oxygenation might have the smallest capital cost, but an additional ~2.8 million dollars would be needed in operational cost per year, quickly exceeding P inactivation costs. Further, the operation of an oxygenation system in shallow Missisquoi Bay may require additional controls, most notably an automated sensor and operation system that is not part of the anticipated cost. Finally, oxygenation would not be expected to provide more than a 75% reduction in internal loading, as mineralization of organic P will offset some of the decrease in redox-sensitive P control.

Table 14. Probable cost to address internal P loading over a 5,580-ha area of Missisquoi Bay.

Methods	Applicable Units	Cost Range ($)/Unit	Probable Cost to Address 5,580 ha ($ million)	Notes
Dredging (removing 0.3 m)	cubic meter	40-100	558-1,400	5,580 ha X 0.25 m = 14 million m^3
Side-stream saturation oxygen addition	hectare	7,500-10,000	42-56	Operating cost of about $2.8 million ($500/ha) per year not included
P inactivation by aluminum	hectare	9,000-9,500	50-53	Assumes one quarter to one half of target zone treated at any one time; 12-year program

Dredging is the most expensive approach but may provide benefits for the longest time. However, the impacts of the process may complicate implementation beyond the cost and the redox P in the sediment that would be exposed is not negligible. Dredging can be expected to reduce internal P loading by up to 80% but the duration of benefits will depend on watershed management progress.

P inactivation carries the lowest combination of capital and operational costs and would be expected to reduce internal P loading by as much as 90%. The duration of benefits is uncertain, with the analysis of Huser et al. (2016) suggesting that 6 years of control is typical in shallow waterbodies like Missisquoi Bay. Applied doses and ongoing external loads vary greatly among assessed lakes, however, lending substantial variability to any evaluation of duration of benefits. Yet application of P inactivation at a much lower dose than necessary to maximize benefit duration would provide immediate improvement and allow an empirical evaluation of benefits under the complicated scenarios of internal and external loading in this case.

Inactivating the redox-sensitive P in only the upper 1-2 cm of sediment would require an aluminum dose of about 20 g/m^2 and would counter the estimated annual internal P load for several years. Such a treatment could be performed for about $2,700/ha, about $15 million for the 5,580-ha zone believed to be contributing to the internal P load. A wide variety of treatment options representing combinations of area and dose are possible, informed by model predictions and potentially providing immediate improvement even with ongoing external loading. Treating one quarter of the target zone each year for three cycles (12 years) with an annual inflation adjustment would cost about $53 million and would be expected to minimize cyanobacteria blooms and achieve the target chlorophyll *a* of 20 µg/L after the first cycle. Such treatment could be accomplished with 42 days of treatment per year, most likely in late spring.

Treating half of the target zone in a year would accelerate achievement of the chlorophyll *a* target and should allow two years of inactivity after two years of initial treatment. This would result in treatment in 6 out of 12 years with about 80 days of treatment needed for each half of the target zone. A total cost of slightly less than $50 million is estimated for this 12-year program, slightly lower than for the annual treatment of one quarter of the target area as a consequence of reduced labor costs. Treating the target area in halves at the start of the program and then shifting to treatment of one quarter of the area annually, as needed, could minimize cyanobacteria blooms quickly and allow the greatest flexibility in maintaining desired conditions through the remainder of the program.

Permitting is almost as big a factor as price in moving this project forward. Uncertainty in how Vermont will permit P inactivation projects going forward and approval processes across international boundaries are both concerns. Permitting processes seek to protect resources and ensure that proposed projects do no harm but are not set up to solve environmental problems; trade-offs are not necessarily acceptable. While action in only Vermont or Quebec is possible with some benefit, it will be necessary to take action in both countries for lasting and maximal benefit.

6. Conclusions

The combination of comprehensive environmental monitoring data analysis coupled with many simulations of our AEM3D model of Missisquoi Bay enables us to make a number of conclusions related to: 1) the nature and drivers of internal phosphorus loading in Missisquoi Bay, 2) the role of internal P loading in the occurrence of cyanobacteria blooms, and 3) assessing the impact and potential feasibility of an intervention aimed at suppressing the internal loading of legacy P. As other studies have previously demonstrated, our data suggest the dominant mechanism responsible for internal P loading in Missisquoi Bay is the reductive dissolution of redox-sensitive Fe and Mn minerals upon which legacy phosphorus has adsorbed. Thus, loading, versus accumulation of P in Missisquoi Bay sediment, is driven by the transient occurrence (or lack thereof) of low oxygen conditions around the SWI that can trigger such reactions.

Because of Missisquoi Bay's shallow depth and large surface area, wind is the primary driver of the occurrence and duration of low oxygen conditions in the summer–fall bloom season, and thus internal P loading (as opposed to seasonal turnover dynamics typical of deeper lakes). Missisquoi Bay has a very low threshold for wind to mix, as evident by the frequent mixing events captured within our high-frequency, multi-year dataset from the HFB. Yet due to MB's relatively high sediment oxygen demand in summer, low level and brief stratification under calm winds can cause low oxygen conditions to rapidly develop that trigger internal P loading. Indeed, in this study we were able to leverage high-frequency monitoring data to determine when to collect spatially distributed samples to examine the spatial extent of internal loading during these highly transient events. During the two August 2021 low SWI oxygen excursions that we sampled, signals of internal loading were detected in different regions of the bay. In one instance, loading appeared hyper-local in the one region of the bay in the lee of the dominant southwest summer wind. Conversely, the larger and more prolonged event manifest in over half of the bay, and elevated concentrations throughout the bay (with minimal riverine input) suggest that this event impacted the entire bay's P inventory. These data, coupled with model simulations of low DO, indicate that most of the bay's sediments can be exposed to low DO conditions and thus contribute to internal P loading. Furthermore, while there were hot spots of high concentration and mass of redox-sensitive sediment P within the bay, all of the sediment cores collected across the bay were well above a concentration that promotes an internal loading problem. Probably the most significant conclusion derived from our geochemical data is that due to the wide distribution of lake bottom that can be exposed to low oxygen conditions, coupled with ubiquitous high concentrations of redox-sensitive P in the sediments of the bay, an intervention aimed at suppressing internal P loading in the bay would need to target almost the entire bay irrespective of approach.

The monitoring data also allowed us to develop and enhance our process based computational model of the Missisquoi Bay system (AEM3D), which enabled us to further examine the role internal vs. riverine P loading plays over time with various external and internal P loading reduction scenarios. We could then examine how reductions in either or both loading mechanisms impacted water quality in the context of the TMDL and the occurrence of cyanobacteria blooms over time. A key conclusion of this modeling work is that while very aggressive reductions in external loading will be critical to reach the TMDL P target and suppress the build-up of legacy P in the bay's sediment (the origin of the internal loading water quality issue), those external changes will have minimal impact on the occurrence and severity of cyanobacteria blooms. This is because most of the external loading of phosphorus occurs in the shoulder seasons, particularly early spring and late fall, when water is colder than optimal for cyanobacteria growth and the residence time of riverine dissolved P in the bay is short (often on the order of days). Conversely, internal loading is the dominant source of P when the water is warm and conducive to blooms, and the residence time of P in the bay is also longer due low riverine flow and limited exchange with the Inland Sea. As such, when we implemented scenarios that included internal P loading reductions, this facilitated a pronounced decrease in summer cyanobacteria bloom severity. The extent of that impact varied most on treatment area and duration**.** The model also further supported the geochemical data-based conclusion that internal loading would need to be addressed in most of the bay rather than select hot spots to achieve bloom suppression goals over time, with reapplication until full external load reduction targets are reached. Ultimately, a key take home point from the modeling is that by implementing an internal loading suppression approach (assuming that it is effective at 90% internal P reduction), the bay would have almost instantaneous improvement in water quality, particularly with respect to blooms. This notable improvement could be achieved as the agencies continue to work towards achieving the targets set forth by the TMDL in the bay's watershed, albeit at high cost.

The particularly large scale of the pollution problem in MB presents many challenges to successfully implementing and realistically paying for suppression of internal P loading. While dredging would likely be highly effective, it is also cost prohibitive and could come with substantial ecological costs due to disturbance. Other common approaches involving water column mixing and/or oxygenation would face technical and cost hurdles to implementation that make them similarly infeasible and less likely to succeed. Hypolimnetic water removal would not be feasible given the dynamic nature of the system coupled with the fact that P enriched water would simply be transferred to other lake segments that are also threatened by eutrophication. Thus, we concluded that P inactivation via chemical amendment of the sediment is likely the only potentially feasible approach to mitigating internal loading in this particular lake system with current technology. Both the scenario model results produced in this project and latest practice in lake management suggest implementation of low-rate, partial-area P inactivation treatments, performed sequentially across the entire internal P contributing area of MB, could provide the highest water quality benefit with minimal potential adverse impact on the ecology of MB.

Given the polymictic condition of MB and high level of riverine P loading, individual low-rate treatments would not last particularly long in the bay, with reapplication required every ~4 years until the TMDL-mandated watershed reductions are achieved. Thus, this treatment program would represent a sustained cost to taxpayers (in both the U.S. and Canada). Furthermore, there would certainly be significant regulatory and public messaging hurdles that would need to be overcome, some of which may not be consistent between the two countries. While we are confident that the internal loading reduction could be achieved and could significantly improve water quality, we are less confident that getting to an implementation is feasible given the complexities associated with the policy and governance of the issue and the relatively high cost to taxpayers.

7. Deliverables Completed

Task 1. Convene PAC:

- Project advisory committee meetings were held on four dates to present interim results and solicit feedback: July 30, 2020; April 9, 2021; March 4, 2022; and June 8, 2023.

Task 2. Prepare QAPP:

- A primary and secondary data QAPP, approved on September 17, 2020, and a QAPP update, approved January 31, 2022 (Appendix A).

Tasks 3 and 4, Map Sediment P, Years 1 and 2:

- A technical memo to Matthew Vaughan outlining proposed changes in the Year 2 Missisquoi Bay sampling plan.
- Missisquoi Bay sediment P concentration data submitted to LCBP; Map included in Figure 6.
- Missisquoi Bay interim monitoring deliverables, including spatial and tabular data of P and metals concentrations in sediment and water.
- Sediment assay results prepared by Dr. Emily Lesher of St. Joseph's College (Standish, Maine), enabling direct comparison of P concentrations following ascorbate and bicarbonate-dithionite extraction.

Tasks 5 and 6, Analyze Hydrologic and Hydrodynamic Responses Years 1 and 2:

- Missisquoi Bay AEM3D modeling deliverables (spatial and tabular model results) submitted to Matthew Vaughan.
- A technical memo distributed to the PAC and Vermont DEC regarding the plan for implementing external and internal P loading reductions in the Missisquoi Bay AEM3D model (for concurrence by Vermont DEC).

Tasks 7 and 8, Evaluate Internal P Loading Strategies:

- An interim report submitted April 1, 2022 by lead author Ken Wagner reviewing management alternatives for Missisquoi Bay provided preliminary evaluations for discussion with the PAC.
- Section 4 and Section 5 of this final report provide these evaluations. Internal P loading management alternatives (including a map of treatment areas and potential P inactivation agent amounts) are evaluated in Section 5 and in the ArcGIS Storymap. In Section 4 we modeled specific P inactivation scenarios to characterize their effectiveness.

Task 9, Develop Implementation Plan:

- An interim report submitted April 1, 2022 by lead author Ken Wagner reviewing management alternatives for Missisquoi Bay.

- The management alternatives interim report was refined and extended as Section 5 of this final report, which includes our findings.

Tasks 10, Visualization Tools—HydroHub:

- HydroHub was used with video editing software to prepare videos of AEM3D model simulations. The videos may be viewed through the ArcGIS StoryMap.

Task 11, Visualization Tools—Story Map:

- An ArcGIS StoryMap was created to provide an overview of insights gained in this project and to present the results of the internal P loading inactivation evaluation. The StoryMap is accessible at the following URL: (https://storymaps.arcgis.com/stories/2df5114a2fd945408521bcedddaa0526).

Task 12, Reporting:

- Quarterly reports were submitted providing updates on the progress of each task and describing any problems encountered.
- Interim reports were submitted related to the sediment monitoring, AEM3D modeling, and management alternatives evaluation. The substance of these reports is incorporated in this final report.
- This final report was presented to the LCBP TAC on September 6, 2023, and was revised in August 2024 following additional review by the PAC.

Additionally, aspects of this project were presented at two conferences and published in Water Resources Research:

- Ashton Kirol and Meghan Arpino made an oral presentation of this work at the 2022 Northeast Aquatic Biologists Conference in Portland, ME on March 4, 2022.
- Co-PI Andrew Schroth presented interim project findings at the Lake Champlain Research Conference in Burlington, VT on May 24, 2022.
- The citation for the Water Resources Research publications is:
  Kirol, A.P., Morales-Williams, A.M., Braun, D.C., Marti, C.L., Pierson, O.E., Wagner, K.J., & Schroth, A.W. (2024). Linking sediment and water column phosphorus dynamics to oxygen, temperature, and aeration in shallow eutrophic lakes. *Water Resources Research*, 60, https://doi.org/10.1029/2023WR034813

8. References

Bennett, N.D., B.F.W. Croke, G. Buariso, J.H.A Guillaume, S.H. Hamilton, A.J. Jakeman, S. Marsili-Libeli, L.T.H. Newham, J.P. Norton, C. Perrin, S.A. Peirce, B. Robson, R. Seppelt, A.A. Voinov, B.D. Fath, and V. Andreassian. 2013. Characterizing performance of environmental models. *Environ Model Softw*., 40:1-20.

Bocaniov, S.A., L.F. Leon, Y.R. Rao, D.J. Schwab, and D. Scavia. 2016. Simulating the effect of nutrient reduction on hypoxia in a large lake (Lake Erie, USA-Canada) with a three-dimensional lake model. *J. Great Lakes Res.,* 42: 1228-1240. https:// doi.org/10.1016/J.JGLR.2016.06.001.

Brattebo, S., E. Welch, H. Gibbons, M. Burghdoff, G. Williams, and J. Oden. 2017. Effectiveness of alum in a hypereutrophic lake with substantial external loading. *Lake Reserv. Management,* 33:108-118.

Bruce, L.C., D. Hamilton, J. Imberger, G. Gal, M. Gophen, T. Zohary, and K.D. Hambright. 2006. A numerical simulation of the role of zooplankton in C, N and P cycling in Lake Kinneret, Israel. *Ecol. Modell.,* 193: 412-436.

Burger D.F., D.P. Hamilton, C.A. Pilditch, and M.M. Gibbs. 2007. Benthic nutrient fluxes in a eutrophic, polymictic lake. *Hydrobiologia*, 584: 13-25.

Burger, D.F., D.P. Hamilton, and C.A. Pilditch. 2008. Modelling the relative importance of internal and external nutrient loads on water column nutrient concentrations and phytoplankton biomass in a shallow polymictic lake. *Ecological Modelling,* 211: 411-423.

Cavalcante, H., F. Araújo, V. Becker, J.E. Lucena-Barbosa. 2021. Control of internal phosphorus loading using coagulants and clays in water and the sediment of a semiarid reservoir susceptible to resuspension. *Hydrobiologia*, https://doi.org/10.1007/s10750-021-04737-0

Celikkol, S., N. Fortin, N. Tromas, H. Andriananjamanantsoa, and C.W. Greer. 2021. Bioavailable nutrients (N and P) and precipitation patterns drive cyanobacterial blooms in Missisquoi Bay, Lake Champlain. *Microorganisms,* 2021, 9, 2097. https://doi.org/10.3390/microorganisms9102097.

Chung S.W., J. Imberger, M.R. Hipsey, and H.S. Lee. 2014. The influence of physical and physiological processes on the spatial heterogeneity of a Microcystis bloom in a stratified reservoir. *Ecological Modelling*, 289: 133-149.

Giles, C.D., P.D.F. Isles, T. Manley, Y. Xu, G.K. Druschel, and A. Schroth. 2016. The mobility of phosphorus, iron, and manganese through the sediment–water continuum of a shallow eutrophic freshwater lake under stratified and mixed water-column conditions. *Biogeochemistry,* 127:15–34. doi:10.1007/s10533-015-0144-x.

Godfrey, P., R. Kortmann, S. Souza, and K. Wagner. 2003. Recommendations for the management of Neponset Reservoir for control of excessive, nutrients, algae and macrophytes. Prepared for the Town of Foxborough and NRRC, Foxborough, MA.

Griffin, S.L., M. Herzfeld, and D.P. Hamilton. 2001. Modelling the impact of zooplankton grazing on phytoplankton biomass during a dinoflagellate bloom in the Swan River Estuary, Western Australia. *Ecological Engineering*, 16: 373-394.

Hanson, P.C., R. Ladwig, C. Buelo, E.A. Albright, A.D. Delany, C.C. Carey. 2023. Legacy phosphorus and ecosystem memory control future water quality in eutrophic lake. *Journal of Geophysical Research: Biogeosciences*, 128:1-17, https://doi.org/10.1029/2023JG007620

Hodges, B., and C. Dallimore. 2018. Aquatic Ecosystem Model: AEM3D. v1.0 User Manual. In *HydroNumerics*.

Hodges, B.R., J. Imberger, A. Saggio, and K.B. Winters. 2000. Modelling basin-scale internal waves in a stratified lake. *Limnol. Oceanogr.,* 45: 1603-1620.

Huisman, J., G.A. Codd, H.W. Paerl, B.W. Ibelings, J.M.H. Verspagen, and P.M. Visser. 2018. Cyanobacterial blooms. *Nat. Rev. Microbiol.*, 16(8), 471-483, doi:10.1038/s41579-018-0040-1.

Huser, B., S. Egemose, H. Harper, M. Hupfer, H. Jensen, K.M. Pilgrim, K. Reitzel, E. Rydin, and M. Futter. 2016. Longevity and effectiveness of aluminum addition to reduce sediment phosphorus release and restore lake water quality. *Water Res.*, 97:122-132.

Imberger J., and J.C. Patterson. 1990. Physical Limnology. *Advances in Applied Mechanics,* 27: 303-475.

Isles, P.D.F., C.D. Giles, T.A. Gearhart, Y. Xu, G.K. Druschel, and A.W. Schroth. 2015. Dynamic internal drivers of a historically severe cyanobacteria bloom in Lake Champlain revealed through comprehensive monitoring. *Journal of Great Lakes Research*, 41: 818-829.

Isles, P.D.F. 2016. A Multiscale Analysis of the Factors Controlling Nutrient Dynamics and Cyanobacteria Blooms in Lake Champlain. University of Vermont Ph.D. Thesis, Burlington, VT. https://scholarworks.uvm.edu/graddis/561.

Isles, P.D.F., D.M. Rizzo, Y.Y. Xu, and A.W. Schroth. 2017a. Modeling the drivers of interannual variability in cyanobacterial bloom severity using self-organizing maps and high-frequency data. *Inland Waters*, 7(3), 333-347, doi:10.1080/20442041.2017.1318640.

Isles, P.D. F., Y.Y. Xu, J. D. Stockwell, and A.W. Schroth. 2017b. Climate-driven changes in energy and mass inputs systematically alter nutrient concentration and stoichiometry in deep and shallow regions of Lake Champlain. *Biogeochemistry*, 133(2), 201-217, doi:10.1007/s10533-017-0327-8.

James, W., and J. Bischoff. 2015. Relationships between redox-sensitive phosphorus concentrations in sediment and the aluminum: phosphorus binding ratio. *Lake Reserv. Manage.*, 31:339-346.

Kirol, A. 2023. Assessing the Drivers of Legacy Phosphorus Loading and Distribution in Shallow Eutrophic Lake Sediments and the Impacts of Intervention. MS Thesis, UVM, Burlington, VT.

Leon, L.F., J. Imberger, R.E. Smith, R.E. Hecky, D.C. Lam, and W.M. Schertzer. 2005. Modeling as a tool for nutrient management in Lake Erie: a hydrodynamics study. *Journal of Great Lakes Research*, 31: 309-318, https ://doi.org/10.1016/S0380 -1330(05)70323 -3

Leon, L.F., R.E.H. Smith, M.R. Hipsey, S.A. Bocaniov, S.N. Higgins, P.E. Hecky, J.P. Antenucci, J. Imberger, and S.J. Guildford. 2011. Application of a 3D hydrodynamic-biological model for seasonal and spatial dynamics of water quality and phytoplankton in Lake Erie. *Journal of Great Lakes Research*, 37: 41-53.

Levine, S.N., A. Lini, M.L. Ostrofsky, L. Bunting, H. Burgess, P.R. Leavitt, D. Reuter, A. Lami, P. Guilizzoni, and E. Gilles. 2012. The eutrophication of Lake Champlain's northeastern arm: Insights from paleolimnological analyses. *Journal of Great Lakes Research*, 38, 35-48, doi:10.1016/j.jglr.2011.07.007.

Levine, S. N., A. Lini, M.L. Ostrofsky, H. Burgess-Grant, A. Lami, E. Collyer-Gilles, D. Reuter, L. Schwarting-Miller, and N. Kamman. 2018. The relative roles of point and nonpoint phosphorus sources in the eutrophication of Lake Champlain as recorded in sediment cores. *Journal of Great Lakes Research*, 44(5), 1043-1056, doi:10.1016/j.jglr.2018.06.005.

LimnoTech. 2012. Development of a Phosphorus Mass Balance Model for Missisquoi Bay. Prepared for the Lake Champlain Basin Program under contract to NEIWPCC. LimnoTech, Ann Arbor, MI.

LimnoTech. 2015. Missisquoi Bay Phosphorus Model – Extended Load Reduction Simulation Period Results. Memo to LCBP. LimnoTech, Ann Arbor, MI.

Lürling M, M. Mucci, and G. Waajen. 2020. Removal of positively buoyant *Planktothrix rubescens* in lake restoration. *Toxins*, 2020, 12, 700, https://doi.org/10.3390/toxins12110700.

Marti, C.L., A.W. Schroth, and A. Zia. 2019. Physical and biogeochemical processes across seasons in Missisquoi Bay, Lake Champlain: Insights from a three-dimensional model. AGU Fall Meeting, December 9-13, 2019, San Francisco, CA, USA. Oral session. H34C-04.

McCarthy, M.J., W.S. Gardner, M.F. Lehmann, A. Guindon, and D.F. Bird. 2016. Benthic nitrogen regeneration, fixation, and denitrification in a temperate, eutrophic lake: Effects on the nitrogen budget and cyanobacteria blooms. *Limnology and Oceanography*, 61(4), 1406-1423, doi:10.1002/lno.10306.

ME DEP. 2001. Lake Sebasticook TMDL. DEPLW 2000-110. ME DEP, Augusta, ME.

Missaghi S., M. Hondzo, and C. Melching. 2013. Three-dimensional lake water quality modeling: sensitivity and uncertainty analyses. *J. Environ. Qual.*, 42(6): 1684-1698, https://doi.org/10.2134/jeq2013.04.0120

Molot, L.A., S.L. Schiff, J.J. Venkiteswaran, H.M. Baulch, S.N. Higgins, A. Zastepa, M.J. Verschoor, and D. Walters. 2021. Low sediment redox potential promotes cyanobacteria blooms across a trophic range: implications for management. *Lake Reserv. Manage.*, 37:120-142.

Mueller, H., D. Hamilton, G. Doole, J. Abell, and C. McBride. 2019. Economic and ecosystem costs and benefits of alternative land use and management scenarios in the Lake Rotorua, New Zealand, catchment, *Global Environmental Change,* 54: 102-112.

Nedeau, 2011. 2011 Freshwater Mussel Survey in Mystic Lake (Barnstable, Massachusetts). Biodrawversity, Amherst, MA.

Ostrofsky, M.L., S.N. Levine, and A. Lini. 2020. Spatial and temporal variation in sedimentary phosphorus species in Lake Champlain (Vermont, New York, Québec). *Journal of Great Lakes Research*, 46:1277-1291.

Oveisy, A., L. Boegman, and J. Imberger. 2012. Three-dimensional simulation of lake and ice dynamics during winter. *Limnol. Oceanogr.*, 57 (43): 43-57, http://dx.doi.org/10.4319/lo.2012.57.1.0043.

Paerl, H.W., T.G. Otten, and R. Kudela. 2018. Mitigating the expansion of harmful algal blooms across the freshwater-to-marine continuum. *Environ. Sci. Technol.,* 52, 5519-5529.

Pearce, A.R., D.M. Rizzo, M.C. Watzin, and G.K. Druschel. 2013. Unraveling associations between cyanobacteria blooms and in-lake environmental conditions in Missisquoi Bay, Lake Champlain, USA, using a modified self-organizing map. *Environmental Science & Technology*, 47(24), 14267-14274, doi:10.1021/es403490g.

Preston A, I.A. Hannoun, E.J. List, I. Rackley, and T. Tietjen. 2014. Three-dimensional management model for Lake Mead, Nevada, Part 2: Findings and applications, Lake and Reservoir Management, 30(3): 303-319, doi: 0.1080/10402381.2014.927942

Randall, M.C., G.T. Carling, D.B. Dastrup, T. Miller, S.T. Nelson, K.A. Rey, N.C. Hansen, B.R. Bickmore, and Z.T. Aanderud. 2019. Sediment potentially controls in-lake phosphorus cycling and harmful cyanobacteria in shallow, eutrophic Utah Lake. PLoS ONE 14(2): e0212238. https://doi.org/ 10.1371/journal.pone.0212238.

Rao, Y.R., R. Valipour, P. Fong, C. Binding, A. Zastepa, and T. Pascoe. 2023. Application of a three-dimensional ecological model to develop nutrient management plans for Lake of the Wood. *Journal of Great Lakes Research*, 49: 97-111.

Robertson, D.M., B.I. Siebers, R. Ladwig, D.P. Hamilton, P. Reneau, C. McDonald, S. Prellwitz, R.C. Lathrop. 2022. Response of Green Lake, Wisconsin, to changes in phosphorus loading, with special emphasis on near-surface total phosphorus concentrations and metalimnetic dissolved oxygen minima. U.S. Geological Survey Scientific Investigations Report 2022–5003; 77 p. https://doi.org/10.3133/sir20225003

Robson, B.J., and D.P. Hamilton. 2004. Three-dimensional modelling of a Microcystis bloom event in the Swan River estuary. West. Aust. *Ecological Modelling*, 174 (1-2): 203-222.

Romero, J.R., J.P. Antenucci, and J. Imberger. 2004. One- and three-dimensional biogeochemical simulations of two differing reservoirs. *Ecological Modelling*, 174(1-2):143-160.

Rosenberg, B.D., and A.W. Schroth. 2017. Coupling of reactive riverine phosphorus and iron species during hot transport moments: impacts of land cover and seasonality. *Biogeochemistry,* 132(1-2), 103-122, doi:10.1007/s10533-016-0290-9.

Schroth, A.W., C.D. Giles, P.D.F. Isles, Y.Y. Xu, Z. Perzan, and G.K. Druschel. 2015. Dynamic coupling of iron, manganese, and phosphorus behavior in water and sediment of shallow ice-covered eutrophic lakes. *Environmental Science & Technology*, 49(16), 9758-9767, doi:10.1021/acs.est.5b02057.

Sherman, F.S., J. Imberger, and G.M. Corcos. 1978. Turbulence and mixing in stably stratified waters. *Annual Review of Fluid Mechanics,* 10: 267-288.

Silva C.P., C.L. Marti, and J. Imberger. 2014a. Mitigating the effects of high biomass algal blooms on the drinking water intakes of the city of Buenos Aires, Argentina. *Journal of Hydraulic Research,* 52: 705-719.

Silva, C.P., C.L. Marti, and J. Imberger. 2014b. Horizontal transport, mixing and retention in a large, shallow estuary. *Environmental Fluid Mechanics,* doi 10.1007/s10652-013-9330-3.

Smeltzer, E., R.A. Kirn, and S. Fiske. 1999. Long-term water quality and biological effects of alum treatment of Lake Morey, Vermont. *Lake Reserv. Manage.*, 15:173-184.

Smith, L.G., M.C. Watzin, and G. Druschel. 2011. Relating sediment phosphorus mobility to seasonal and diel redox fluctuations at the sediment–water interface in a eutrophic freshwater lake. *Limnol. Oceanogr.*, 56:2251–2264.

Sosiak, A. 2022. Assessment of the hypolimnetic withdrawal system at Pine Lake, Alberta. Lake Reserv. Manage., In press. https://doi.org/10.1080/10402381.2021.2001609.

Spigel, R.H., J. Imberger, and K.N. Rayner. 1986. Modeling the diurnal mixed layer. *Limnology and Oceanography,* 31: 533-556.

Steinman, A. and B. Spears (editors). 2020. Internal Phosphorus Loading in Lakes: Causes Case Studies and Management. J. Ross Publishing, Plantation, FL.

Tammeorg, O., G. Nürnberg, J. Niemistö1, M. Haldna, and J. Horppila. 2020. Internal phosphorus loading due to sediment anoxia in shallow areas: implications for lake aeration treatments. *Aquatic Sciences*, 82:54-63. DOI 10.1007/s00027-020-00724-0.

Tranmer, A.W., D. Weigel, C.L. Marti, D. Vidergar, R. Benjankar, D. Tonina, P. Goodwin, and J. Imberger. 2020. Coupled reservoir-river systems: Lessons from an integrated aquatic ecosystem assessment. *Journal of Environmental Management,* 260, 110107, https://doi.org/10.1016/j.jenvman.2020.110107

Trolle, D., T.B. Jørgensen, and E. Jeppesen. 2008. Predicting the effects of reduced external nitrogen loading on the nitrogen dynamics and ecological state of deep Lake Ravn, Denmark, using the DYRESM–CAEDYM model. Limnologica, Integrating approaches in limnological research: from basic to applied and from empirical to theoretical 38: 220-232. https://doi.org/10.1016/j. limno.2008.05.009.

Trolle D., D.P. Hamilton, M.R. Hipsey, K. Bolding, J. Bruggeman, W.M. Mooij, J.H. Janse, A. Nielsen, E. Jeppesen, J.A. Elliott, V. Makler-Pick, T. Petzoldt, K. Rinke, M.R. Flindt, G.B. Arhonditsis, G. Gal, R. Bjerring, K. Tominaga, J.T. Hoen, A.S. Downing, D.M. Marques, C.R.J. Fragoso, M. Søndergaard, and

P.C. Hanson. 2012. A community-based framework for aquatic ecosystem models. *Hydrobiologia*, 683: 25-34.

USEPA. 2016. Lake Champlain Phosphorus TMDL: A Commitment to Clean Water. https://www.epa.gov/tmdl/lake-champlain-phosphorus-tmdl-commitment-clean-water

Valipour, R., P. Fong, C. McCrimmon, J. Zhao, D.R. Van Stempvoort, and Y. Rao. 2023. Hydrodynamics of a large lake with complex geometry and topography: Lake of the Woods. *J. Great Lakes Res.*, 49(1), 82–96.

van der Linden, L., R.I. Daly, and M.D. Burch. 2015. Suitability of a coupled hydrodynamic water quality model to predict changes in water quality from altered meteorological boundary conditions. *Water*, *7*(1), 348-361.

Vilhena L.C., I. Hillmer, and J. Imberger. 2010. The role of climate change in the occurrence of algal blooms: Lake Burragorang, Australia. *Limnology and Oceanography, 55(3):1188-1200.*

VTANR. 2008. Review of SolarBee Performance in St. Albans Bay, Lake Champlain. VT ANR, Waterbury, VT.

VTDEC. 2022. Lake Champlain Long-term Monitoring Project. URL: https://anrweb.vermont.gov/dec/_dec/LongTermMonitoringLakes.aspx

Wagner, K. 2015. Oxygenation and Circulation to Aid Water Supply Reservoir Management. Water Research Foundation, Denver, CO.

Wagner, K. 2017. Preface: Advances in phosphorus inactivation. *Lake Reserv. Manage.*, 33:103-107, DOI: 10.1080/10402381.2017.1316064

Weigel, D.E., L.C. Vilhena, P. Woods, D. Tonina, A. Tranmer, R. Benjankar, C.L. Marti, P. Goodwin. 2017. Aquatic habitat response to climate-driven hydrologic regimes and water operations in a montane reservoir in the Pacific Northwest, USA. *Aquatic Sciences*, doi:10.1007/s00027-017-0544-1.

Welch, E., H. Gibbons, S. Brattebo, and H. Corson-Rikert. 2017. Distribution of aluminum and phosphorus fractions following alum treatments in a large shallow lake. *Lake Reserv. Manage.,* 33:198-204.

Willmott, C.J. 1982. Some comments on the evaluation of model performance. *Am. Meteorol. Soc*. 63 (11): 1309-1313.

Woodward B., C.L. Marti, J. Imberger, M.R. Hipsey, and C.E. Oldham. 2017. Wind and buoyancy driven horizontal exchange in shallow embayments of a tropical reservoir: Lake Argyle, Western Australia. *Limnology and Oceanography,* 62: 1636-1657.

WRS. 2016. 604b Study of Phosphorus Sources to Hummock and Miacomet Ponds. By WRS, Wilbraham, MA for the Town of Nantucket.

WRS. 2021. Woodridge Lake and Wood Pond Cumulative Condition Summary. By WRS, Wilbraham, MA for the Woodridge Lake Association, West Hartford, CT.

Xing Z, L.H. Chua, and J. Imberger. 2014. Evaluation of management scenarios for controlling eutrophication in a shallow tropical urban lake. *Int. J. Environ. Pollut. Remediat.*, 2(2): 66-72

Zhang, J-Z and N.T. Lanning. 2018. Ascorbic Acid as a Reductant for Extraction of Iron-Bound Phosphorus in Soil Samples: A Method Comparison Study. *Communications in Soil Science and Plant Analysis*, 49:17, 2155-2161. DOI:10.1080/00103624.2018.1499751

Zhang, Q., and R.M. Hirsch. 2019. River water-quality concentration and flux estimation can be improved by accounting for serial correlation through an autoregressive model. *Water Resources Research*, https://doi.org/10.1029/2019WR025338.

Zia, A., A.W. Schroth, J.S. Hecht, P. Isles, P.J. Clemins, S. Turnbull, P. Bitterman, Y. Tsai, I.N. Mohammed, G. Bucini, E.M.B. Doran, C. Koliba, A. Bomblies, B. Beckage, J. Winter, E.C. Adair, D.M. Rizzo, W. Gibson, G. Pinder. 2022. Climate change-legacy phosphorus synergy hinders lake response to aggressive water policy targets. *Earth's Future*, v. 10, doi:10.1029/2021EF002234.

Zia, A., A. Bomblies, A.W. Schroth, C. Koliba, P.D.F Isles, Y. Tsai, I.N. Mohammed, G. Bucini, P.J. Clemins, S. Turnbull, M. Rodgers, A. Hamed, B. Beckage, J. Winter, C. Adair, G.L. Galford, D. Rizzo, and J. Van Houten. 2016. Coupled impacts of climate and land use change across a river-lake continuum: insights from an integrated assessment model of Lake Champlain's Missisquoi Basin, 2000-2040. *Environmental Research Letters*, 11(11), doi:10.1088/1748-9326/11/11/114026.

Appendix A:
Quality Assurance Project Plan

QA Project Plan:

Evaluating Alternatives to Control Internal Phosphorus Loading in Missisquoi Bay Using a 3-Dimensional Coupled Hydrodynamic-Aquatic Ecosystem Model

Stone project number 19-150
EPA Grant Number LC00A00605; QAPP ID Q20-043; RFA# 20104
Account L-2020-063; JCC 346-002-001

Version 1

Prepared by:
Stone Environmental, Inc., 535 Stone Cutters Way, Montpelier, VT 05602

Prepared for:
Lake Champlain Basin Program, 54 West Shore Road, Grand Isle, VT 05458

Approved September 17, 2020
Updated January 31, 2022

Dave Braun, Project Manager, Stone Environmental, Inc. Date

Jennifer Cypher, Project QA/QC Manager, Stone Environmental, Inc. Date

Mike Winchell, Vice-President, Stone Environmental, Inc. Date

Andrew Schroth, Project Data Manager, UVM Date

Clelia Marti De Ocampo, Project Model Manager, Curtin University Date

Matthew Vaughan, Project Officer, LCBP Date

Peter Zaykoski, QA Program Manager, NEIWPCC Date

Bryan Dore, Project Officer, EPA Date

Nora Conlon, QA Reviewer, EPA Date

Table of Contents

A – Project Management

A3 – Distribution List

EPA: Bryan Dore, EPA Project Officer, dore.byran@epa.gov
Address: 5 Post Office Sq., Suite 100, Mail Code OEP06-1, Boston, MA 02109-3912
Phone: (617) 918-1211

Nora Conlon, EPA QA Reviewer, conlon.nora@epa.gov
Address: 11 Technology Dr., North Chelmsford, MA 01863
Phone: (617) 918-8335

NEIWPCC: Heather Radcliffe, Water Resource Protection Programs Director, hradcliffe@neiwpcc.org
Alexandra Morneau, Administrative Assistant, qapps@neiwpcc.org
Peter Zaykoski, QA Program Manager, pzaykoski@neiwpcc.org
Address: NEIWPCC, 650 Suffolk St., Suite 410, Lowell, MA 01854
Phone: (978) 323-7929

LCBP: Matthew Vaughan, Project Officer, mvaughan@lcbp.org
Kathy Jarvis, LCBP Office Manager, kjarvis@lcbp.org
Address: LCBP, 54 West Shore Road, Grand Isle, VT 05458
Phone: (802) 372-3213

Stone: Dave Braun, Project Manager, dbraun@stone-env.com
Jennifer Cypher, Project QA Manager, jcypher@stone-env.com
Mike Winchell, Vice-President, mwinchell@stone-env.com
Address: Stone Environmental, 535 Stone Cutters Way, Montpelier, VT 05602
Phone: (802) 229-4541

UVM: Andrew Schroth, Project Data Manager, Andrew.Schroth@uvm.edu
Address: Department of Geology, Delehanty Hall, UVM, Burlington, VT 05405
Phone: (802) 656-3481

Curtin Univ. Clelia Marti De Ocampo, Project Model Manager, marti1clelia@gmail.com
Address: Sustainable Engineering Group, Curtin U., Perth, WA 6102, Australia
Phone: (802) 656-8793

A4 – Project/Task Organization

EPA:

Bryan Dore, EPA Project Officer: General oversight, review and approve all final work products for the EPA.

Nora Conlon, EPA QA Reviewer: QA/QC Approval Authority. Review and approve QAPP and subsequent revisions in terms of quality assurance aspects.

NEIWPCC:
Peter Zaykoski, Quality Assurance Program Manager: Review and approve QAPP and subsequent revisions in terms of quality assurance aspects.

LCBP:
Matthew Vaughan, LCBP Project Officer: Overall coordination of the project and point of communication for all parties. Responsible for maintaining and distributing the official approved QAPP.

Stone Environmental, Inc.:
Dave Braun, Stone Project Manager: Overall coordination and oversight of project and quality assurance activities, including communication with approved subcontractors, as appropriate, and reporting to LCBP. Responsible for communicating potential changes to this QAPP to the LCBP Project Officer.

Jennifer Cypher, Project QA Manager: Responsible for reconciling deviations and corrective actions from this QAPP with the Stone Project Manager and LCBP Project Officer.

Staff members from Stone Environmental, Inc. will report to the Stone Project Manager for technical and administrative direction. Each staff member has responsibility for performance of assigned quality control duties while accomplishing identified tasks. The quality control duties include:

- Completing the assigned task on schedule and in a quality manner in accordance with established procedures.
- Ascertaining that the work performed is technically correct and meets all requirements of this QAPP.

University of Vermont:
Andrew Schroth, UVM Project Data Manager: Responsible for implementation of all primary data collection activities, including sensor data collection and sediment and water sample collection, processing, and analysis. Will report to the Stone Project Manager for administrative direction.

Curtin University:
Clelia Marti De Ocampo, Project Model Manager: Responsible for incorporation of primary and secondary data in the refined Missisquoi Bay Aquatic Ecosystem Model 3D and conducting model simulations. Will report to the Stone Project Manager for administrative direction.

Staff members assisting the UVM Project Data Manager and the Project Model Manager will be responsible for performance of assigned quality control duties while accomplishing identified tasks. The quality control duties include:

- Completing the assigned task on schedule and in a quality manner in accordance with established procedures.
- Ascertaining that the work performed is technically correct and meets all aspects of this QAPP.

A5 – Problem Definition/Background

Missisquoi Bay (MB) of northeastern Lake Champlain underwent anthropogenic eutrophication over the latter half of the 20th century (*Levine et al.*, 2012*; Levine et al.*, 2018). This was primarily due to the intensification of agricultural production and associated macronutrient inputs across the landscape of the MB Basin and their consequent increased riverine loading to MB. As a result, there are persistent and relatively severe cyanobacteria blooms that occur in late summer and early fall in MB, degrading surface water quality and decreasing ecosystem services (*Isles et al.*, 2017a). For most of the bloom season, phosphorus (P) is thought to be the dominant limiting nutrient, although co-limitation with nitrogen and light has also been suggested (*Isles et al.*, 2015; *McCarthy et al.*, 2016). Although the long-term eutrophication of MB was driven by increased riverine nutrient loads, the build-up of legacy P in the sediments, and subsequent release of immediately bioavailable benthic P to the water column (internal P loading), is a critical driver of cyanobacteria bloom initiation, duration, and severity (e.g., *Smith et al.*, 2011; *Pearce et al.*, 2013; *Giles et al.*, 2016; *Isles et al.*, 2017a).

Missisquoi Bay is a shallow system (Figure 1), with a mean depth of 2.8 m and a maximum depth of 4 m (*Levine et al.*, 2012). Due to this shallow bay's particularly high surface area relative to its volume, coupled with its robust inventory of legacy P in surface sediment, nutrient dynamics in MB are strongly impacted by internal P loading, particularly when river inputs are near baseflow. Indeed, roughly 25% of the P flux in the bay on an annual basis is estimated to be derived from internal loading (*Limnotech*, 2012). This number underestimates the impacts of internal P loading in degrading water quality because of the timing and conditions associated with internal P flux (relative to the larger riverine P flux). Much of the riverine P is delivered to the bay from storm and snowmelt-derived high flow events under conditions not conducive to promoting blooms. Specifically, high flow events deliver P to the bay under conditions where the residence time of water (and P) can be the shortest (e.g., days), cyanobacteria buoyancy regulation capabilities are suppressed by mixing of the water column, and relatively cool water conditions of spring/fall are not conducive to bloom development (*Isles et al.*, 2017a).

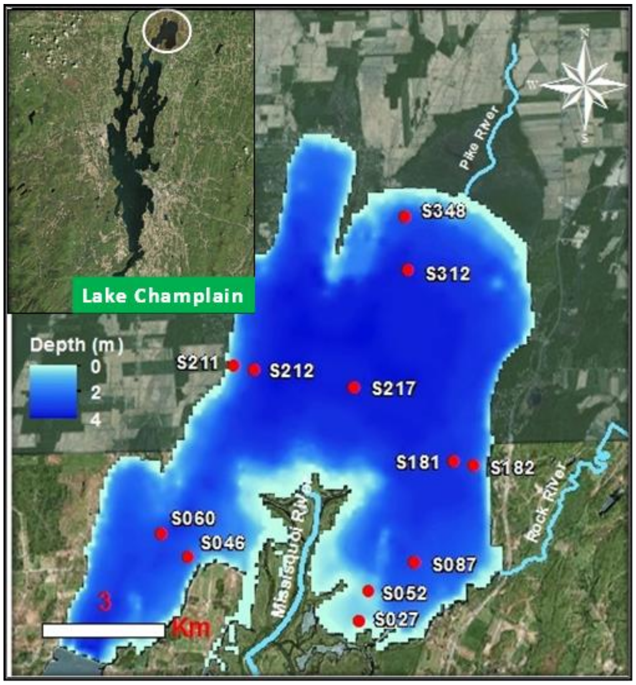

Figure 1. MB site and bathymetry map with sample core locations (red dots) where sectioned cores (to 10 cm) have been analyzed for P inventories at 4 time points in 2013 (June–Sept.). At point S087, there are biweekly time series of sediment P inventories in 2013-14 and 2014-2015. All points have coincident water column physical, chemical and biological data.

Conversely, much of the internal P loading to MB occurs during summer months, when the majority of water column P is likely derived from internal loading, although this relative contribution fluctuates each year due to variability in weather patterns (*Giles et al.*, 2016; *Limnotech*, 2012; *Isles et al.*, 2017a,b). Furthermore, summer internal P loading inherently occurs during periods when bay water residence times will be longest due to low riverine inputs, when temperatures are favorable for cyanobacteria growth, and when the water column is stable and stratified, allowing cyanobacteria to outcompete other phytoplankton for this nutrient due to buoyancy regulation (*Huisman et al.*, 2018). Hydrodynamic conditions that promote internal P loading are a calm, stable water column that enables reducing conditions to develop at the sediment-water interface (SWI) and associated release of P from redox sensitive mineral phases, primarily iron oxyhydroxides in the case of MB (*Schroth et al.*, 2015; *Giles et al.*, 2016). Conversely, wind and riverine inputs promote mixing off the water column, input of riverine sediments, and re-oxidation of the SWI, all of which promote accumulation of P (*Giles et al.*, 2016). The interannual variability in the duration and severity of cyanobacteria blooms in MB has been attributed to the frequency and duration of each of these contradictory water column/SWI conditions when water temperatures are in a range that promote cyanobacteria dominance (*Isles et al.*, 2017a). As such, while the only long-term solution to decreasing legacy P in MB will depend on achieving reductions in watershed loading, those reductions will not suppress cyanobacteria blooms in the coming decades (and perhaps longer), necessitating reduction of internal loading to achieve water quality goals associated with cyanobacteria bloom suppression.

MB is a particularly dynamic hydrodynamic system with a limited water flux and connectivity to the rest of Lake Champlain. It has three major sources of riverine input, the Missisquoi (~80%), Pike (~10%) and Rock (~5%) Rivers, that all export terrestrial-derived P to MB in both dissolved and particulate forms. The concentration and reactivity of particulate P loads have been shown to vary extensively in time and by event (*Rosenberg and Schroth*, 2017). These three input points also exert a strong control on the hydrodynamics of MB, particularly under high flow conditions. Because the system has such a high surface area to volume ratio, MB is particularly sensitive to wind speed and orientation, completely turning over in response to relatively minor wind events (e.g., 1 m/s *Isles et al.,* 2017a), facilitating rapid changes in SWI redox chemistry (*Smith et al.*, 2011). Wind stress and heat fluxes on the surface water, and river discharges interacting with the bay's morphology are the major local forcing mechanisms creating a variable circulation pattern. Four modes of circulation were found to exist in MB (*Manley, T.*, unpublished). First, the "wintertime sluggish" mode, in which water velocities are vertically uniform and very low (< 1 cm/s). Second, the "spring melt", where the three rivers discharge high flow volumes. From May to November when thermally stratified conditions could develop, a third mode, "well-mixed summer", when the water column is well-mixed, or a fourth mode, "two-layer summer", in which stratified conditions are present, will occur. Water retention times vary seasonally ranging from several days during high spring river flows to several months during periods of low summer river flows.

Circulation patterns and retention time affect the fate and transport of biogeochemical constituents within MB. Preliminary monitoring data by Andrew Schroth suggest that these hydrodynamic factors produce variation in the distribution of P across the bay; surface sediments vary in P concentration by a factor of 6. Since 2012, researchers led by Schroth have deployed sensors in MB to capture, at an unprecedented scale, high frequency physical and biochemical dynamics of MB. These data have enhanced our conceptual model of internal loading and cyanobacteria dynamics in MB. These data have been utilized by Clelia Marti to simulate the time- and space varying physical and biogeochemical processes across seasons in MB (Marti et al., 2019) using the Aquatic Ecosystem Model 3D (AEM3D), which couples the hydrodynamic

3-D Estuary, Lake and Coastal Ocean Model (ELCOM) and the Computational Aquatic Ecosystem Dynamics Model (CAEDYM) (*Romero et al.*, 2004; *Silva et al.*, 2014). The independent review by Trolle et al. (2012) judged these models to be the superior choice for standing waters of varying scales from large natural systems, such as Lake Erie (Leon et al., 2005; Leon et al. 2011) to smaller lakes and reservoirs (Romero et al., 2004; Missaghi et al., 2014; Weigel et al., 2017) and widely used for estimating loads reductions necessary to support water quality goals (Burger et al., 2008; Trolle et al., 2012), studying the design and effectiveness of management methods for controlling algal blooms (Xing et al., 2014; Preston et al., 2014), and assessing the response to climate change and nutrient loading projections (Vilhena et al., 2010; van der Linden et al., 2015).

Simulation results produced by Marti using the AEM3D model reveal patterns in the distributions of orthophosphate (PO_4) (Figure 2) and dissolved oxygen (Figure 3) in the bottom water (1 m from bottom) that resemble the sediment grain size map (Figure 4) recently prepared by P. Manley and T. Manley (unpublished), illustrating transient relationships between small particle size and elevated bottom water PO_4 and low dissolved oxygen concentrations.

The approved Total Maximum Daily Load (TMDL) for MB (*US EPA*, 2016) mandates a 64.3% reduction in P loading from the bay's watershed to achieve an in-lake water quality standard of 25 µg/L (annual mean). While such a reduction in external loading would be a remarkable achievement from a management standpoint, modeling data indicate that this would have minor impact on cyanobacteria blooms in coming decades because of the robust legacy P pool in MB and its high bioavailability (*Zia et al.*, 2016; *Zia et al.*, submitted). Furthermore, characteristics of ongoing and projected climate change in the Lake Champlain Basin will continue to enhance cyanobacteria bloom occurrence (i.e., warmer, more stratified water promotes cyanobacteria reproduction and the advantages of buoyancy regulation capabilities), which have a synergistic effect with internal P loading to sustain blooms (*Zia et al.*, 2016; *Zia et al.*, submitted). Therefore, mitigating internal loading of legacy P is

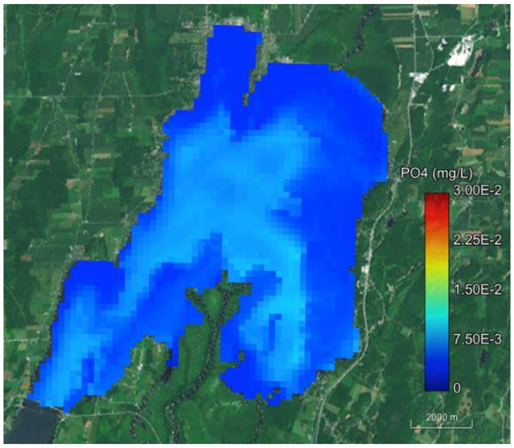

Figure 4. Predicted orthophosphate (PO_4) concentrations in MB 1 m from bottom.

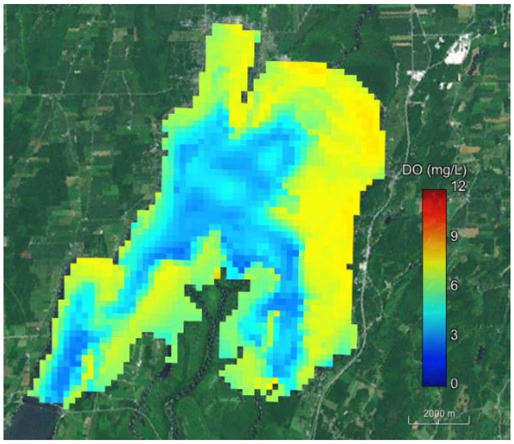

Figure 4. Predicted dissolved oxygen concentrations in MB 1 m from bottom.

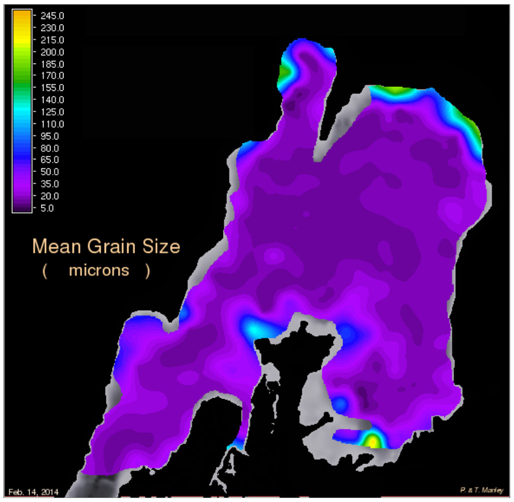

Figure 4. Sediment grain size in MB (P. Manley and T. Manley, unpublished).

required in concert with external nutrient loading reduction to achieve water quality and bloom suppression goals and preserve the credibility of management entities with the public. However, what kind of approach is optimal for mitigating internal loading of legacy P in this particular system and when it should be implemented are unknown.

There is a suite of potential remediation options available to address internal P loading (e.g., *Paerl et al.*, 2018), only some of which are likely well-suited to address the unique configuration of MB's hydrodynamic, biogeochemical, and ecological systems. Of the roughly dozen approaches to managing cyanobacteria, many suffer from some constraint that would greatly limit their application to MB. For example, flushing requires a tremendous amount of water and MB already has a short detention time. Bacterial additives have a short and mixed track record with virtually no supporting peer reviewed literature. Most successful internal P loading control efforts involve one or more of four techniques: dredging, circulation, oxygenation, and/or P inactivation. These will be the focus of our assessments and model scenario runs (e.g., *Xing et al.*, 2014).

In this study, the project team will utilize and refine the previously developed conceptual and process-based model of MB's hydrodynamic-biogeochemical system to meet the following objectives:

Objectives:

I. Design and implement a robust sampling campaign to further spatially identify and map P distribution in MB, with particular focus on hot spots of accumulation and release from the sediments.
II. Establish the physical and chemical drivers of P distribution.
III. Asses the capacity of different intervention strategies to control internal P loading and achieve bloom suppression goals.
IV. Predict the efficacy and appropriate timing of potential interventions over multiple decades in the context of EPA-mandated watershed nutrient reductions; and
V. Present the effective internal P loading reduction strategies through an accessible, visually appealing tool enabling managers to view the simulated results of various management interventions over time.

A6 – Project/Task Description

The project team will undertake the following tasks (Table 1):

Table 1. Project tasks

	Task	Objective	Deliverables & Outputs	Timeline
1.	Convene PAC	Objectives I–V	Engaged Advisory Committee; hold three meetings	July 2020 – March 2022
2.	Prepare QAPP	Objectives I–IV	Approved Quality Assurance Project Plan	July - August 2020
3	Map Sediment P, Year 1	Objective I	Map and data of MB sediment P concentrations	Aug. – Dec. 2020
4	Map Sediment P, Year 2	Objective I	Map and data of MB sediment P concentrations	Jan. – Dec. 2021
5	Analyze Hydrologic and	Objective II	Model output including bay-wide maps of P	June – Dec. 2020

	Task	Objective	Deliverables & Outputs	Timeline
	Hydrodynamic Responses, Year 1		accumulation, cumulative summer P release, and zones of low dissolved oxygen, high chlorophyll-a, and sediment resuspension	
6	Analyze Hydrologic and Hydrodynamic Responses, Year 2	Objective II	Model output including bay-wide maps of P accumulation, cumulative summer P release, and zones of low dissolved oxygen, high chlorophyll-a, and sediment resuspension	Jan. – Dec. 2021
7	Evaluate Internal P Loading Strategies—Technical Feasibility and Cost	Objective III	Evaluation and ranking of internal P loading reduction strategies per technical feasibility and cost A map showing amount of inactivation agent needed to achieve short term inactivation of sediment P	Jan. – Dec. 2021
8	Evaluate Internal P Loading Strategies—Ecological Impacts, Permitting, and Public Acceptability	Objective III	Evaluation and ranking of internal P loading reduction strategies per ecological impacts, permitting feasibility, and public acceptability	Jan. – Dec. 2021
9	Develop Implementation Plan	Objective IV	An optimized plan for controlling internal P loading and associated AEM3D model simulation results	June 2021 – March 2022
10	Visualization Tools—HydroHub	Objectives V	HydroHub interface enabling lake managers to examine effects of internal P reduction strategies	June 2021 – March 2022
11	Visualization Tools—Story Map	Objectives V	ArcGIS story map to communicate the optimized plan to the public	June 2021 – May 2022
12	Reporting	Objectives I–V	Approved quarterly progress reports for: 2020 (Q2, Q3, Q4); 2021 (Q1, Q2, Q3, Q4); and 2022 (Q1)	Due each quarter June 2020 – March 2022
			Approved Final Report and presentation to TAC	By June 30, 2022
	QAPP expiration			December 31, 2022

A7 – Quality Objectives and Criteria for Measurement Data

Objectives. The project data-quality objective is to collect, assemble, and analyze valid geographic, environmental, and cost data. Data quality will be measured in terms of accuracy and precision, representativeness, comparability, and completeness.

Intended use of the data. All primary data generated, and all non-direct data assembled in this project will be used in characterizing conditions in Missisquoi Bay and in evaluating and ranking internal P loading reduction strategies.

Spatial data sets will be used primarily in refining the MB AEM3D model parameterization. Primary, tabular environmental data will be used in developing AEM3D model parameter sets and spatial data layers of sediment P. Cost data will be used in preparing cost projections for intervention strategies to reduce internal P loading in MB.

Performance and acceptance criteria. Sediment and water chemistry data acquired through the monitoring program (Tasks 3-4) led by the UVM Project Data Manager will be accepted unless these appear inaccurate based on data acceptance criteria in Table 2 and the UVM Project Data Manager's professional judgement during data review and post-processing. If determined to be inaccurate per the data acceptance criteria in Table 2, measurements or sample collection and analysis will be repeated where possible or rejected if necessary. Spatial datasets and tabular environmental data to be used in this project (including flow measurements and meteorological data) produced by State and Federal Agencies are subject to their own quality criteria and procedures. These will be assumed to be accurate and will not be vetted. Cost estimates will be assembled from a variety of sources and the quality of the data will be documented to the best of our ability. Multiple cost values or estimates will be obtained in each cost category and median values/estimates generally applied in cost calculations for the intended purpose of providing cost projections for internal P loading intervention strategies. Note that more specific and complete cost estimates will be produced if the overall project advances to implementation.

The precision of primary data collection will be assessed through repeated measurements of water quality parameters measured in the field, collection and analysis of duplicate water samples and sediment cores, and triplicate analysis of processed sediment core sections (Table 2). Water and sediment samples will be collected such that at least 10% of the total sample loads are collected in duplicate. Precision of the sediment analyses will be further quantified through triplicate analysis of sediment samples and calculation of standard error.

Table 2. Data Quality Requirements and Assessments

Matrix	Parameter	PQL[1]	Accuracy[2]	Precision[3]	Method range
water	dissolved P	0.005 mg/L	<=±10% of known conc. of ref. material	field duplicate, RPD<=30%	0.005–10 mg/L
water	dissolved Al	0.05 mg/L	<=±10% of known conc. of ref. material	field duplicate, RPD<=30%	0.05–10 mg/L
water	dissolved Ca	0.05 mg/L	<=±10% of known conc. of ref. material	field duplicate, RPD<=30%	0.05–10 mg/L
water	dissolved Fe	0.02 mg/L	<=±10% of known conc. of ref. material	field duplicate, RPD<=30%	0.02–10 mg/L
water	dissolved Mn	0.02 mg/L	<=±10% of known conc. of ref. material	field duplicate, RPD<=30%	0.02–10 mg/L
sediment digestate	total P	0.05 mg/L	<=±10% of known conc. of ref. material	field duplicate: RPD<=50%; triplicate analysis: SE<=15%	0.05–10 mg/L
sediment digestate	total Al	0.05 mg/L	<=±10% of known conc. of ref. material	field duplicate: RPD<=50%; triplicate analysis: SE<=15%	0.05–10 mg/L
sediment digestate	total Ca	0.05 mg/L	<=±10% of known conc. of ref. material	field duplicate: RPD<=50%; triplicate analysis: SE<=15%	0.05–10 mg/L
sediment digestate	total Fe	0.02 mg/L	<=±10% of known conc. of ref. material	field duplicate: RPD<=50%; triplicate analysis: SE<=15%	0.02–10 mg/L
sediment digestate	total Mn	0.02 mg/L	<=±10% of known conc. of ref. material	field duplicate: RPD<=50%; triplicate analysis: SE<=15%	0.02–10 mg/L
sediment extract	redox sensitive P	0.05 mg/L	<=±10% of known conc. of ref. material	field duplicate: RPD<=50%; triplicate analysis: SE<=15%	0.05–10 mg/L
sediment extract	redox sensitive Al	0.05 mg/L	<=±10% of known conc. of ref. material	field duplicate: RPD<=50%; triplicate analysis: SE<=15%	0.05–10 mg/L
sediment extract	redox sensitive Ca	0.05 mg/L	<=±10% of known conc. of ref. material	field duplicate: RPD<=50%; triplicate analysis: SE<=15%	0.05–10 mg/L
sediment extract	redox sensitive Fe	0.02 mg/L	<=±10% of known conc. of ref. material	field duplicate: RPD<=50%; triplicate analysis: SE<=15%	0.02–10 mg/L
sediment extract	redox sensitive Mn	0.02 mg/L	<=±10% of known conc. of ref. material	field duplicate: RPD<=50%; triplicate analysis: SE<=15%	0.02–10 mg/L
sediment	dry bulk density	note 4	note 4	field duplicate, RPD<=30%	note 4

sediment	redox sensitive P (dithionite)	note 5	note 5	field duplicate, RPD<=30%	note 5
water	temperature	NA	-5–35°C: ±0.01°C; 35–50°C: ±0.05°C	triplicate measurement, RSD<=10%	-5– +50°C
water	pH	NA	±0.1 units within ±10°C of calibration temp.; ±0.2 units for entire temp. range	triplicate measurement, RSD<=10%	0–14 units
water	conductivity	NA	0-100 mS/cm: ±0.5% of reading or 0.001 mS/cm, whichever is greater; 100-200 mS/cm: ±1% of reading	triplicate measurement, RSD<=10%	0–200 mS/cm
water	dissolved oxygen	NA	0-20 mg/L: ±1% of reading or 0.1 mg/L; 20-50 mg/L: ±5% reading	triplicate measurement, RSD<=10%	0–50 mg/L
water	turbidity	NA	0-999 FNU: 0.3 FNU or ±2% of reading, whichever is greater; 1000-4000 FNU: ±5% of reading	triplicate measurement, RSD<=10%	0–4000 FNU
water	fDOM	0.07 ppb QSU	r^2>0.999 for serial dilution of 300 ppb Quinine Sulfate solution	triplicate measurement, RSD<=10%	0–300 ppb QSU
water	chlorophyll a / phycocyanin	NA	**Chl:** r^2>0.999 for Rhodamine WT, full range; **PC:** r^2>0.999 for Rhodamine WT, full range	triplicate measurement, RSD<=10%	Chl: 0–100 RFU; PC: 0–100 RFU (see note 6)

1. PQL (Practical Quantitation Limit) is the lower limit of quantitation/reporting.
2. Accuracy of field-measured water quality parameters per manufacturer specifications.
3. RPD = relative percent difference; RSD = relative standard deviation; SE = standard error
4. No PQL or range is given for this method due to the fact that all samples will have a measurable bulk density. The method accuracy is undefined.
5. Redox sensitive P quantitated following sediment P inactivation assay, per Lesher et al. (Appendix C)
6. Pigment concentration ranges of algae sensors were determined in monocultures of specific algae species. This range will vary depending on algae assemblage and environmental conditions.

A8 – Special Training/Certifications

Personnel with considerable expertise and experience in performing the project tasks will conduct all sampling and analysis for the project. UVM Project Data Manager or designee will be responsible for continued coordination of field operations and maintenance of consistency among field sampling personnel. This consistency will be aided using standard forms for sample retrieval and processing (Appendix A). All personnel performing the project tasks will have training in their respective duties and shall have read the applicable procedures. Training records for UVM employees will be maintained at UVM. Training records for Stone employees will be maintained at Stone's Montpelier office.

Sediment digestions and subsequent digestate and water sample analysis for P and metals concentrations will occur at the University of Vermont's Geology Department and Rubenstein Ecosystem Science Laboratories. Phosphorus and metals concentrations in sediment digestates and extracts will be analyzed by the inductively coupled plasma optical emission spectrophotometer (ICP-OES) at UVM. Appropriate blanks, replicates and reference materials will be run on the ICP-OES following the Schroth lab's existing protocols.

A small number of sediment grab samples will be submitted for analysis by the laboratory operated by Dr. Emily Lesher of St. Joseph's College of Maine in Standish, ME, following the Lesher lab's existing protocols (Appendix C).

A9 – Documents and Records

Generated environmental data will be stored in formats compatible with the method or instrument of generation. Processed data will be stored in ESRI ArcMap, Microsoft Word, Microsoft Excel, Microsoft Access, and/or Adobe Acrobat formats.

Paper records will be scanned and maintained electronically. Electronic files will be transferred to and maintained on secure computer networks at UVM and Stone Environmental, as appropriate. Electronic files maintained at Stone Environmental will be backed up daily to cloud-based servers. Electronic files maintained by UVM will be backed up to cloud-based servers weekly or more frequently. Electronic files will be archived for a minimum of seven years following completion of the project.

B – Data Generation and Acquisition

B1 – Model Development and Implementation and Sampling Process Design

AEM3D Model Description

The hydrodynamics component in AEM3D predicts velocity, temperature, salinity and tracer distributions in standing waters that are subjected to external forcing from the atmosphere, river surface in and out flows, groundwater flows and built structures. The hydrodynamic simulation method solves the unsteady, viscous Navier-Stokes equations for incompressible flow with an option of using the hydrostatic assumption for pressure (Hodges et al., 2000). Simulated processes include explicit algorithms for baroclinic and barotropic responses, rotational effects, tidal forcing, wind stresses, surface thermal forcing, inflows, outflows, ice formation dynamics, internal mixing and transport of salt, heat, and passive scalars. The hydrodynamic algorithms in AEM3D are based on the Euler-Lagrange method for advection of momentum with a conjugate-gradient solution for the free surface. Passive and active scalars (i.e., tracers, salinity and temperature) are advected using a conservative ULTIMATE QUICKEST scheme. AEM3D has been optimized for computational efficiency and has typical real time to simulation time ratios of O (100 to 1000):1 depending on the grid resolution and domain size. Calibration of the hydrodynamics component of AEM3D requires few parameter tests because the algorithms are intentionally generic process models and coefficients are process-based, not site-dependent. The values (or at least the appropriate range) of most of the coefficients can be specified from literature values.

The water quality component in AEM3D is dynamically coupled to the hydrodynamics component to simulate the fate and transport of physical, chemical and biological state variables (Romero et al., 2004; Vilhena et al., 2010; Weigel et al., 2017). AEM3D houses a series of mathematical equations representing biogeochemical processes that influence water quality including primary and secondary production, nutrient and metal cycling, oxygen dynamics and movement of the sediment.

AEM3D simulates state variables at the chemical and biological species level (e.g., organic and inorganic nitrogen, carbon and phosphorus species, and phytoplankton species) and provides aggregate measures to compare with typical observed variables (e.g., Total Suspended Solids (TSS), Total Nitrogen (TN), Total Phosphorus (TP), chlorophyll-a (Chl-a)). Higher trophic levels are included in AEM3D and the utility of the model in this regard has been demonstrated with simulations of the microbial loop and secondary production associated with zooplankton grazing (e.g., Bruce et al., 2006). The water quality component requires specification of several parameters used to simulate the biogeochemical processes, but they are also constrained within ranges found in literature.

Technical specifications of AEM3D may be found in the Science and User Manuals (Hodges and Dallimore, 2018) and are available at: http://www.hydronumerics.com.au/#software. The manual does not list any hardware requirements as it may be run on most modern personal computers.

The configuration of AEM3D is flexible so that the user can select to model the processes of interest, or within the limitations set by the availability of data and parameters. The model allows the user to define a range of outputs and extract model results at selected spatial and temporal scales.

Development of the AEM3D of Missisquoi Bay

The physical model domain of Missisquoi Bay was discretized with a uniform horizontal grid size of 200 m by 200 m, and a vertical resolution of 0.25 m. The model used a time step of 200 s. The model performance was tested against a high-frequency physical and biogeochemical dataset for the years 2017 and 2018.

The hydrodynamics component activated the appropriate algorithms to include atmospheric exchange, inflow dynamics, turbulent mixing dynamics, Coriolis forcing, and ice formation dynamics. The water quality component was configured to simulate nitrogen and phosphorus in both particulate and dissolved organic forms and dissolved inorganic forms to include particulate organic nitrogen (PON), dissolved organic nitrogen (DON), ammonium (NH_4), nitrate (NO_3), particulate organic phosphorus (POP), dissolved organic phosphorus (DOP), orthophosphate (PO_4), dissolved oxygen (DO), particulate organic carbon (POC), dissolved organic carbon (DOC), one group of suspended solids, and two phytoplankton groups: cyanobacteria, and diatoms simulated as Chl-a, with a constant carbon to chlorophyll a ratio.

The parameters relevant to the hydrodynamic processes were not adjusted and minimal adjustment of the water quality parameters was performed using literature values or direct estimates within default literature ranges.

Assessing Model Performance and Uncertainty

A three-step approach will be taken to assess model performance and address model uncertainty as follows:

1. Descriptive visualization will be used to compare simulated time series and contour plots against observed data and assess whether the model is reproducing the observed characteristics over the correct temporal and spatial scales.
2. Statistical performance tests such as regression testing, correlation coefficients, least squares differences, and more complex tests (see Bennett et al. 2013) will be used if required. The most appropriate performance measures will be selected after a review of the available validation

data. The performance indicators will accommodate the combination of potential spatial and/or temporal (i.e., phase) inaccuracies within the model that may be tolerable but weaken single point and time comparisons against data.

3. Uncertainty inherent in deterministic process-based models such as AEM3D is typically exhaustive, because of the algorithm complexities and the number of parameters they require. Therefore, a list of identified uncertainties will be qualitatively ranked in terms of the level of uncertainty and the likely level of impact that uncertainty has on the project outcomes. A select number of uncertainties with the highest ranking (i.e., high uncertainty with the potential to have a high impact on the project outcomes) will be quantitatively assessed through an ensemble of sensitivity runs that captures the range of the uncertainty. The same metrics used to assess performance against validation data will be used to report uncertainty, and the final selection of both will be made in consultation with the technical reviewer(s). All relevant findings and quantifications of uncertainty will be included in the final report.

The biogeochemical processes algorithms in AEM3D contain numerous rate coefficients that depend on the species in the water and certain site-specific characteristics (e.g., bottom sediment organic content). However, given a particular species group, these coefficients may be viewed as generic and this has been shown in various publications for pathogens, phytoplankton, and up to zooplankton (e.g., Bruce et al. 2006).

The accuracy of simulations will hinge on the availability of adequate boundary condition validation data at strategically placed locations.

The water quality component of AEM3D requires calibration as a result of different species assemblages (e.g., phytoplankton), inadequate mathematical representation of some biogeochemical processes, and state variables or constituents not explicitly included in the model. The ability to have a sound physical basis for the model, both as a result of measurements and because of the physical basis of the model, provides a good foundation upon which to undertake calibration of the ecological component of the model. Wherever possible the ecological theory (e.g., stoichiometry, allometric scaling, etc.), careful consideration of relevant state variables, and literature, will be used to minimize dependence on calibration of the ecological model.

The performance of each iteration of the model undertaken during the calibration exercise will be assessed using the performance criteria identified above. Batches of multiple situations within a range of parameters and/or configurations will be automated. Further calibration and validation will be undertaken against the new field data collected.

Sampling Design

The existing AEM3D model of MB will be used in developing a sediment sampling plan. Sediment cores and bottom water will be collected across MB at locations indicated by the model. The sediment and water data will enable further model refinement and development of a spatial sediment P inventory for MB and an associated conceptual model of the hydrodynamic and biogeochemical drivers of P distributions. The calibrated and validated model will then be used to run scenarios evaluating the effectiveness of P inactivation strategies under differing conditions of future watershed loading. Predicted transient chlorophyll-a and dissolved oxygen concentration distributions across MB will be interpreted to assess impacts on the occurrence of blooms, while water column P concentrations will be used to assess impacts on P dynamics in MB. The cost, permitting feasibility, public acceptance, and ecological impacts of internal P loading management strategies will also be evaluated, compared, and ranked by Stone. When compiled and synthesized, these project outputs will provide the management community with a holistic perspective of available options and possible outcomes associated with interventions aimed at suppressing internal P loading and cyanobacteria blooms in MB.

B2 – Sampling Methods

Existing UVM sediment P data will be supplemented by collection of sediment cores at predetermined locations to capture the spatial distribution of P accumulation and release hot spots in the bay. Schroth and colleagues' existing data indicate that P concentrations vary in time (up to 2X), depth (up to 5X), and space (up to 6X) (*Schroth*, unpublished data). UVM's calibrated AEM3D model will be used to identify areas in the MB of low oxygen and associated P release to guide the monitoring program in its first year (2020). In Year 1, transects (Figure 5) will be developed based on simulation of the number of days each bottom water cell experiences low oxygen conditions (<3 mg/L). Initial plans will have sampling points along each transect (2 North-South, 2 East-West) that are equidistant, but if quartiles of bottom water DO are not capturing the regions of particular concern (areas with the most sustained low DO conditions), we will switch to a stratified approach wherein sampling points are selected at random within each quartile of bottom water DO. We will not sample regions of MB that are 1.5 meters or less, because those shallow waters are not a source of internal P loading and DO conditions never reach this threshold. The sampling plan will be adjusted as needed in Year 2 based on analysis of Year 1 data and consultation with the PAC in February of 2021, as mentioned elsewhere in this QAPP.

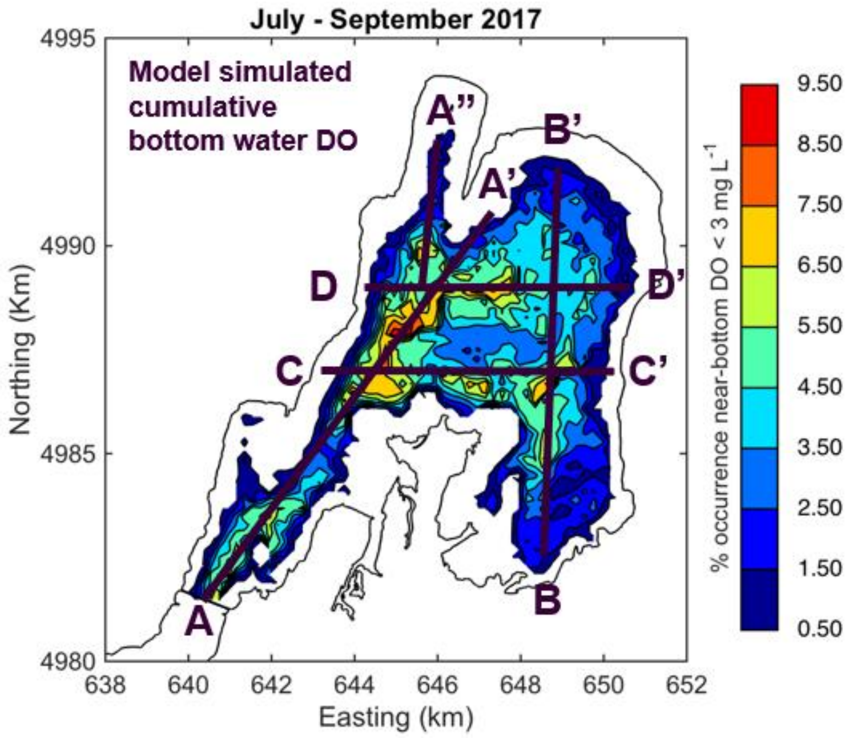

Figure 5. Year 1 sampling transects

One sampling event is planned for the first field season. UVM will collect sediment cores using a gravity corer and polycarbonate core tubes at locations identified using model simulations. A minimum of 10% of sediment cores will be collected and analyzed in duplicate to quantify precision using calculation of percent relative difference (RPD). Sediment cores will be capped and stored in their polycarbonate tubes in a cooler until transported to the shore (or the lab) for in-situ sectioning. Once sectioned, polycarbonate tubes will be rinsed with lake water, and then repurposed for collection of subsequent sediment core samples. Sediment samples will be sectioned as soon as possible on land, frozen, and subsequently freeze dried at the UVM Department of Geology prior to undergoing digestion and extraction procedures.

At the same time and location that each sediment core is collected, a manual cast using a YSI EXO2 sonde will be performed to measure temperature, conductivity, pH, dissolved oxygen, turbidity, fluorescent dissolved organic matter (fDOM), and chlorophyll-a/phycocyanin fluorescence. Data will be collected at half meter intervals from the bottom with an additional measurement made as close to the SWI and surface as possible. At each depth where sensor data are collected, triplicate measurements will be made to quantify precision using relative standard deviation (RSD).

At selected sediment core locations, a 250-mL filtered bottom water sample will be collected using an in-line 0.45 micrometer Pall Supor filter attached to acid clean tubing and a peristaltic pump. A minimum of 10% of water samples will be collected and analyzed in duplicate to quantify precision using calculation of percent relative difference (RPD). Schroth et al. 2015, Giles et al. 2016, Joung et al. 2017 are all examples of the implementation of these sampling protocols.

The field sampling campaign in Year 1 will be performed when conditions on the water are safe. Schroth typically assesses this based on NOAA forecasts with particular emphasis on wind speed, direction, and potential for thunderstorms. In Schroth's 8 years conducting work on Missisquoi Bay, he has found that optimal conditions that are safe for sediment sampling occur with forecasts of 10 mph or lower. If winds are forecast to be higher than that threshold, sampling will not occur. If there is a low percent chance of thunderstorms, the sky and radar will be monitored for potential cells, and the team will stop sampling and take shelter on land if either indicate a thunderstorm in the vicinity of MB. If there is a 50% or greater chance of thunderstorms, the team will not go out. In Year 2 the team will conduct seasonal sampling events under these same safety protocols, but target specific seasonal dynamics based on the historical context of environmental drivers. The team will target the period following peak spring runoff (late May/early June, depending on safe boating conditions), the pre-bloom period, the late summer bloom period in August/early September, and the post bloom fall period (October). The particular dates within these time frames will be determined by safe boating conditions as outlined above and researcher availability, which also may need to be adjusted to manage potential Covid-19 disruptions. These sampling periods are informed by robust contextual information provided by years of monitoring MB that distinguishes these time periods in the context of distinct bloom and P biogeochemical behaviors (e.g. Giles et al. 2016, Isles et al. 2015, 2017a,b).

Spatial distributions of sediment P observed in 2020 will be used to improve the MB AEM3D model parameterization and the simulation of P distributions and dynamics. The refined model will then be used to design a second field campaign (Task 4), in 2021, with input on sampling locations from the project advisory committee. The objectives of the second field campaign will be to further ground truth and refine model simulations, characterize temporal variation in sediment chemistry, and fill in areas either not sampled in 2020 or where discrepancies were observed in 2020. The Year 2 sample number estimates in Table 3 are subject to change based on the Year 1 results and input from the project advisory committee. In Year 2, water samples will be collected at every site where we collect time series sediment cores to help inform trends in the concentrations of P in sediment over time in response to water column seasonal dynamics. The same sediment and water sampling procedures and YSI EXO2 sonde deployment methods will be employed in Year 2 as in Year 1.

In Year 2, approximately 5 grab samples will be collected from zones spanning the range of observed ascorbate-extractable sediment P concentration to evaluate the efficiency of P reactions with aluminum using an assay method (Appendix C). These assay data will be used in estimating the amount of aluminum that would need to be applied (as aluminum sulfate or sodium aluminate) to control internal loading of P from sediment. Grab samples will be collected using a petite ponar dredge. Table 3 summarizes the number of sediment and water samples that we anticipate collecting under this QAPP.

Table 3. Sediment and water sample numbers

		Sediment core intervals	Water samples	Sediment grab samples
Year 1				
	Locations	42	20	0
	Periods/events	x1	x1	0
	Depth intervals	x3	x1	0
	Duplicates	x1.1	x1.1	0
	Year 1 subtotal	139	22	0
Year 2				
	Locations	20	20	5
	Periods/events	x4	x4	X1
	Depth Intervals	x3	x1	x1
	Duplicates	x1.1	x1.1	x1.1
	Year 2 subtotal	264	88	6
Total		403	110	6

Trained personnel will be responsible for sampling operations and collection of field data. Monitoring and sampling methods will be consistent for the duration of the project. Field personnel will be responsible for recording failures of monitoring instruments and taking corrective actions.

B3 – Sample Handling and Custody

Sediment cores will be sectioned at 0-1cm, 1-4 cm, and 4-10 cm depth intervals following Schroth lab's longstanding sediment analysis protocols (Appendix B). Depth splits will be placed in sealed plastic bags. Filtered water samples will be acidified to 1% HNO_3.

Sediment depth splits and water samples will be labelled with unique IDs, project name, sampler identification, and sample date. Samples will be transported on ice in coolers to the laboratory.

Sediment samples will be frozen on arrival at the Rubenstein Ecosystem Science Lab. Table 4 summarizes the preservation conditions by sample type.

Table 4. Sample types to be collected

Matrix	Analytical parameters	Container	Preservation	Hold Time (days)
Sediment	1. Total P, Al, Ca, Fe, Mn 2. Redox sensitive P, Al, Ca, Fe, Mn	Polycarbonate core tube	Frozen after sectioning and then freeze dried	Indefinite after freeze drying
Sediment	Dry bulk density	250-mL plastic jar	None	28 days
Sediment	Redox sensitive P (dithionite)	1-L Ziplock bag	Frozen	Indefinite after freezing
Water	Dissolved P, Al, Ca, Fe, Mn	250-mL plastic bottle	Filtered (0.45 µM Pall Supor); acidified to 1% HNO_3; cool (<4°C)	28 days

B4 – Analytical Methods

After lyophilization, sediment samples will be homogenized and then extracted by ascorbate extraction to determine redox sensitive P and aqua regia to determine total P per Schroth lab's established methods (Appendix B, following *Smith et al.*, 2011 and *Giles et al.*, 2016). Subsequent solutions will be analyzed for P concentration on the UVM Department of Geology's ICP-OES. Filtered and acidified water samples will be analyzed using the same approach for Ca, Mn, and Fe, but the SEAL Autoanalyzer will be used for DP(see those references or specifics of the methods as outlined in Appendix B). These analysis protocols (Table 5) are consistent with data requirements needed to assess internal P loading intervention strategies.

Table 5. Analytical methods

Sample matrix	Analytical parameter	Lab	Method	Reference
Sediment	Total P, Al, Ca, Fe, Mn	Schroth	Extraction: Aqua regia Analysis: ICP-OES	Smith et al. 2011
Sediment	Redox sensitive P, Al, Ca, Fe, Mn	Schroth	Extraction: Ascorbate Analysis: ICP-OES	Smith et al. 2011
Sediment	Redox sensitive P (dithionite)	Lesher	Preparation: Aluminum assay Extraction: Ammonium chloride, Bicarbonate-dithionite, and sodium hydroxide Analysis: Molybdate blue method / Hach spectrophotometer	Lesher et al. (Appendix C)
Sediment	Dry bulk density	AETL	Gravimetry	Grossman and Reinsch 2002.
Water	Dissolved Al, Ca, Fe, Mn	Schroth	ICP-OES	Schroth et al. 2015
Water	Dissolved P	Schroth	Determination of Phosphorus by Semi-Automated Colorimetry (SEAL)	EPA Method 365.1, Revision 2.0

B5 – Quality Control

All data acquired or generated will be documented as to original source, quality, and history. Should any data be determined to be unacceptable, the cause of the failure will be identified where possible. Response actions will typically include repeating questionable measurements.

Accuracy

Accuracy for sediment extractions and digestions will be assessed based on recoveries of an internal reference material, a previously characterized, homogenized sample of Missisquoi Bay sediment. No travel blanks will be collected because the parameters are not susceptible to cross contamination during transport.

Water sample analysis accuracy will be confirmed by analyzing a standard reference material every 10 unknown samples run on the Seal. The reference material for the metals analyses in water is SLRS-6: River Water Certified Reference Material for Trace Metals and other Constituents (http://www.speciation.net/Database/Materials/National-Research-Council-of-Canada-NRC--CNRC/SLRS6-River-Water-Certified-Reference-Material-for-Trace-Metals-and-other-Constituents-;i1312). The reference material for P analysis in water run on the Seal is the Nutrient (low concentration) sample available from USGS (https://bqs.usgs.gov/srs).

Accuracy of sonde measurements will be confirmed during calibration and maintenance prior to each sampling event using standard manufacturer protocols for the YSI EXO2 (e.g. Chapter 4 https://www.ysi.com/File%20Library/Documents/Manuals/EXO-User-Manual-Web.pdf). The date and personnel performing the calibration will be documented in the project records.

Precision

The overall precision of sample collection and analysis will be assessed through collection and analysis of duplicate water samples and sediment cores and grab samples. 10% of water samples and sediment cores and grab samples will be collected and analyzed in duplicate. The relative percent difference (RPD) between analyses of duplicated water samples and duplicated sediment core samples (sectioned at equivalent depths) and grab samples (for the sediment P inactivation assay method) will be calculated as:

$$RPD = (x2 - x1)/((x2 + x1)/2) \times 100$$

Analytical method precision will be assessed through calculation of the standard error of triplicate analysis of homogenized, unknown sediment samples. Every homogenized sediment sample will be analyzed in triplicate. The standard error (SE) calculation is:

$SE = \sigma/\sqrt{(n)}$, where σ = sample standard deviation and n = number of samples

If the standard error of these triplicate analyses is greater than 15%, the associated unknown sample set will be reanalyzed in triplicate.

Precision of the YSI EXO2 sensors will be quantified by taking triplicate readings at each measurement depth and calculating the relative standard deviation among the results at each depth.

Representativeness

In the context of this study, representativeness expresses the degree to which the data gathered accurately and precisely represent field conditions. The sampling program is designed to achieve representativeness by characterizing conditions across Missisquoi Bay. Data representativeness for primary source data will be accomplished through implementing standard sampling procedures and analytical methods which are appropriate for the intended data uses.

Comparability

Comparability expresses the confidence with which one data set can be compared to another. Comparability of the field measurements is ensured by adhering to consistent standard sampling techniques and protocols. Such consistency will be reinforced by training and supervision of field staff.

Completeness

Completeness is a measure of the percentage of planned samples collected or the percentage of usable data points per measurement, with a usable result defined as one that meets criteria for accuracy, precision, and representativeness. Project specific completeness goals account for all aspects of sample handling, from collection through reporting. The minimum completeness objective for the key parameters is determined to be 95 percent.

% Completeness = # of Usable Points / Total # of Data Points Collected x 100

Traceability

Traceability is defined as the ability to trace the generation of each analytical result from sample collection through analysis and reporting. To accomplish this, all activities must be documented. Specific requirements will be met for documenting operation and maintenance of field instrumentation, sample tracking, analytical methodology including NIST traceable standards, record-keeping, data reduction procedures, and data presentation; these requirements are described elsewhere in this document. The data quality objective for traceability with respect to all primary data analyses for all samples is 100 percent.

B6 – Instrument/Equipment Testing, Inspection, and Maintenance

The YSI EXO2 sonde requires routine maintenance per the manufacturer’s operating instructions (https://www.ysi.com/File%20Library/Documents/Manuals/EXO-User-Manual-Web.pdf). Sonde sensors will be inspected, cleaned, and recalibrated in the Rubenstein Ecosystem Science Laboratory prior to each sampling event.

The sediment sampling instruments require minimal maintenance. Field staff will wipe visible material off the sediment coring device and clean the core barrel with water between successive samples. The petite ponar dredge used to collect sediment grab samples will be wiped down to remove visible material and rinsed with water between successive samples,

B7 – Instrument/Equipment Calibration and Frequency

The YSI EXO2 sonde calibration and maintenance information is covered above in B5.

The ICP-OES and Seal calibrations will utilize four standards spanning the anticipated concentration ranges that are synthesized in the matrix of the digestant or extractant under analysis (e.g. ascorbate diluted in 1% HNO_3 or diluted aqua regia) or synthesized in straight 1% HNO_3-acidified water for analysis of collected bottom water samples. Calibration occurs during each instrument run and instrument stability is monitored by running two mid-range P standards for every 10 unknowns run. If a standard deviates from its known concentration by more than 10%, the instrument is recalibrated and those 10 samples preceding the standard that deviated by more than 10% will be rerun. B8 – Inspection Acceptance of Supplies and Consumables

Standards and reference materials will be inspected at the laboratory by the UVM Project Data Manager or designee. Materials will be inspected for signs of defect and their expiration dates will be checked.

B9 – Non-Direct Measurements

Existing data to be assembled, manipulated, and analyzed in completing this evaluation include publicly available, published spatial datasets and tabular water quality, streamflow, and meteorological data. We will acquire weather data and satellite monitoring from NOAA, streamflow data from USGS and Water Canada, and long-term lake and tributary monitoring data from VTDEC/LCBP. These data will be accepted as valid as published by the respective organizations.

Sources of supplementary data considered in this project will include existing sediment and water chemistry and water temperature data from UVM and sediment particle size distribution data from Middlebury College. These unpublished data collected by researchers under other projects are listed in Table 6. These have and will continue to be used to calibrate the initial version of the model and will be leveraged to inform the researchers' sampling plan (along with initial model output, as discussed above). Otherwise, these data are considered contextual information (e.g. Giles et al., 2015; Isles et al., 2015, 2017; Schroth et al., 2015; Joung et al., 2017) that the researchers can draw on from their past experience in interpreting new data derived from this study, but these historical unpublished data are in no way a product of this research, and should not be considered as such by either the funding agency or the research team. Datasets lacking appropriate metadata will not be used in any analysis or delivered to outside agencies. Documentation of provisional datasets will be reviewed to verify references to the use and limitations of the data.

Table 6. Historical data collected at different spatial-temporal scales in MB will be used to calibrate and validate the MB model employed in this study

Organization	Relevant Parameters	Time interval	Source
UVM	Air temperature, relative humidity, shortwave radiation, wind speed and direction, pressure	15 minute (2012-2015, 2017-2020) at UVM monitoring station	Schroth
UVM	Chl-a, phycocyanin, turbidity, conductivity, water temperature, dissolved oxygen, pH, fluorescence, dissolved organic matter[1]	Hourly depth profiles, May through Nov 2012-2020 (excluding 2016) at UVM monitoring station	Schroth
UVM	Missisquoi Bay water and sediment transport (spatially distributed water level, ADCP sensors) and temperature chains	2012-2015 15 minutes from May through Oct.	T. Manley/Co-PI Marti
UVM	Sediment transport analysis (bay-wide composite sampling for grain size distribution analysis)	Composite samples collected in 2014 on a 500-meter grid	P. and T. Manley

Organization	Relevant Parameters	Time interval	Source
UVM	Dissolved and total nutrients, and metals time series	Bottom and surface water total nutrients (3 times per day, May - early Nov., 2012-2015), dissolved nutrients and metals at two depths, weekly over the same time period	Schroth
UVM	Total sediment P and redox sensitive sediment P, metals (top 1 cm of sediment)	Biweekly at UVM monitoring station (S087), Jan.– Nov. 2013, 2014 and 2015	Schroth
UVM	Total sediment P and redox sensitive sediment P, metals (top 1 cm of sediment)	2013 (June, July, Aug., and Sep.) at 12 locations in MB	Schroth
Middlebury College	Sediment grain size distribution map	Summer 2013	P. Manley and T. Manley

[1] *Measured using a YSI EXO2 vertical profiling system.*

B10 – Data Management

The UVM Project Data Manager or designee will be responsible for organization of primary data generation, disbursement, processing, and storage so that the data will be documented, accessible, and secure for the foreseeable time period of its use. The Stone Project Manager will periodically check datasets for completeness.

Standard sample retrieval forms will be used to document field conditions and the location, collection date and time, and personnel responsible for collection of all samples. Copies of all forms will be maintained by UVM.

Secondary data will be used for parameterizing and calibrating models as described in Section B9. At the conclusion of the project all relevant information and electronic data will submitted to the LCBP Project Officer

C – Assessment/Oversight

C1 – Assessments and Response Actions

The Stone Project Manager or designee will review all project outputs. The Stone Project Manager or designee will have the authority to issue a stop work order upon finding a significant condition that would adversely affect the quality and usability of the data. Any corrective actions implemented will be documented by the Stone Project Manager in the quarterly reports described in Section C2 and in the final project report.

If water or sediment quality data are suspect (e.g., RPD of duplicated samples too high, standard error of triplicated sediment analyses regularly exceeding the precision criterion, unusual extreme concentrations), the first response will be to verify that no simple errors have been made. If questions cannot be resolved and suspect concentration data remain, the concentration data may be rejected for that constituent for the sampling event in question.

UVM will conduct and document internal assessments of the MB AEM3D model input data and model parameters to ensure the model is used and performing as intended and that outputs are consistent with inputs and applied assumptions. Quality control checks will be carried out by an independent researcher who has expertise in water quality modelling but has not performed the original model setup and simulations to verify that transfer of field data to model inputs and model parameters is accurate.

NEIWPCC may implement, at its discretion, various audits or reviews of this project to assess conformance and compliance to the Quality Assurance Project Plan in accordance with the NEIWPCC Quality Management Plan. NEIWPCC may issue a stop work order and require corrective action(s) if nonconformance or noncompliance to the Quality Assurance Project Plan is found.

C2 – Reports to Management

The Stone Project Manager will submit quarterly progress reports and a final project report to the LCBP Project Officer. This final report will include a discussion regarding the appropriate use and limitations of the data in terms of quality, as well as all datasets developed within the scope of this project. Additional reports or other information related to project status, concerns, completed deliverables, or any other project needs will be provided when requested.

D – Data Validation and Usability

D1 – Data Review, Verification, and Validation

The data quality will be reviewed for logical consistency and coding errors as identified in appropriate standards. UVM Project Data Manager or designee will be responsible for primary review and decisions regarding the usability or rejection of the data and whether certain samples should be reanalyzed or retaken. Stone Project Manager will be a secondary reviewer responsible for final approval of the data and determining whether any corrective actions are necessary, in accordance with the project objectives and use of the data.

D2 – Verification and Validation Methods

Covered in sections above.

D3 – Reconciliation with User Requirements

At various times throughout the project, situations may arise that will require some degree of corrective action or reconciliation of data, ranging from simple corrections on routine field documentation to systematic problems that may necessitate shutting down a process until the problem is corrected. Deviations from stated work plans and this QAPP will be reconciled with the LCBP Project Officer and the Project QA Manager. Reconciliations will be documented as a memorandum, sent to the LCBP Project Officer, and noted in the final report. If a change is planned that requires an amendment to the QAPP, the amended QAPP will be approved before the change is implemented. If there are limitations regarding the use of data, these will be documented as such, reported to the LCBP Project Officer, and noted in the final report.

In the field, numerous situations, such as equipment or instrument malfunction, may occur that require corrective action. Wherever possible, immediate corrective action will be taken following manufacturer guidelines, and clearly described on an appropriate form. Field personnel noting the problem will document it and bring it to the attention of UVM Project Data Manager. Reconciliation of the situation will be fully documented and included in the final report if data quality may have been impacted.

References Cited Within the QAPP

Bennett ND, Croke BFW, Guariso G, et al. 2013. Characterizing performance of environmental models. Environmental Modelling & Software, 40: 1-20.

Bruce LC, Hamilton D, Imberger J, Gal G, Gophen M, Zohary T, and Hambright KD. 2006. A numerical simulation of the role of zooplankton in C, N and P cycling in Lake Kinneret, Israel. Ecological Modelling 193 (3): 412-436.

Burger DF, Hamilton DP, and Pilditch CA. 2008. Modelling the relative importance of internal and external nutrient loads on water column nutrient concentrations and phytoplankton biomass in a shallow polymictic lake. Ecological Modelling 211: 411-423.

Giles, C.D., P.D.F. Isles, T. Manley, Y.Y. Xu, G.K. Druschel, and A.W. Schroth. 2016. The mobility of phosphorus, iron, and manganese through the sediment-water continuum of a shallow eutrophic freshwater lake under stratified and mixed water-column conditions. Biogeochemistry, 127(1), 15-34, doi:10.1007/s10533-015-0144-x.

Grossman, R.B., and Reinsch, T.G. 2002. Bulk Density and Linear Extensibility. *In* J. H. Dane & G. C. Topp (Eds.), Methods of soil analysis: Part 4, SSSA book series, 5 (pp. 201-210). Madison, WI: SSSA.

Hodges BR, Imberger J, Saggio A, and Winters KB. 2000. Modeling basin-scale internal waves in a stratified lake. Limnology and Oceanography, 45(7): 1603-1620.

Hodges B. and Dallimore C. 2018. Aquatic Ecosystem Model: AEM3D v1.0 User Manual. Hydronumerics.

Huisman, J., G.A. Codd, H.W. Paerl, B.W. Ibelings, J.M.H. Verspagen, and P.M. Visser. 2018. Cyanobacterial blooms. Nat. Rev. Microbiol., 16(8), 471-483, doi:10.1038/s41579-018-0040-1.

Isles, P.D.F., C.D. Giles, T.A. Gearhart, Y.Y. Xu, G.K. Druschel, and A.W. Schroth. 2015. Dynamic internal drivers of a historically severe cyanobacteria bloom in Lake Champlain revealed through comprehensive monitoring. Journal of Great Lakes Research, 41(3), 818-829, doi:10.1016/j.jglr.2015.06.006.

Isles, P.D.F., D.M. Rizzo, Y.Y. Xu, and A.W. Schroth. 2017a. Modeling the drivers of interannual variability in cyanobacterial bloom severity using self-organizing maps and high-frequency data. Inland Waters, 7(3), 333-347, doi:10.1080/20442041.2017.1318640.

Isles, P.D. F., Y.Y. Xu, J. D. Stockwell, and A.W. Schroth. 2017b. Climate-driven changes in energy and mass inputs systematically alter nutrient concentration and stoichiometry in deep and shallow regions of Lake Champlain, Biogeochemistry, 133(2), 201-217, doi:10.1007/s10533-017-0327-8.

Joung, D., Leduc, M. Ramcharitar, B., Xu, Y., Isles, P.D.F., Stockwell, J.D., Druschel, G.K.,Manley, T., Schroth, A.W. 2017, Winter weather and lake-watershed physical configuration drive phosphorus, iron and manganese dynamics in water and sediment of ice-covered lakes. *Limnology and Oceanography.*

Leon LF, Imberger J, Smith RE, Hecky RE, Lam DC, and Schertzer WM. 2005. Modeling as a tool for nutrient management in Lake Erie: a hydrodynamics study. J Great Lakes Res 31: 309-318. https ://doi.org/10.1016/S0380 -1330(05)70323 -3

Leon LF, Smith REH, Hipsey MR, Bocaniov SA, Higgins SN, Hecky RE, Antenucci JP, Imberger J, and Guildford SJ. 2011. Application of a 3D hydrodynamic-biological model for seasonal and spatial dynamics of water quality and phytoplankton in Lake Erie. Journal of Great Lakes Research 37: 41-53.

Levine, S.N., A. Lini, M.L. Ostrofsky, L. Bunting, H. Burgess, P.R. Leavitt, D. Reuter, A. Lami, P. Guilizzoni, and E. Gilles. 2012. The eutrophication of Lake Champlain's northeastern arm: Insights from paleolimnological analyses. Journal of Great Lakes Research, 38, 35-48, doi:10.1016/j.jglr.2011.07.007.

Levine, S. N., A. Lini, M.L. Ostrofsky, H. Burgess-Grant, A. Lami, E. Collyer-Gilles, D. Reuter, L. Schwarting-Miller, and N. Kamman. 2018. The relative roles of point and nonpoint phosphorus sources in the eutrophication of Lake Champlain as recorded in sediment cores. Journal of Great Lakes Research, 44(5), 1043-1056, doi:10.1016/j.jglr.2018.06.005.

Marti CL, Schroth AW, and Zia A. 2019. Physical and biogeochemical processes across seasons in Missisquoi Bay, Lake Champlain: Insights from a three-dimensional model. AGU Fall Meeting, 9-13 December 2019, San Francisco, USA. Oral session. H34C-04.

McCarthy, M.J., W.S. Gardner, M.F. Lehmann, A. Guindon, and D.F. Bird. 2016. Benthic nitrogen regeneration, fixation, and denitrification in a temperate, eutrophic lake: Effects on the nitrogen budget and cyanobacteria blooms. Limnology and Oceanography, 61(4), 1406-1423, doi:10.1002/lno.10306.

Missaghi S, Hondzo M, and Melching C. 2013. Three-dimensional lake water quality modeling: sensitivity and uncertainty analyses. J Environ Qual 42(6): 1684-1698. https://doi.org/10.2134/jeq20 13.04.0120

Paerl, H.W. 2018. Mitigating toxic planktonic cyanobacterial blooms in aquatic ecosystems facing increasing anthropogenic and climatic pressures. Toxins, 10, 76; doi:10.3390/toxins10020076

Paerl, H.W., T.G. Otten and R. Kudela. 2018. Mitigating the expansion of harmful algal blooms across the freshwater-to-marine continuum. Environ. Sci. Technol., 52, 5519-5529.

Pearce, A.R., D.M. Rizzo, M.C. Watzin, and G.K. Druschel. 2013. Unraveling associations between cyanobacteria blooms and in-lake environmental conditions in Missisquoi Bay, Lake Champlain, USA, using a modified self-organizing map. Environmental Science & Technology, 47(24), 14267-14274, doi:10.1021/es403490g.

Preston A, Hannoun IA, List EJ, Rackley I, and Tietjen T. 2014. Three-dimensional management model for Lake Mead, Nevada, Part 2: Findings and applications, Lake and Reservoir Management, 30(3): 303-319, doi: 0.1080/10402381.2014.927942

Romero, J.R., J.P. Antenucci, and J. Imberger. 2004. One- and three-dimensional biogeochemical simulations of two differing reservoirs. Ecol Modell, 174(1-2):143-160.

Rosenberg, B.D., and A.W. Schroth. 2017. Coupling of reactive riverine phosphorus and iron species during hot transport moments: impacts of land cover and seasonality. Biogeochemistry, 132(1-2), 103-122, doi:10.1007/s10533-016-0290-9.

Schroth, A.W., C.D. Giles, P.D.F. Isles, Y.Y. Xu, Z. Perzan, and G.K. Druschel. 2015. Dynamic Coupling of Iron, Manganese, and Phosphorus Behavior in Water and Sediment of Shallow Ice-Covered Eutrophic Lakes. Environmental Science & Technology, 49(16), 9758-9767, doi:10.1021/acs.est.5b02057.

Silva C.P., C.L. Marti, and J. Imberger. 2014. Mitigating the effects of high biomass algal blooms on the drinking water intakes of the city of Buenos Aires, Argentina. Journal of Hydraulic Research, 52: 705-719.

Smith, L., M.C. Watzin, and G. Druschel. 2011. Relating sediment phosphorus mobility to seasonal and diel redox fluctuations at the sediment-water interface in a eutrophic freshwater lake. Limnology and Oceanography, 56(6), 2251-2264, doi:10.4319/lo.2011.56.6.2251.

Trolle D., D.P. Hamilton, M.R. Hipsey, K. Bolding, J. Bruggeman, W.M. Mooij, J.H. Janse, A. Nielsen, E. Jeppesen, J.A. Elliott, V. Makler-Pick, T. Petzoldt, K. Rinke, M.R. Flindt, G.B. Arhonditsis, G. Gal, R. Bjerring, K. Tominaga, J.T. Hoen, A.S. Downing, D.M. Marques, C.R.J. Fragoso, M. Søndergaard, and P.C. Hanson. 2012. A community-based framework for aquatic ecosystem models. Hydrobiologia, 683: 25-34.

U.S. Environmental Protection Agency. 2016. Phosphorus TMDLs for Vermont Segments of Lake Champlain. 72 pp. Retrieved from https://ofmpub.epa.gov/waters10/attains_impaired_waters.show_tmdl_document?p_tmdl_doc_blobs_id=79000

van der Linden L, Daly RI, and Burch MD. 2015. Suitability of a Coupled Hydrodynamic Water Quality Model to Predict Changes in Water Quality from Altered Meteorological Boundary Conditions. Water, *7*(1), 348-361.

Vilhena LC, Hillmer I, and Imberger J. 2010. The role of climate change in the occurrence of algal blooms: Lake Burragorang, Australia. *Limnology and Oceanography, 55(3): 1188-1200.*

Weigel DE, Vilhena LC, Woods P, Tonina D, Tranmer A, Benjankar R, Marti CL, and Goodwin P. 2017. Aquatic habitat response to climate-driven hydrologic regimes and water operations in a montane reservoir in the Pacific Northwest, USA. Aquatic Sciences, doi:10.1007/s00027-017-0544-1.

Xing Z, L.H. Chua, and J. Imberger. 2014. Evaluation of management scenarios for controlling eutrophication in a shallow tropical urban lake. Int J Environ Pollut Remediat, 2(2): 66-72

Zia, A., et al. 2016. Coupled impacts of climate and land use change across a river-lake continuum: insights from an integrated assessment model of Lake Champlain's Missisquoi Basin, 2000-2040. Environmental Research Letters, 11(11), doi:10.1088/1748-9326/11/11/114026.

Appendix A: Sample collection and processing forms

Sediment Core Collection Form

Personnel:______________________________ Date collected:__________________ Weather:____

Coring device: Aquatic Research Instruments NLA Gravity Corer Core tube inside diameter: __6.8 cm

Latitude	Longitude	Core ID	Water depth (m)	Sonde cast file name	Core sample depth intervals (cm)	Bottom water sample collected?	Duplicates collected?	Comment
		MB – __________ – _______ (mmddyyyy) location				Y N	Y N	
		MB – __________ – _______ (mmddyyyy) location				Y N	Y N	
		MB – __________ – _______ (mmddyyyy) location				Y N	Y N	
		MB – __________ – _______ (mmddyyyy) location				Y N	Y N	
		MB – __________ – _______ (mmddyyyy) location				Y N	Y N	
		MB – __________ – _______ (mmddyyyy) location				Y N	Y N	
		MB – __________ – _______ (mmddyyyy) location				Y N	Y N	
		MB – __________ – _______ (mmddyyyy) location				Y N	Y N	
		MB – __________ – _______ (mmddyyyy) location				Y N	Y N	
		MB – __________ – _______ (mmddyyyy) location				Y N	Y N	

Sediment Core Processing Form

Core ID ______________________________

Core Section ID	Freeze Dried?	Subsample collected for BD?	BD subsample volume (mL)	AR Digestion (mmddyyyy)	Asc Extraction (mmddyyyy)	ICP Analysis (mmddyyyy)	ICP Filename
MB – __________ – _______ – _______ – ______ (mmddyyyy) location depth interval (cm)	Y N	Y N					
MB – __________ – _______ – _______ – ______ (mmddyyyy) location depth interval (cm)	Y N	Y N					
MB – __________ – _______ – _______ – ______ (mmddyyyy) location depth interval (cm)	Y N	Y N					
MB – __________ – _______ – _______ – ______ (mmddyyyy) location depth interval (cm)	Y N	Y N					
MB – __________ – _______ – _______ – ______ (mmddyyyy) location depth interval (cm)	Y N	Y N					
MB – __________ – _______ – _______ – ______ (mmddyyyy) location depth interval (cm)	Y N	Y N					
MB – __________ – _______ – _______ – ______ (mmddyyyy) location depth interval (cm)	Y N	Y N					
MB – __________ – _______ – _______ – ______ (mmddyyyy) location depth interval (cm)	Y N	Y N					

Appendix B: Schroth et al. Sediment Analysis Protocols (following *Smith et al.*, 2011)

ASCORBATE EXTRACTION FOR REACTIVE PHOSPHORUS AND METALS

BACKGROUND AND APPLICATION OF THE ASCORBATE EXTRACTION FOR FRESHWATER SEDIMENTS:

The ascorbic acid extraction for reactive P and metals is based on the method of Anschutz et al. (2000) and was first used for Missisquoi Bay sediments by Smith et al. (2011). At alkaline pH (8-8.5), ascorbic and citric acids are deprotonated and take on a net negative charge. Ascorbate will donate an electron (alt.: accept a proton) under these conditions and promote the reductive dissolution of amorphous iron (Fe^{3+} -> Fe^{2+}) and manganese (Mn^{3+} -> Mn^{2+}) oxyhydroxides in the sediment mineral structure. Citrate, a hydroxytricarboxylic acid, will chelate solubilized metals in the 3+ oxidation state, and to a lesser extent, those in the 2+ oxidation state. With the reductive dissolution of amorphous metal-hydroxides, comes the solubilization of P compounds (primarily orthophosphate) associated with this sediment fraction. Amorphous metal-hydroxides are particularly vulnerable to redox shifts and are therefore considered the most ‘reactive’ in environments, which undergo bouts of sediment sub-oxia and anoxia (e.g., eutrophic freshwater lakes, wetlands, marine environments; Wetzel 1999). Phosphorus and metals (Fe, Mn, Ca, Al, etc.) in these extractions tend to be interpreted as the most ‘mobile’ fraction of the sediment, and have been used to estimate sediment P flux in previous studies of Missisquoi Bay (Smith et al., 2011).

REAGENTS

Extraction Solution: To prepare 0.2 L of extractant solution dissolved sodium citrate (10 g) and sodium bicarbonate (10 g) in 0.2 L of deaerated distilled water. Add 4 g L-Ascorbic acid and adjust pH to 8 using sodium hydroxide (10 N) or hydrochloric acid (5 N). The pH can be checked with universal pH strips.

EXTRACTION PROTOCOL:

0.1-0.2 g freeze-dried and ground sediment and 1.5 mL of extractant solution is added to each extraction tube (2 mL, PP snap-cap centrifuge). Tubes are sealed and placed horizontally on a shaker table at 400 rpm for 24 hours at room temperature. At the end of the extraction period, tubes are centrifuged in a microcentrifuge at 14,000 rpm for 10 minutes. One mL of extract supernatant is transferred to a clean 15 mL conical tube (polypropylene or polycarbonate) and diluted to ten mL with distilled water for ICP analysis. Two ICP measurements are made from each tube to ensure sufficient replication, while minimizing the consumption of disposables.

CALCULATING SEDIMENT REACTIVE PHOSPHORUS AND METALS CONCENTRATIONS:

The concentration of reactive P and metals in the sediment (C_{sed}) is calculated as follows:

$$C_{Sed}\left[\frac{mg}{g}\right] = \ \{C_{ICP}\left[\frac{mg}{L}\right] \cdot V_{ext}\ [L]\ \cdot DF\ \}\ /\ DW\ [g]$$

Where C_{ICP} is the concentration in the extract prepared for ICP analysis, V_{ext} is the total volume of the extract (e.g., 0.0015 L), DF is the ICP dilution factor (e.g., 10), and DW is the dry weight of the sediment, which was extracted.

AQUA REGIA ACID DIGESTION FOR PHOSPHORUS AND METALS

BACKGROUND:

The aqua regia digestion method for solids is based on the EPA 3050B method and has been modified for use in an aspirated Gerhardt Kjeldahl digestion block. This method is not a *total* digestion, as it does not target elements bound in silicate structures. The targeted fraction is related to the total fraction of sediment P and metals that would eventually become environmentally available (EPA 3050B). Sediments are heated and refluxed at 100°C in the presence of nitric acid (HNO_3), hydrogen peroxide (H_2O_2), and hydrochloric acid (HCl) for several hours and then allowed to cool and settle overnight. The final digestion solution is diluted ten-fold and then analyzed using inductively-coupled-plasma-optical-emission-spectroscopy (ICP-OES) or ICP-atomic-emission-spectroscopy (ICP-AES).

DIGESTION APPARATI AND MAINTENANCE:

Gerhardt Kjeldahl aluminum digestion block with 40 x 100 mL glass tubes and an aspirator system (Property Jane Hill, jane.hill@dartmouth.edu). Digestions must be carried out in a fume hood with access to a tap. As of January 2014, the digestion unit is located at the University of Vermont, Rubenstein Ecosystem Science Laboratory, Room 204. The aspirator system is attached to the tap by ½" tubing and the tap left to run for the duration of the digestion procedure. Alternatively, the aspirator does not need to be on, so long as the block temperature is sufficient to maintain a gentle boil. For this reason, the prescribed 95°C of the EPA method has been increased to 100-105°C. If aspiration is used, frequently check the attachment of the hose at the back of the aspiration unit, as it has a tendency to detach.

The borosilicate glass digestion tubes (100 mL) must be thoroughly cleaned with Alcanox detergent and acid-rinsed (7.5% HCl bath) prior to use. A tube brush is useful in cleaning the inside bottom of these long tubes. The tubes should be fully dry before adding sediments to prevent the sediments from sticking to the sidewalls (a potential loss of material and source of error in the final measurement). Note that the tubes have been calibrated and marked at the 40 mL line. Check that all lines are visible prior to digestion as this is the final level that the digestion mixture must be brought to with water after the final cooling step. If there is not time to wash and acid-rinse the tubes immediately after emptying them of the digestion contents, they should at least be rinsed with tap water, as dried acid and sediment will be difficult to remove later.

REAGENTS:

1. Nitric Acid, HNO_3 (concentrated)
2. 1:1 (v/v) $H_2O:HNO_3$
3. Hydrogen Peroxide (H_2O_2, 30%)
4. Hydrochloric Acid, HCl (concentrated)
5. Distilled Deionized Water (DDI H_2O)

REACTION PROTOCOL:

***Note:** All steps requiring acid and peroxide should be conducted under a fume hood.*

Step 1: Weigh 0.3 – 0.4 g dry sediment into clean, dry digestion tubes. Prepare a labeling chart, which defines where each sample is in the tube rack as tube labels/ tape will melt and ruin the tubes. Include at least 2 each of blanks and positive controls in each run. Blank tubes contain no sediment. The available positive controls are NIST 1575 (Pine Needles; P = 0.12±0.02%) and NIST 2781 (Domestic Sludge; P = 2.42±0.05%). When the tube rack is prepared it can be placed on the cool digestion block in the fume hood.

Step 2: Add 2 mL of concentrated HNO_3 to each tube using the electronic peristaltic pipettor in rm 204. A 50 mL serological pipet (acid-rinsed borosilicate glass) is filled and 2 mL aliquots of the acid are dispensed into each of the digestion tubes. When the HNO_3 addition is complete, rinse the pipet multiple times with DDI H_2O in the hood sink. Dispense the first two rinses into a waste container.

Step 3: Mix the contents of each tube on a vortex mixer to suspend the sediment.

Step 4: Heat the samples to 100^oC and reflux 10 minutes without boiling. To set the temperature on the control manifold, hold the arrow down in the direction that is needed.

Step 5: Allow the samples to cool for 5 minutes by lifting the tubes out of the block and setting the rack on the upper supports.

Step 6: Add 0.8 mL DDI H_2O to each tube using the electronic repeat pipettor and 20 mL plastic pipet tip.

Step 7: Add 1.2 mL 30% H_2O_2 using a different 20 mL pipet tip. The sample will react strongly to the addition of H_2O_2, particularly if the temperature is still high. Save the pipet tip for Step 8.

Step 8: Carefully vortex each tube and then heat at 100^oC until effervescence subsides.

Step 9: Continue to add 0.4 mL aliquots of 30% H_2O_2 with warming until effervescence is minimal or the general appearance of the sample is unchanged (typically 5x). For organic-rich materials, sample appearance may become lighter in color as dark organic acids are oxidized by the H_2O_2. Do not add more than 4 mL H_2O_2 in this step. Rinse the H_2O_2 tip thoroughly with DDI H_2O after use.

Step 10: Continue heating the HNO_3/H_2O_2 mixture until the volume is reduced to 2 mL or by 30% (2-3 h).

Step 11: Remove the tube rack from heating and place on the upper holder. Allow to cool (5-10 min).

Step 12: Add 4 mL concentrate HCl using a 50 mL pipet (acid-rinsed borosilicate, NOT the same as used for HNO_3) and electronic peristaltic pipettor. Rinse the glass pipet as described in Step 2.

Step 13: Heat at 100^oC for 15-20 min and then cool completely (shut off digestion unit).

Step 14: When the tubes are completely cool, fill the tubes to the 40 mL mark with DDI H_2O. Vortex a final time before allowing the tubes to sit overnight in the hood.

Step 15: Using at 1000 uL pipet, carefully draw off 1 mL of settled digestion solution and transfer into a clean 15 mL conical tube for ICP-OES analysis. Add 9 mL DDI H_2O to each ICP tube to achieve a dilution factor (DF) of 10.

Appendix C: Lesher et al. Sediment P Inactivation Assay Protocol

Analysis of Sediment for Available Phosphorus and Response to Inactivation

Authors: Dr. Emily Lesher, Shaylee Davis, Amanda Darby, Saint Joseph's College

Date Created: 2 October 2020
Last Modified: 21 December 2021

Lab Procedures:

Drying and LOI

1. For each sample, add 5 to 10 grams of the wet sediment pre-massed aluminum trays (for Psenner extractions) and/or crucibles (for LOI). Depending on water content and amount of dry sample needed, consider multiple trays per sample. Tray weight should be recorded to the 0.001 g.
2. Weigh the trays with wet sediment and record weight to the 0.001 g.
3. Place into preheated oven (100-115℃) and dry for 18 hours.
4. After drying, weight the trays or crucibles to determine the water content. Recombine and homogenize dry sediment material from trays and store for Psenner extractions in an airtight, acid-washed container.
5. For loss on ignition, transfer crucibles to a 550℃ furnace for 4 hours.

Alum Dosing and Water Extractions

Aluminum Stock Solutions

The solution preparation instructions that follow are for making aluminum sulfate and sodium aluminate solutions from crystalline hydrated aluminum sulfate and a sodium aluminate concentrated solution sourced from a company that manufactures it for lake remediation projects. Other sources may be used.

- Aluminum Sulfate stock: 100 ml 0.200 M $Al_2(SO_4)_3$, 0.400 M Al^{3+}, **10792 mg/L Al^{3+}** solution. Aluminum Sulfate information:
    - $Al_2(SO_4)_3 \times 18H_2O$
    - *Aluminum Sulfate Hydrate (Crystalline/Certified ACS), Fisher Chemical, Quantity: 500g, Packaging: Poly Bottle, CAS: 7784-31-8, White, Grade: Certified ACS, Melting Point: 86 deg.C, Molecular Formula: Al2H36O30S3 [Al2(SO4)3*18H2O], Molecular Weight: 666.401, Percent Purity: 98.0 to 102.0%, pH: 3 to 4*
    - 0.1 L (0.2 mol of $Al_2(SO_4)_3$/1L)(666.42 g/mol) = 13.33g crystalline hydrated aluminum sulfate.
    - Instructions:
        1. Fill 100 mL plastic volumetric flask halfway with DI water.
        2. Add 13.33 g of aluminum sulfate (solid) and dissolve.
        3. Fill to line.
        4. Confirm concentration against primary standard using ICP-OES

- Sodium Aluminate stock: 100 ml 0.871 M $NaAlO_2$, 0.871 M AlO_2^-, **23500 mg/L Al**. Sodium aluminate information:
    - Made from the raw aluminate solution. "Liquid sodium aluminate", Holland Company does not specify aluminum concentration in this product; lists product as 1.4-1.6 specific gravity, pH >12.5. Assume that aluminum content can vary batch to batch.
    - Instruction below assume an 87 mg/ml (87,000 mg/L) aluminum content.
    - Instructions:
        1. Pipette 27.0 mL raw Holland liquid sodium aluminate product in plastic 100 mL volumetric flask, dilute to 100 mL mark with DI water.
            - 87 mg/mL * 0.27 (DF) = 23.5 mg/mL = 23,500 mg/L
        2. ICP analysis of the diluted stock solution against a primary standard is required. Variations in concentration of stock solution are acceptable and may be accounted for in dosing calculations.

Lake Water Filtration Preparation

1. Water samples should be collected from the target waterbody with no disturbance of sediment or extraneous collection of solids that will interfere with filtration. Filtered lake water is required to initiate alum dosing. Thirty (30) ml of filtered water are required for each dosing for each sample. Depending on the scale of the experiment, 1-2 L are typically collected in acid washed plastic 1L bottles.
2. Rinse bottles with lake water three times and discard, avoiding perturbation.
3. Fill bottles to the top and close tightly. If water will be frozen, allow room for expansion.
4. Transport in cooler with ice pack and keep cold until use within 2 days or frozen for later use.
5. Filter using a 0.45 um glass fiber filter with clean acid washed glassware and vacuum filtration apparatus.
6. Refrigerate filtered water until use within 2 days or frozen for later use.

Sample Preparation: Dosing sediments with variable amounts of alum

1. Label one 50 ml centrifuge tube and four or five (4 or 5) 50 ml Digitubes (SCP Science) for each sample. Digitubes should have sample ID and the following suffixes
    a. _SN (*for supernatant*)
    b. _water (*for water extraction, optional*)
    c. _NH_4Cl (*for filtered ammonium chloride extraction*)
    d. _BD (*for filtered bicarbonate-dithionite extraction*)
    e. _NaOH (*for filtered sodium hydroxide extraction*)
2. Transfer 2 g (+/- 0.05 g) of dried, homogenized sediment into separate, tared 50 ml centrifuge tubes, one for each sequential extraction. Take mass to 0.001 g.
3. Add 30 mL of the filtered lake water using a clean 50 mL tube graduated cylinder or Digitube.
4. Add appropriate volume of aluminum sulfate and sodium aluminate stock solutions by micropipette.
    a. Determine what fraction of the target sediment mass is represented by the 2 g dried sediment placed in tubes for testing = 2 g/(1,000,000 g/m^3 X target sediment depth (m) X solids content of sediment (%/100) X specific gravity).
    b. Choose target dose(s) of Al to be tested (usually ranging from 10 to 100 g/m^2)

   c. For any chosen Al dose, determine the amount of Al to be added to container with 2 g of dried target sediment = dose (g/m^2) X fraction of target sediment represented by 2 g dried target sediment. Convert to mg.
   d. Determine amount of aluminum sulfate stock solution (mL) to be added to container with target sediment = (target Al dose to 2 g sediment (mg) X 2)/(3 X stock aluminum sulfate Al concentration (mg/mL)). This assumes an alum: aluminate ratio by volume of 2:1; alternative ratios can replace the 2 and 3 in this equation if needed.
   e. Determine amount of sodium aluminate stock solution (mL) to be added to container with target sediment = (target Al dose to 2 g sediment (mg) X 1)/(3 X stock sodium aluminate Al concentration (mg/mL)). This assumes an alum: aluminate ratio by volume of 2:1; alternative ratios can replace the 1 and 3 in this equation if needed.

5. Measure and record the pH.
6. If necessary, add small volumes of 0.1 M NaOH to adjust pH to between 6.5 and 7.5. Record final pH.
7. Shake samples for 48 hours (+/- 4 hours) on orbital rotator.
8. After 48 hours, centrifuge tubes at 3000 RPM for 15 minutes.
9. After centrifugation, pour as much of the supernatant into the labeled Digitube (hold the inverted centrifuge tube until almost no water comes out, the pellet should remain fairly intact in the bottom of the centrifuge tube). The centrifuge tube containing the pellet of sediment is retained for the Psenner Extraction procedure in the next section.
   a. If the pellet does not remain intact, centrifuge a second time, and consider increasing the RPM.
   b. The supernatant is the "Water Extraction". Filter and analyze this solution according to steps c-j below only if there is an interest in the amount of P released during this process, which is usually inconsequential in the context of Psenner analysis. Discard if no analysis is needed.
   c. Attach a 0.45 um Digifilter (SCP Sciences) to the Digitube containing the supernatant.
   d. Place the red plug into the Digifilter hole that is on the same side of the filter as the water so no water leaks out.
   e. Attach a second Digitube to the other side of the Digifilter.
   f. Invert the apparatus and connect to a Digifilter manifold port, by way of the second hole, which is now below the filter.
   g. Open any valves that are in use to provide suction, ensure any that are not in use are closed.
   h. Turn on vacuum pump to filter samples.
   i. Remove the digitube with the now filtered water and add 2 drops of 50% HNO_3 using a plastic transfer pipette, if storing for potential analysis. Cap tightly.

<u>Psenner Extractions</u>

Psenner Extraction Solutions

1. Ammonium chloride (extraction 1, 1 M NH_4Cl, extracts labile P fraction)
   a. Partially fill a 1L plastic volumetric flask with fresh DI water.

   b. Add 67 grams of solid ammonium chloride.
   c. Let dissolve fully.
   d. Fill to the 1L mark with more water.
   e. Adjust the pH between 7-8 if necessary, by adding 1M of sodium hydroxide (this raises the pH).
2. Bicarbonate-dithionite (BD) solution (extraction 2, 0.11 M bicarbonate, 0.11 M dithionite, extracts iron-bound/reducible P fraction)
   a. Partially fill a 1L plastic flask with fresh DI water
   b. Add 9.2 grams of sodium bicarbonate.
   c. Let dissolve fully.
   d. Fill to the 1L mark with more water.
   e. Before each dithionite extraction, add 4.8 grams of sodium hydrosulfite (sodium dithionite) to 250 mL of the bicarbonate solution. This step must be completely the day this extraction takes place.
3. Sodium hydroxide solution (extraction 3, 0.1 M NaOH, extracts aluminum-bound and organic P fraction)
   a. Partially fill a 1L plastic flask with fresh DI water
   b. Add 40.00 grams of sodium hydroxide pellets.
   c. Let dissolve fully.
   d. Add more water to bring to the 1L mark.
   e. Dilute this 10x (100 mL to 1L) to get to 0.1M that will be used in the extractions.

Psenner Extractions Procedure

1. First extraction step:
   a. Add 30 mL of 1 M NH_4Cl to each sediment sample, which are in the 50 ml centrifuge tubes.
   b. Vigorously shake the suspensions by hand for 10 seconds, and then load onto orbital rotator or shaker table and shake for 2 hr.
   c. Centrifuge suspensions at 3000 RPM for 15-20 min
   d. After centrifugation, pour as much of the supernatant into the "_SN" labeled Digitube (hold the inverted centrifuge tube until almost no liquid comes out, the pellet should remain fairly intact in the bottom of the centrifuge tube). The centrifuge tube containing the pellet of sediment is retained for the second extraction.
      i. If the pellet does not remain intact, centrifuge a second time, and consider increasing the RPM.
      ii. Attach a 0.45 um Digifilter (SCP Sciences) to the Digitube containing the supernatant.
      iii. Place the red plug into the Digifilter hole that is on the same side of the filter as the water, so no water leaks out.
      iv. Attach a second Digitube ("_NH_4Cl") to the other side of the Digifilter.
      v. Invert the apparatus and connect to a Digifilter manifold port, by way of the second hole, which is now below the filter.
      vi. Open any valves that are in use to provide suction, ensure any that are not in use are closed.
      vii. Turn on vacuum pump to filter samples.
   e. Acidify the supernatant with 6 drops of 50% HNO_3

    f. Discard Digifilter. Retain and rinse the "_SN" Digitube for re use.

2. Second extraction step: *NOTE - Before starting BD solution-making, make sure the ICP is available to run BD extracts the next day. BD extracts must be run within 24 hours and ideally immediately after filtration.
    a. Add 30 mL of 0.11 M bicarbonate-dithionite (BD) to the wet sediment pellet retained from the previous extraction in the 50 ml centrifuge tube.
    b. Vigorously shake the suspensions by hand for 10 seconds, and then load onto orbital rotator or shaker table and shake for 24 hr.
    c. Centrifuge suspensions at 3000 RPM for 15-20 min
    d. After centrifugation, pour as much of the supernatant into the "_SN" labeled Digitube (hold the inverted centrifuge tube until almost no liquid comes out, the pellet should remain fairly intact in the bottom of the centrifuge tube). The centrifuge tube containing the pellet of sediment is retained for the third extraction.
        i. If the pellet does not remain intact, centrifuge a second time, and consider increasing the RPM.
        ii. Attach a 0.45 um Digifilter (SCP Sciences) to the Digitube containing the supernatant.
        iii. Place the red plug into the Digifilter hole that is on the same side of the filter as the water, so no water leaks out.
        iv. Attach a second Digitube ("_BD") to the other side of the Digifilter.
        v. Invert the apparatus and connect to a Digifilter manifold port, by way of the second hole, which is now below the filter.
        vi. Open any valves that are in use to provide suction, ensure any that are not in use are closed.
        vii. Turn on vacuum pump to filter samples.
    e. Just prior to ICP analysis, dilute 1:10 with DI water. Pipette 1 mL of BD extraction solution into a 15 ml centrifuge tube and add 9.0 mL of DI water by mass (9.00 g). Acidify with 2 drops of 50% HNO_3.

3. Third extraction step:
    a. Add 30 mL of 0.1 M sodium hydroxide (NaOH) to the wet sediment pellet retained from the previous extraction in the 50 ml centrifuge tube.
    b. Vigorously shake the suspensions by hand for 10 seconds, and then load onto orbital rotator or shaker table and shake for 24 hr.
    c. Centrifuge suspensions at 3000 RPM for 15-20 min
    d. After centrifugation, pour as much of the supernatant into the "_SN" labeled Digitube (hold the inverted centrifuge tube until almost no liquid comes out, the pellet should remain fairly intact in the bottom of the centrifuge tube). Discard or archive the centrifuge tube containing the pellet of sediment.
        i. If the pellet does not remain intact, centrifuge a second time, and consider increasing the RPM.
        ii. Attach a 0.45 um Digifilter (SCP Sciences) to the Digitube containing the supernatant.
        iii. Place the red plug into the Digifilter hole that is on the same side of the filter as the water, so no water leaks out.
        iv. Attach a second Digitube ("_NaOH") to the other side of the Digifilter.

   v. Invert the apparatus and connect to a Digifilter manifold port, by way of the second hole, which is now below the filter.
   vi. Open any valves that are in use to provide suction, ensure any that are not in use are closed.
   vii. Turn on vacuum pump to filter samples.

e. Just prior to ICP analysis, dilute 1:100 with DI water. Pipette 0.1 mL of NaOH extraction solution into a 15 ml centrifuge tube and add 9.9 mL of DI water by mass (9.90 g). Do not acidify.

ICP-OES Analysis of Extracts

ICP-OES Standard Preparation

Analyze NH_4Cl and BD extractions against a calibration curve composed of acidified standards. These standards are stable for 2 months. For NaOH extractions, make standards in 0.01 M NaOH, which are only stable for 24 hours.

For acidified standards:

The calibration standards contain concentrations of P, Fe, Al defined in the table below.
The Primary Standard is called QCP-QCS-1(Perkin-Elmer) and contains 500 mg/L P, 100 mg/L Al, Fe
Notes on using primary standards:

- NEVER put anything into the primary standard container (pipette or anything else.) Pour a bit of the standard (just a little more than you need) into a clean tube and pipette from there.

Dilution table for Standards (make them in the order listed):

Standard	aliquot of QCP-QCS-1, mL	aliquot of STANDARD 4, mL	Total volume, ml	[P], mg/L in standard	[Al], [Fe] in standard
4	5		50		10
3	0.5		50	5	1
2		1	50	1	0.2
1		0.1	50	0.1	

1. Standard 4: Pipette 5.000 mL of QCP-QCS-1 into a 50ml plastic Digitube (SCP Science). Fill with DI water and 6 drops of 50% HNO_3 (trace metal grade, sometimes labelled as 1+1 HNO_3) to the 50 mL mark. It is probably best to use a 1 mL (1000 uL pipette) 5 times.
2. Standard 3: Pipette 0.500 mL (500 uL) of QCP-QCS-1 into a 50ml plastic Digitube (SCP Science). Fill with DI water and 6 drops of 50% HNO_3 to the 50 mL mark.
3. Standard 2: Pipette 1.000 mL (1000 ul) of Standard 4 into a 50 mL plastic Digitube (SCP Science). Fill with DI water and 6 drops of 50% HNO_3 to the 50 mL mark.

4. Standard 1: Pipette 0.100 mL (100 uL) of Standard 4 into a 50 mL plastic Digitube (SCP Science). Fill with DI water and 6 drops of 50% HNO_3 to the 50 mL mark.

For standards in NaOH (for running NaOH extracts)

Dilution table for NaOH Standards (make them in the order listed, same as for acidified):

Standard	aliquot of QCP-QCS-1, mL	aliquot of STANDARD 4, mL	dil to, ml	[P], mg/L	[Al], [Fe], [Ca]
4	5		50	50	10
3	0.5		50	5	1
2		1	50	1	0.2
1		0.1	50	0.1	0.02

5. Standard 4: Pipette 5.000 mL of QCP-QCS-1into a 50ml plastic Digitube (SCP Science). Fill with DI water and 0.45 mL 0.1 M NaOH to the 50 mL mark. It is probably best to use a 1 mL (1000 uL pipette) 5 times.
6. Standard 3: Pipette 0.500 mL (500 uL) of QCP-QCS-1 into a 50ml plastic Digitube (SCP Science). Fill with DI water and 0.45 mL 0.1 M NaOH to the 50 mL mark.
7. Standard 2: Pipette 1.000 mL (1000 ul) of Standard 4 into a 50 mL plastic Digitube (SCP Science). Fill with DI water and 0.45 mL of 0.1M NaOH to the 50 mL mark.
8. Standard 1: Pipette 0.100 mL (100 uL) of Standard 4 into a 50 mL plastic Digitube (SCP Science). Fill with DI water and 0.45 mL of 0.1M NaOH to the 50 mL mark.

Creation of Spike Samples

- Combine 7 mL of the desired sample (diluted samples in the case of BD and NaOH extracts) and add 0.2 mL of the standard making solution (QCP-QCS-1) in a 15 ml centrifuge tube.

ICP-OES Analysis Procedure

1. Most details and instrument specific parameters will vary with the spectrometer. Sample and gas flow rates, power, wavelength ranges and baselines should be optimized. Calibrate detector according to instrument manual.
2. Run phosphorus in axial mode, iron and aluminum in radial mode.
3. Construct a calibration curve using the following standards
    a. P: blank and standards 1, 2, and 3
    b. Fe and Al: blank and standards 2, 3, and 4
    c. Calibration curves for all elements should have greater than 0.999 correlation coefficient.
4. Run Standard 3 as a Continuing Calibration Verification (CCV) QA every 10 samples, or more frequently.

Spectroscopic Determination of Aluminum vs. Organic-bound P

The NaOH extraction dissolves aluminum oxides and solubilizes organic matter. Thus, two pools of phosphate are present in this extract: phosphate that was bound as a surface complex to solid phase aluminum, and phosphorus contained in organic compounds and natural organic matter. The ICP-OES analysis of the NaOH extract measures both forms, giving us a Total P in this extraction. A UV-Vis spectrophotometric determination of P, via the production of the blue-colored phosphomolybdenum complex, gives us the inorganic aluminum-bound phosphate because only phosphate reacts through the reaction mechanism of this technique, not P within an organic molecule.

Sample Preparation

1. Make a 1:50 dilution of the 0.01 M NaOH extract with DI water, combining 1 mL of the extract in a digitube and diluting to 50 ml.
2. Neutralize. Add one drop of phenolphthalein to each sample; the sample should turn pink. Add 1M H_2SO_4 dropwise until pink color just disappears.

Standard Preparation

Calibrate the UV-Vis spectrophotometer with 5 standard solutions for the initial calibration. Once a calibration curve is established, subsequent analyses can rely on the 100 ppb standard as a check standard. Run a full calibration curve every 6 months.
All standards are made from a 5 mg/L (ppm) phosphate stock solution. For each standard, pipette the stock solution into a clean, labeled 50mL Digitube, and fill carefully to the 50 mL mark with DI water.
Use a 100-1000 ul pipette for volumes greater than 0.2 ml. Use twice if necessary. Use a 20-200 ul pipette for 0.1 or 0.2 ml.

- 10 ppb = 0.10 mL (100 uL) of 5 ppm stock dilute to 50 mL
- 20 ppb = 0.20 mL (200 uL) of 5 ppm stock dilute to 50 mL
- 50 ppb = 0.50 mL (500 uL) of 5 ppm stock dilute to 50 mL
- 100 ppb = 1.00 mL (1000 uL) of 5 ppm stock dilute to 50 mL – best for NaOH extracts
- 150 ppb = 1.50 mL (750 ul TWICE) of 5 ppm stock dilute to 50 mL

Reagent Preparation

General Reagent Prep Requirements

- The Combined Reagent must be made fresh and used within 2 hours. The ingredients for the Combined Reagent must be freshly made or stored properly prior to use. The ascorbic acid MUST be prepared fresh right before use.
- All reagents must be prepared in dedicated or freshly acid-washed plasticware or glassware (depending on the reagent).
- DI water must be freshly drawn and stored for the day in acid washed containers or wash bottles.
- When making the Combined Reagent, all reagents must reach room temperature before they are mixed and must be mixed in the order given below.
- Instructions for preparation and storage of reagents:
    1. Sulfuric acid solution, 5N: Slowly add 70 mL of conc. H_2SO_4 (CASRN 7664-93- 9) to approximately 400 mL of reagent water. Cool to room temperature and dilute to 500 mL with reagent water.

2. Antimony potassium tartrate solution: Weigh 0.3 g K(SbO)C4H4O6•1/2H2O (CASRN 28300-74-5) and dissolve in 50 mL reagent water in 100 mL volumetric flask, swirl, then fill to 100ml mark (dilute to volume). Store at 4°C (REFRIGERATOR) in a dark bottle, ideally with a glass stopper**.** A funnel can help transfer in the antimony potassium tartrate. Rinse the funnel and the dish into the flask to ensure full mass is transferred
3. Ammonium molybdate solution: Dissolve 4 g $(NH_4)_6Mo_7O_{24}\cdot 4H_2O$ (CASRN 12027-67-7) in 100 mL reagent water, stir, then fill to 100ml mark. Store in a plastic bottle at 4°C (REFRIGERATOR).
4. Ascorbic acid, 0.1M: Dissolve 1.8 g of ascorbic acid (CASRN 50-81-7) in 100 mL of reagent water, stir, then fill to 100ml mark. MAKE FRESH DAILY.

All reagents must reach room temperature before they are mixed and must be mixed in the order given below. If turbidity forms in the combined reagent, shake and let stand for a few minutes until the turbidity disappears before processing. This combined reagent is good for four hours.

- Each 50 mL sample needs 8 mL of combined reagent. Multiply the number of samples to be analyzed by 8 to calculate how much combined reagent will be needed, including standards.
- To make 100mL of combined reagent, add these reagents, in the order listed, in a graduated cylinder. Mix cylinder contents after each solution is added.
    - 50 mL 5 N H_2SO_4
    - 5 mL potassium antimony tartrate
    - 15 mL ammonium molybdate
    - 30 mL ascorbic acid solution (freshly made)

Sample Analysis/Generation of the Phosphomolybdenum Blue Complex:

1. Samples and standard(s) should be in 50 ml digitubes, at a volume of 50 ml.
2. If constructing a new calibration curve, begin by analyzing the standards, and generate a curve of absorbance versus concentration. If using a previous calibration, begin the analysis by measuring absorbance on the 100 ppb check standard. Only when the calibration curve is built, or the check standard verifies the existing calibration, should you begin adding combined reagent to samples.
3. To analyze samples or standards, add 8 mL of combined reagent (measured in a graduated cylinder) to each sample or standard in the Digitubes. There is enough room above the graduations to add the reagent directly.
4. Measure absorbance at a wavelength of 890 nm after 10 minutes but **before** 30 minutes has elapsed.
5. Using the previously defined calibration curve, convert absorbance of each unknown to ppb P.

Appendix D: Method 365.1, Revision 2.0: Determination of Phosphorus by Semi-Automated Colorimetry

Appendix B

Supplemental Tables and Figures for Model Parameterization, Calibration, and Verification

Table A1. *Relevant sampling stations and data used for this study.*

	Sampling locations		**Automated sensors**				**Manual sampling**				
	Site name/code	**Details**	**Meteorology**	**Water level/ discharge**	**Water quality**		**Water quality**		**Phyto-plankton**	**Sediment physical char.**	**Sediment chemical char.**
					Profiling[1]	**Samples[2]**	**Profiling[3]**	**Samples[4]**			
Missisquoi Bay Catchment	04294000[5]	Missisquoi River (44° 55.00' N, 73° 7.73' W)		1990-2021 15min/daily[6]							
	MISS07[7]	Missisquoi River (44° 55.23' N, 73° 07.63' W)						1990-2021 biweekly[8,9,10]			
	030424[11]	Pike River (45° 09.52' N, 73° 03.05' W)		2001-2021 15min/daily[6]							
	PIKE01[7]	Pike River (45° 07.38' N, 73° 04.18' W)						1990-2021 biweekly[8,9,10]			
	030425[11]	Rock River (45° 01.32' N, 73° 00.97' W)		2001-2021 15min/daily[6]							
	ROCK02[7]	Rock River (44° 59.49' N, 73° 04.22' W)						2007-2021 biweekly[8,9,10]			
Missisquoi Bay	50[12,13]	Located near the outlet of the bay (depth ~4 m) (45° 00.80' N, 73° 10.43' W)					1992-2021 biweekly[8,14]	1992-2021 biweekly[9,15]			
	53[12,13]	Located in the center of the bay (depth ~5 m) (45° 02.13' N, 73° 07.53' W)					2006-2021 biweekly[8,14]	2006-2021 biweekly[9,15]			
	High-Frequency Buoy (HFB)[16]	Located in the southeast quadrant of the bay (depth ~ 3.5 m) (44° 59.51' N, 73° 6.78' W)			2017-2021 hourly[8,17]	2017-2021 daily/weekly[8,18]			2017 weekly[8,19]		
	Philipsburg[20]	Located in the northeast corner of the bay (45° 2.38' N, 73° 4.77' W)		2017-2021 15min/daily[6,21]							
	Bed[22]	Survey across multiple locations								2013[23]	2013/2014[24], 2020[25]
External	04295000[6]	Richelieu R (Lake Champlain) at Rouses Point, NY (44° 59.76' N, 73° 21.62' W)		2007-2021 15min/daily[6, 21]							
	Colchester Reef[26]	Located in Lake Champlain, VT (44° 33.31' N, 73° 19.74' W)	1996-2021 15 min[6]								
	Burton Island[27]	Located in Lake Champlain, VT (44° 45.992' N, 73° 12.801' W)	2010-2021 15 min[6]								
	Venise Bay[28]	Located in the northwest part of the bay (45° 5' N, 73° 9' W)	2012-2021 15 min[6]								
	Burlington International Airport[29]	(44° 28.09' N, 73° 8.99' W)	2017-2020 hourly/daily[6]								

Note: For the locations of the sampling stations, see Figure 13

[1] Depth, water temperature, dissolved oxygen, pH, conductivity, turbidity, phycocyanin fluorescence, and chlorophyll *a* fluorescence. [2] Ammonia, nitrate, total dissolved nitrogen, total nitrogen, soluble reactive phosphorus, total dissolved phosphorus, and total phosphorus. [3] Depth, water

---

temperature, dissolved oxygen, pH, conductivity, and chlorophyll *a* fluorescence. [4]Ammonia, nitrite+nitrate, total nitrogen, soluble reactive phosphorus, dissolved phosphorus, total phosphorus, dissolved organic carbon, dissolved inorganic carbon, total organic carbon, dissolved silica, total suspended solids, water temperature, dissolved oxygen, pH, conductivity, chlorophyll *a*, and Secchi disk depth. [5]U.S. Geological Survey monitoring gage (https://waterdata.usgs.gov/usa/nwis/uv?#). [6]Recorded *throughout the year.* [7]Lake Champlain Long-term Monitoring - Tributary monitoring site (https://anrweb.vermont.gov/dec/_dec/LongTermMonitoringTributary.aspx). [8]Sampled from May to mid-October each year (exact dates varied among years). [9]Dissolved oxygen, chlorophyll *a*, dissolved silica, and Secchi disk depth not sampled in the tributaries.[10]Sample obtained using depth and velocity-integrating sampling devices. [11]Quebec Ministère de l'Environnement et de la Lutte contre les changements climatiques monitoring gauge (https://www.cehq.gouv.qc.ca/hydrometrie/historique_donnees/fiche_station.asp?NoStation=#). [12]Lake Champlain Long-term Monitoring - Lake Champlain monitoring site (https://anrweb.vermont.gov/dec/_dec/LongTermMonitoringLakes.aspx). [13]Lake Champlain Long-term Monitoring - Multi-Probe sonde Profiles site (https://anrweb.vt.gov/DEC/_DEC/MultiProbeSonde.aspx). [14]Measurements taken in vertical profiles at discrete depths (every ~1 m). [15]Water samples taken at discrete depths and then combined to form vertical water column composites.[16]VT EPSCoR BREE high-frequency monitoring buoy (http://epscor.uvm.edu/StAlbans/). [17]Measurements taken at discrete depths (every ~0.50 m). [18]Samples taken for surface (~0.5 m below surface) and bottom (~0.5 m above bottom) water column conditions. [19]Samples taken as a vertically integrated composite of the photic zone, defined as twice the Secchi disk depth. [20]Government of Canada Water Office monitoring gauge (https://wateroffice.ec.gc.ca/report/historical_e.html?stn=02OH001). [21]Recorded water level only. [22] Sampled opportunistically in space and time. [23]Sediment cores taken within the top 15 cm of the bottom and analyzed for grain size distribution (Manley, P. and Manley, T., *unpublished*). [24]Sediment cores taken within the top 1 cm of the bottom and analyzed for reactive phosphorus (Giles et al., 2016). [25]Sediment cores taken within the top 10 cm of the bottom and analyzed for total phosphorus and dry bulk density. [26]The Forest Ecosystem Monitoring - Colchester Reef Meteorological Monitoring (https://www.uvm.edu/femc/data/archive/project/colchester-reef-meteorological-monitoring-38-m). [27]The Forest Ecosystem Monitoring - Burton Island Meteorological Monitoring (https://www.uvm.edu/femc/data/archive/project/burton-island-meteorological-monitoring). [28]Middlebury College (Manley, T.). [29]NOAA - National Centers for Environmental Information - Local Climatological Data (https://www.ncdc.noaa.gov/cdo-web/datatools/lcd).

Table A2. *Missisquoi Bay model: bathymetry, parameters, boundary forcing and initial conditions, validation and calibration data sources.*

Model components	Sub-components	Calibration/Validation
Bathymetry and setup	Domain grid type	Uniform
	Horizontal grid discretization	250 m
	Vertical grid discretization	0.25 m
	Time step	200 s
	Simulation period	1 June 2017 - 31 December 2019 (Calibration) 1 January 2020 - 31 December 2021 (Validation) 1 January 2010 - 31 December 2021 (Baseline period)
Parameters	Hydrodynamic and biogeochemical processes	Parameters relevant to the hydrodynamic processes were not adjusted. Minimal adjustment to the biogeochemical processes parameters was performed using literature values or direct estimates within default literature ranges. See Table A3.
Boundary forcing	Meteorological	Assumed uniform over the free surface of the model domain. 15 min time series of air temperature (Colchester Reef, Burton Island, Venise Bay and HBF), relative humidity (Colchester Reef, Burton Island, Venise Bay and HBF), shortwave radiation (Colchester Reef, Burton Island and HBF), wind speed and direction (Colchester Reef, Burton Island, Venise Bay and HBF), hourly time series of cloud cover (Burlington Airport), and daily time series of rainfall (Burlington Airport).
	Inflows	Daily time series of discharge rates for the Missisquoi River (04294000[1]), Pike River (030424) and Rock River (030425). Daily time series of water temperature[2] and dissolved oxygen[3] for all inflows. Daily time series of nutrients and suspended solids concentrations for all inflows[4]. Monthly time series of chlorophyll *a* concentrations for each algal group simulated[5].
	Open boundary[6]	Daily time series of water level (04295000).
Initial conditions	Water surface elevation	Uniform (04295000)
	Water temperature and DO	Horizontally and vertically interpolated (50[7] and 53[7]).
	Chlorophyll *a* and algae groups	Horizontally interpolated and vertically uniform (50[8] and 53[8]).
	Nutrients and suspended solids	Horizontally interpolated and vertically uniform (50[8] and 53[8]).
Validation and calibration	Water level	Daily times series of water level (Philipsburg).
	Water temperature and DO	Profiles (HFB[9], 50[7], 53[7]) and discrete depth samples (50[8], 53[8]).
	Chlorophyll *a*	Discrete depth samples (50[8], 53[8]).
	Nutrients	Discrete depth samples (HFB[10], 50[8], 53[8]).

Note: Sampling stations in brackets (see Figure 13 for locations and Table A1).

[1] Divided into four tributaries discharging into Missisquoi Bay: Dead Creek (57%), Missisquoi River branches: North East (15%), Central (14%) and North West (14%), numbers in brackets indicate percentage of the total discharge assigned to each tributary (Mainly, T., *pers. comm.*). [2] Estimated as four-day running average of 15-minute time series of air temperature (Colchester Reef, Burton Island, Venise Bay and HBF) (Silva et al., 2014b). [3] Computed dissolved oxygen concentration at saturation as a function of water temperature and corrected by altitude (Tranmer et al., 2020). [4] Estimated using WRTDS-K (Zhang and Hirsch, 2019) from continuous discharge and intermittent concentration data (total nitrogen, dissolved phosphorus, total phosphorus and total suspended solids) using historical data for Missisquoi River (04294000 and MISS01), Pike River (030424 and PIKE01), and Rock River (030425 and ROCK02). [5] Obtained from a previous study (LimnoTech, 2012). [6] Located at southern edge of the model grid at the Highway 78 bridge causeway (Figure 1). [7] Manual sampling - Water quality profiling. [8] Manual sampling - Water quality sample lab-analyzed. [9] Automated sampling - Water quality profiling. [10] Automated sampling - Water quality sample lab-analyzed.

Table A3. *List of selected parameters used for AEM3D simulations presented in this study.*

Parameter description	Units	Values and references
Thermodynamics		
Mean albedo for short-wave radiation	-	0.08[a]
Mean albedo for long-wave radiation	-	0.03[a]
Background extinction coefficient of pure water	m^{-1}	0.25[a]
Extinction coefficient for near infrared radiation	m^{-1}	1.0[a]
Extinction coefficient for ultraviolet A wavelength	m^{-1}	1.0[a]
Extinction coefficient for ultraviolet B wavelength	m^{-1}	2.5[a]
Bulk transfer coefficient for heat at air-water interface	-	0.0013[b]
Bulk transfer coefficient for momentum at air-water interface	-	0.0013[b]
Turbulent mixing		
Mixing coefficients: Wind stirring	-	1.33[c]
Bottom generation of TKE	-	2.2[d]
Shear generation of TKE	-	0.15[c]
Energy generated from conv. overturn	-	0.2[c]
Dissipation of excess energy	-	1.15[c]
Bottom drag coefficient	-	0.002
Dissolved oxygen (DO)		
Temperature multiplier of sediment fluxes	-	1.08[e]
DO half-saturation constant for nutrient sediment fluxes	mg DO L^{-1}	1.0[f]
Static DO consumption rate by sediments	g DO m^{-2} day^{-1}	2.0[g]
Phosphorus (P), Filterable Reactive Phosphorus (PO$_4$), Dissolved Organic Phosphorus (DOP)		
Ratio of P to Chlorophyll *a*	mg P [mg Chl-*a*]$^{-1}$	0.3[h]
Max mineralization of DOP labile to PO$_4$	day^{-1}	0.01[i]
Release rate of PO$_4$ from sediments	g P m^{2} day^{-1}	0.012[j]
Nitrogen (N), Nitrate (NO$_3$), Ammonium (NH$_4$), Dissolved Organic Nitrogen (DON)		
Ratio of N to Chlorophyll *a*	mg N [mg Chl-*a*]$^{-1}$	9.0[h]
Max mineralization of DON labile to NH$_4$	day^{-1}	0.03[i]
Nitrification stoichiometry ratio of DO to N	mg DO [mg N]$^{-1}$	3.43[h]
Release rate of NH$_4$ from sediments	g N m^{-2} day^{-1}	0.30[i]
Nitrification rate	day^{-1}	0.075[j]
DO half-saturation constant for nitrification	mg DO L^{-1}	1.0[j]
Denitrification rate	day^{-1}	0.25[f]
DO half-saturation constant for denitrification	mg DO L^{-1}	1.0[j]
Cyanobacteria, diatoms		
Photosynthetic stoichiometry ratio of DO to Carbon (C)	mg DO [mg C]$^{-1}$	2.67[h]
Ratio of C to Chlorophyll *a*	mg C [mg Chl-*a*]$^{-1}$	60[k], 40[k]
Fraction of algal DO lost to photosynthetic respiration	-	0.014[l]
Maximum growth rates of algae	day^{-1}	0.875[e], 1.75[e]
Respiration rate coefficient	day^{-1}	0.05[e], 0.039[e]
Half-saturation constant for P uptake	mg P L^{-1}	0.006[j], 0.007[e]
Minimum internal P concentration	mg P [mg Chl-*a*]$^{-1}$	0.1[j], 0.25[e]
Maximum internal P concentration	mg P [mg Chl-*a*]$^{-1}$	1.0[j], 1.0[e]
Maximum rate of P uptake	mg P [mg Chl-*a*]$^{-1}$ [day]$^{-1}$	1.5[j], 1.0[e]
Half-saturation constant for N uptake	mg N L^{-1}	0.01[j], 0.01[f]
Minimum internal N concentration	mg N [mg Chl-*a*]$^{-1}$	1.0[j], 5.0[e]
Maximum internal N concentration	mg N [mg Chl-*a*]$^{-1}$	5.0[j], 7.5[e]
Maximum rate of N uptake	mg N [mg Chl-*a*]$^{-1}$ [day]$^{-1}$	0.9[j], 10[e]

Parameter description	Units	Values and references
Standard temperature for algal growth	◦C	20[j], 16[e]
Optimum temperature for algal growth	◦C	28[j], 20[e]
Maximum temperature for algal growth	◦C	33[j], 29[e]
Temperature multiplier for growth rates of algae	-	1.09[j], 1.05[e]
Temperature multiplier for respiration rates of algae	-	1.08[j], 1.05[e]
Constant settling velocity	m day^{-1}	-0.20[g]; 0.05[g]

Sources: [a] Woodward et al. (2017); [b] Imberger and Patterson (1990); [c] Spigel et al. (1986); [d] Sherman et al. (1978); [e] Robson and Hamilton (2004); [f] Burger et al. (2007); [g] Estimated; [h] Stoichiometry relation; [i] Chung et al. (2014); [j] Missaghi et al. (2013); [k] Griffin et al. (2001); [l] Romero et al. (2004).

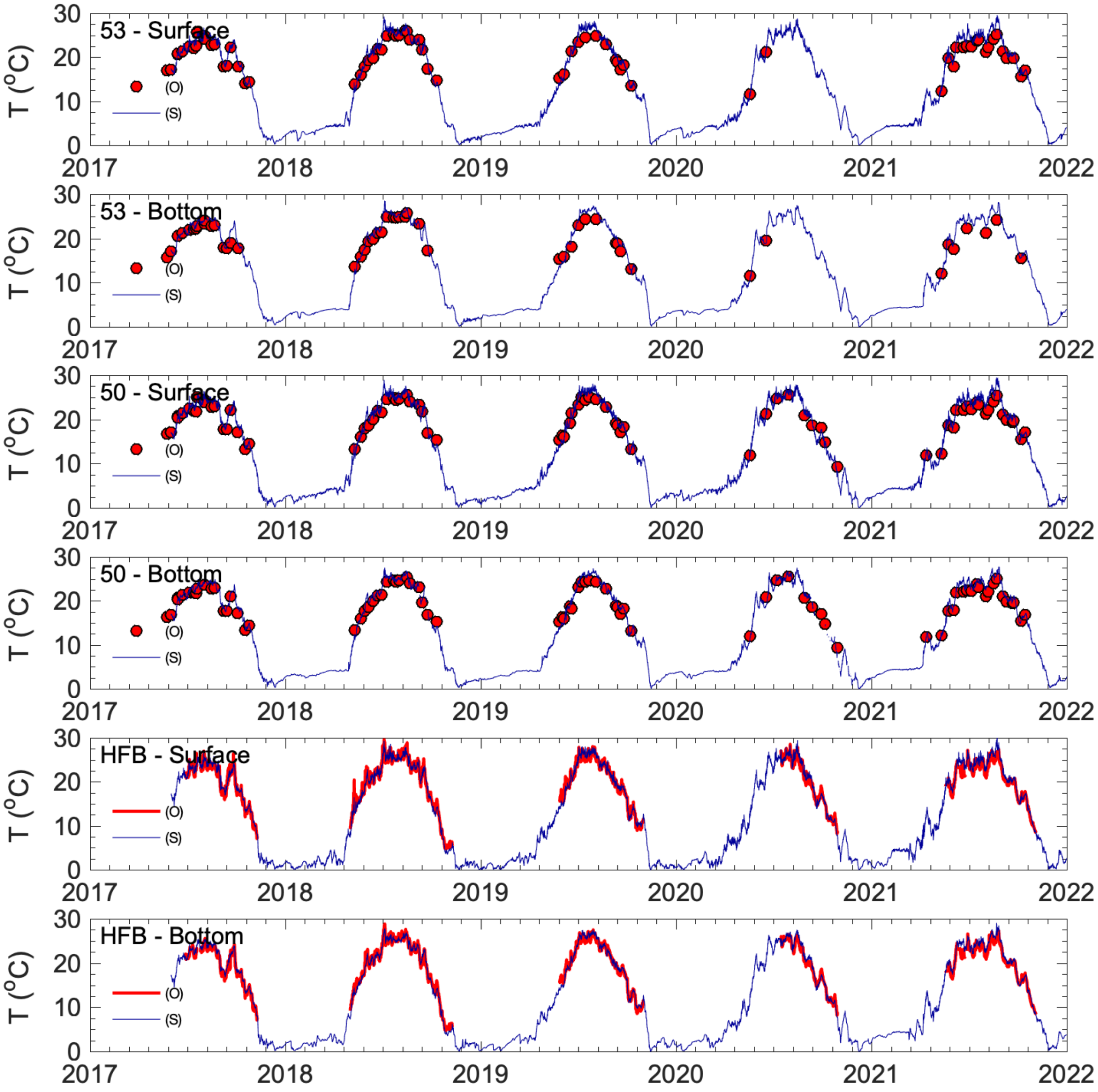

Figure A1. Comparison of model simulation results against field observations (red circles) in the surface (1 m), and bottom waters (0.5 m above the bottom) at different monitoring stations (LTMP stations 53 and 50, and VT EPSCoR BREE HFB) in Missisquoi Bay during the calibration and validation period for water temperature.

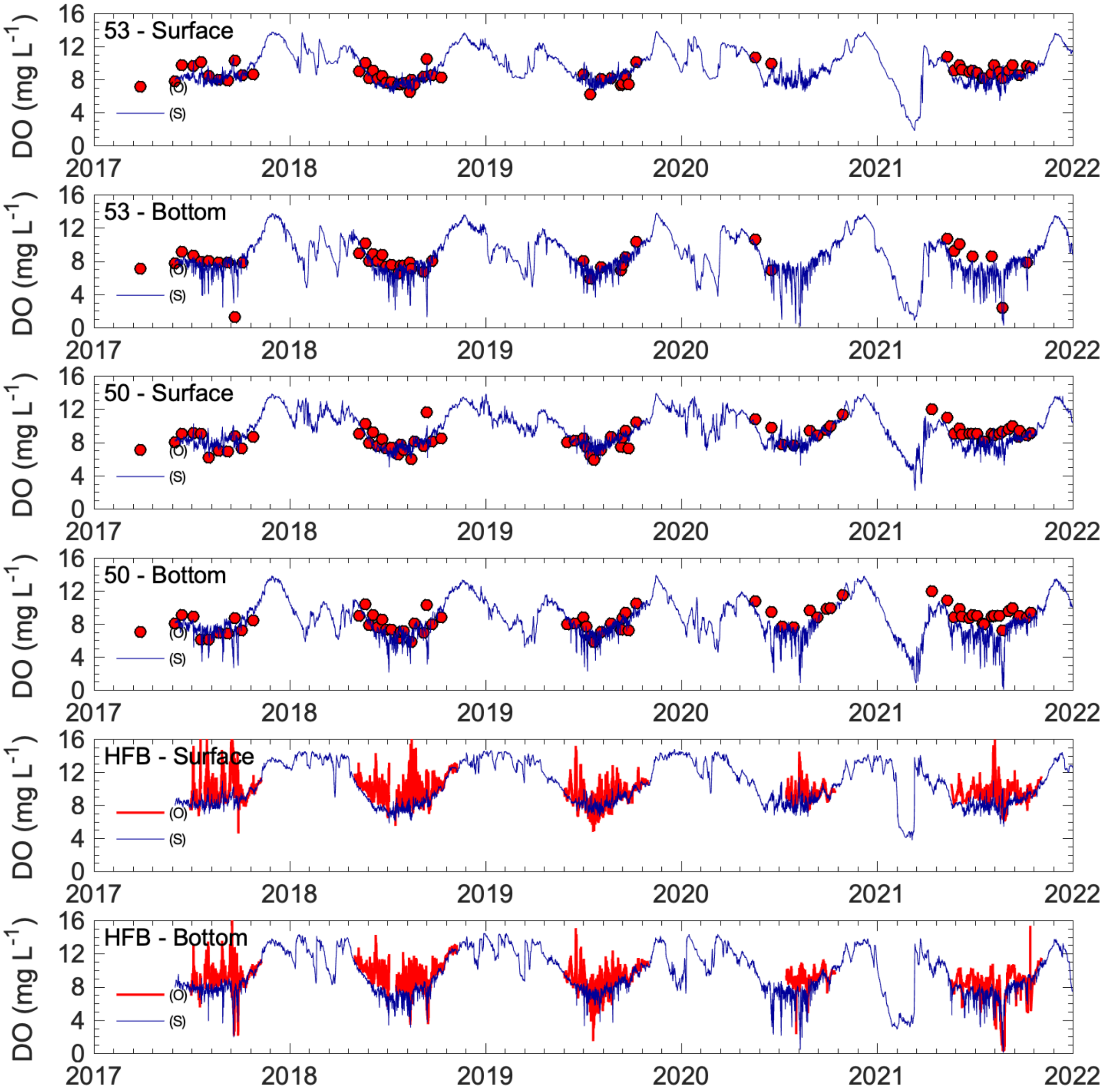

Figure A2. Comparison of model simulation results against field observations (red circles) in the surface (1 m), and bottom waters (0.5 m above the bottom) at different monitoring stations (LTMP stations 53 and 50, and VT EPSCoR BREE HFB) in Missisquoi Bay during the calibration and validation period for dissolved oxygen.

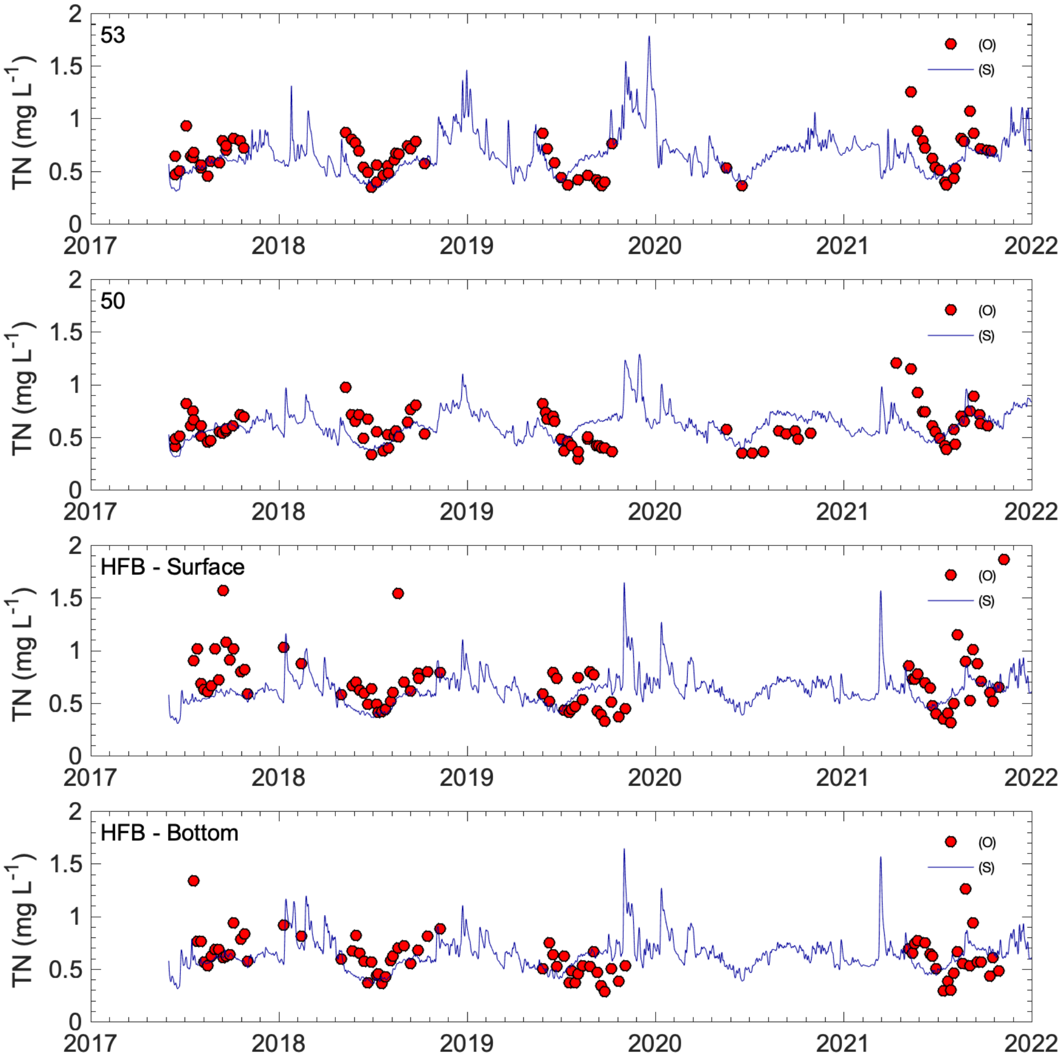

Figure A3. Comparison of model simulation results against field observations (red circles) at different monitoring stations (LTMP stations 53 and 50 – euphotic zone, and VT EPSCoR BREE HFB - the surface (1 m) and bottom waters (0.5 m above the bottom)) in Missisquoi Bay during the calibration and validation period for Total Nitrogen.

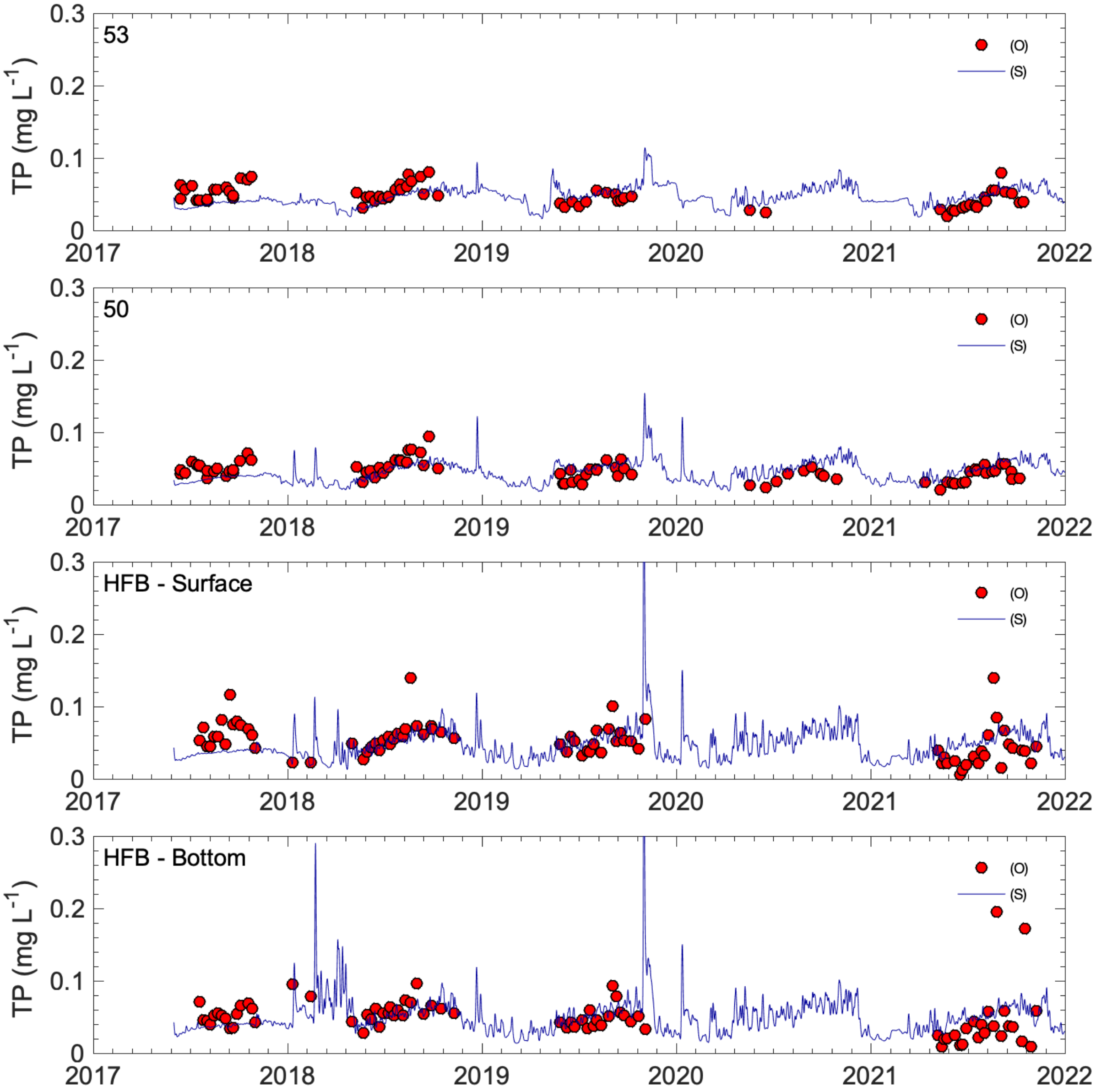

Figure A4. Comparison of model simulation results against field observations (red circles) at different monitoring stations (LTMP stations 53 and 50 – euphotic zone, and VT EPSCoR BREE HFB - the surface (1 m) and bottom waters (0.5 m above the bottom)) in Missisquoi Bay during the calibration and validation period for Total Phosphorus.

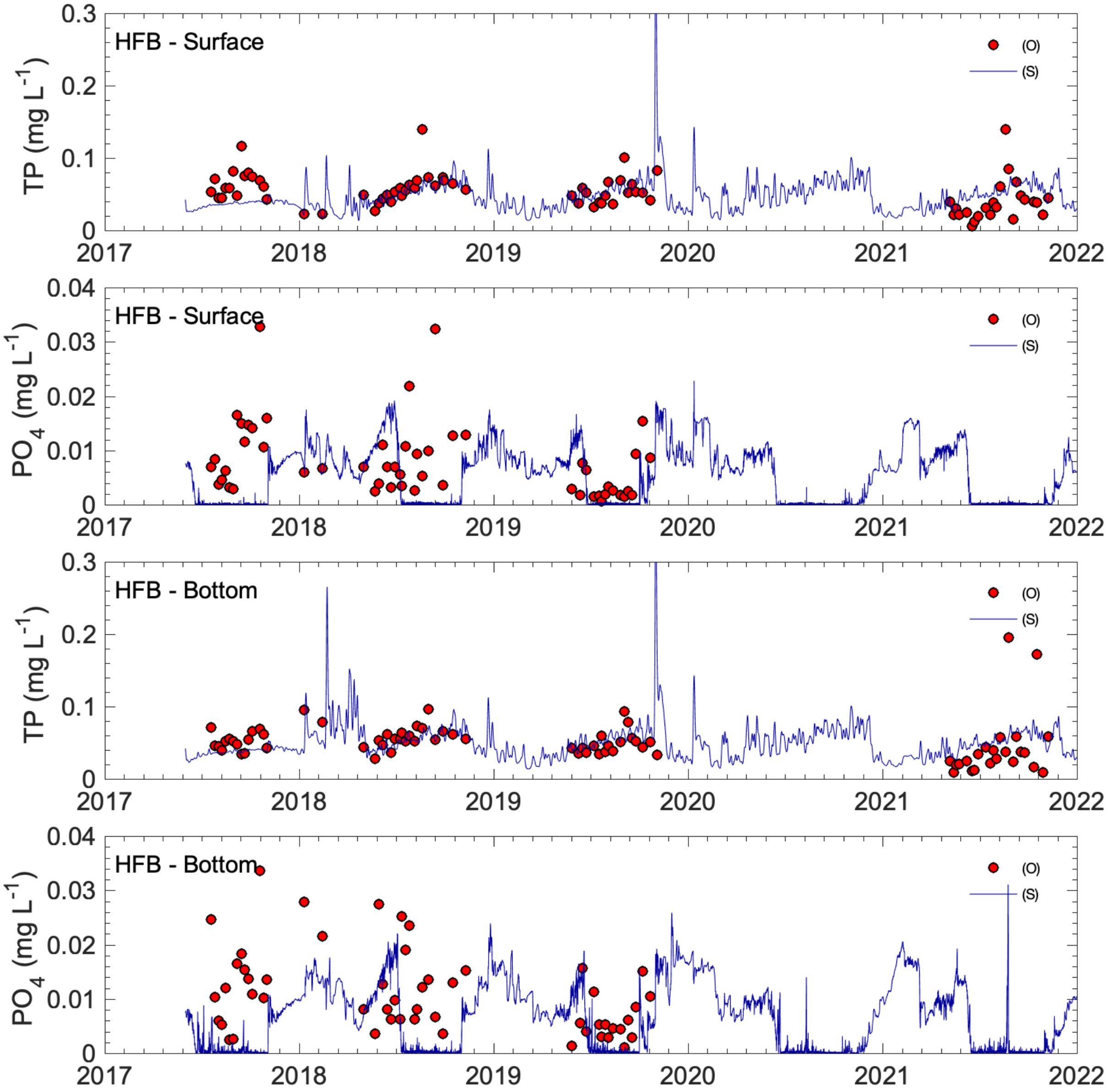

Figure A5. Comparison of model simulation results against field observations (red circles) at the VT EPSCoR BREE HFB monitoring station (the surface (1 m) and bottom waters (0.5 m above the bottom)) in Missisquoi Bay during the calibration and validation period for Total Phosphorus and Phosphate.

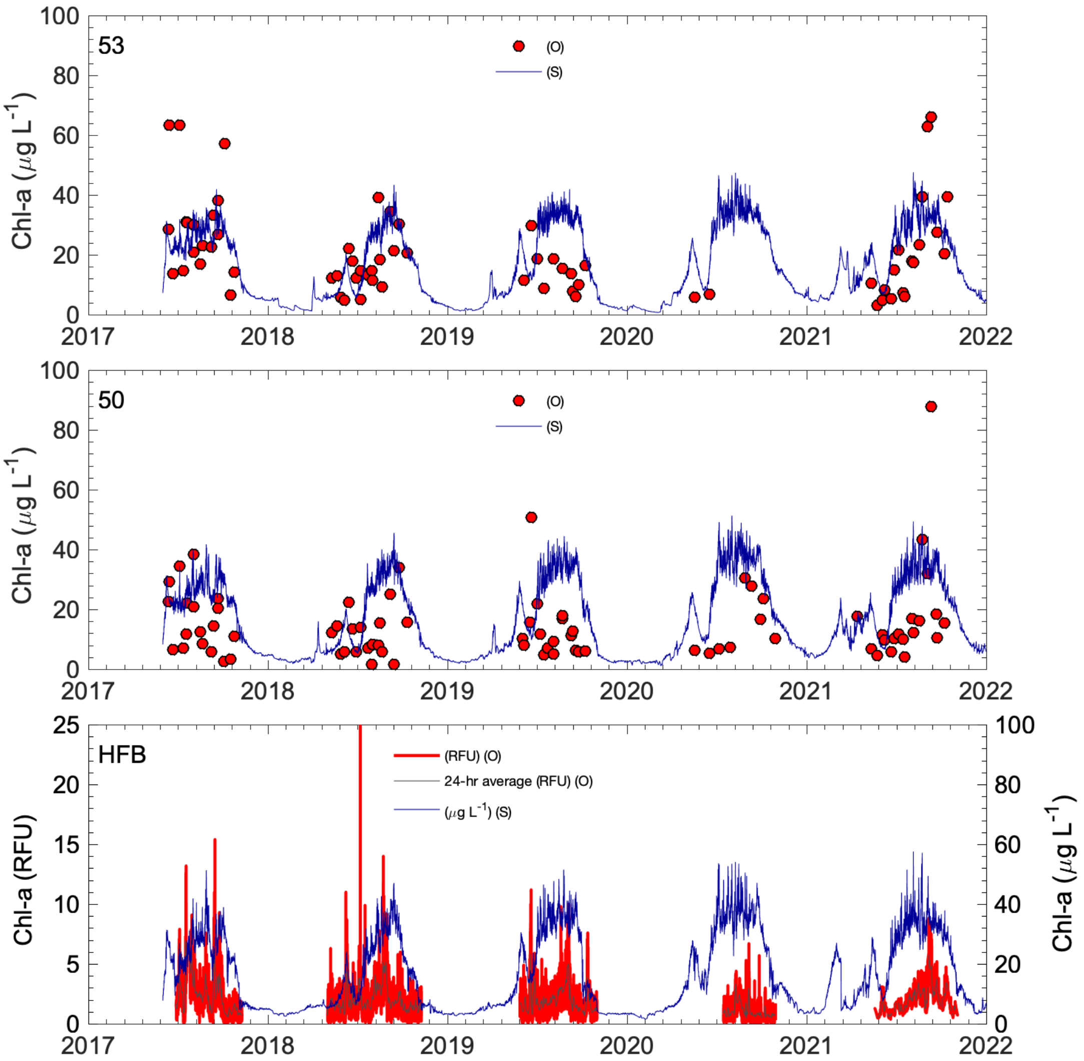

Figure A6. Comparison of model simulation results against field observations (red circles) in the euphotic zone at different monitoring stations (LTMP stations 53 and 50, and VT EPSCoR BREE HFB) in Missisquoi Bay during the calibration and validation period for chlorophyll *a*.

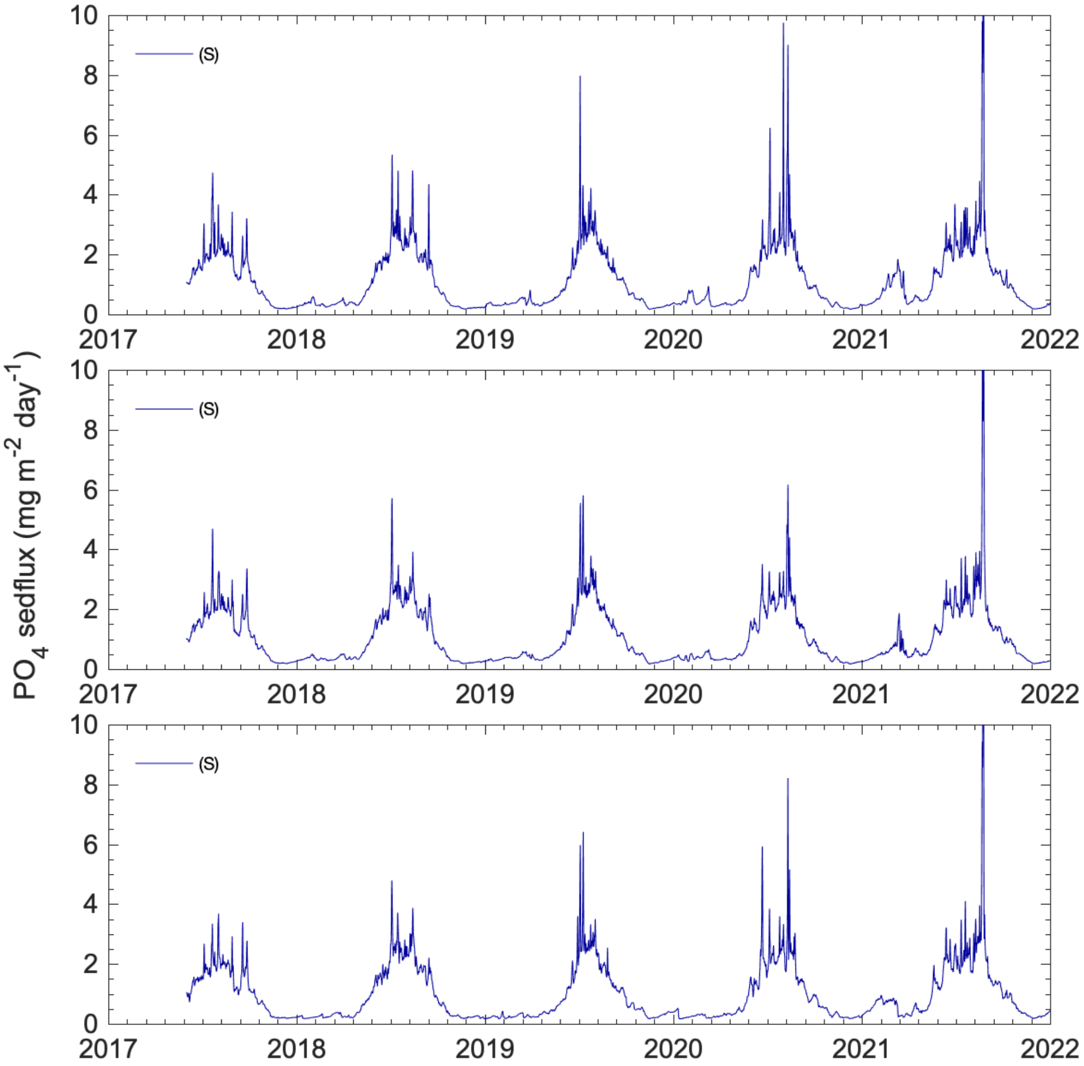

Figure A7. Simulated PO_4 release rate at LTMP stations 53 (top panel) and 50 (middle panel) and VT EPSCOR HFB (bottom panel).

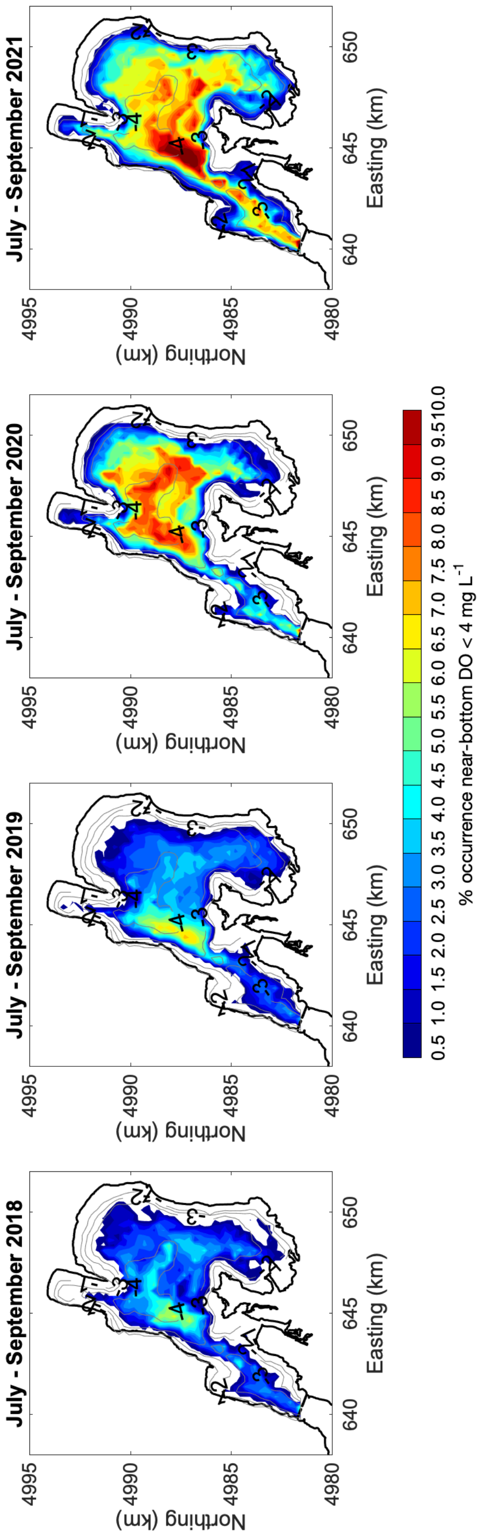

Figure A8. Simulated spatial distribution of areas of low DO concentrations (July-September). The colormap represents the % occurrence of near bottom DO concentrations below 4 mg/L.

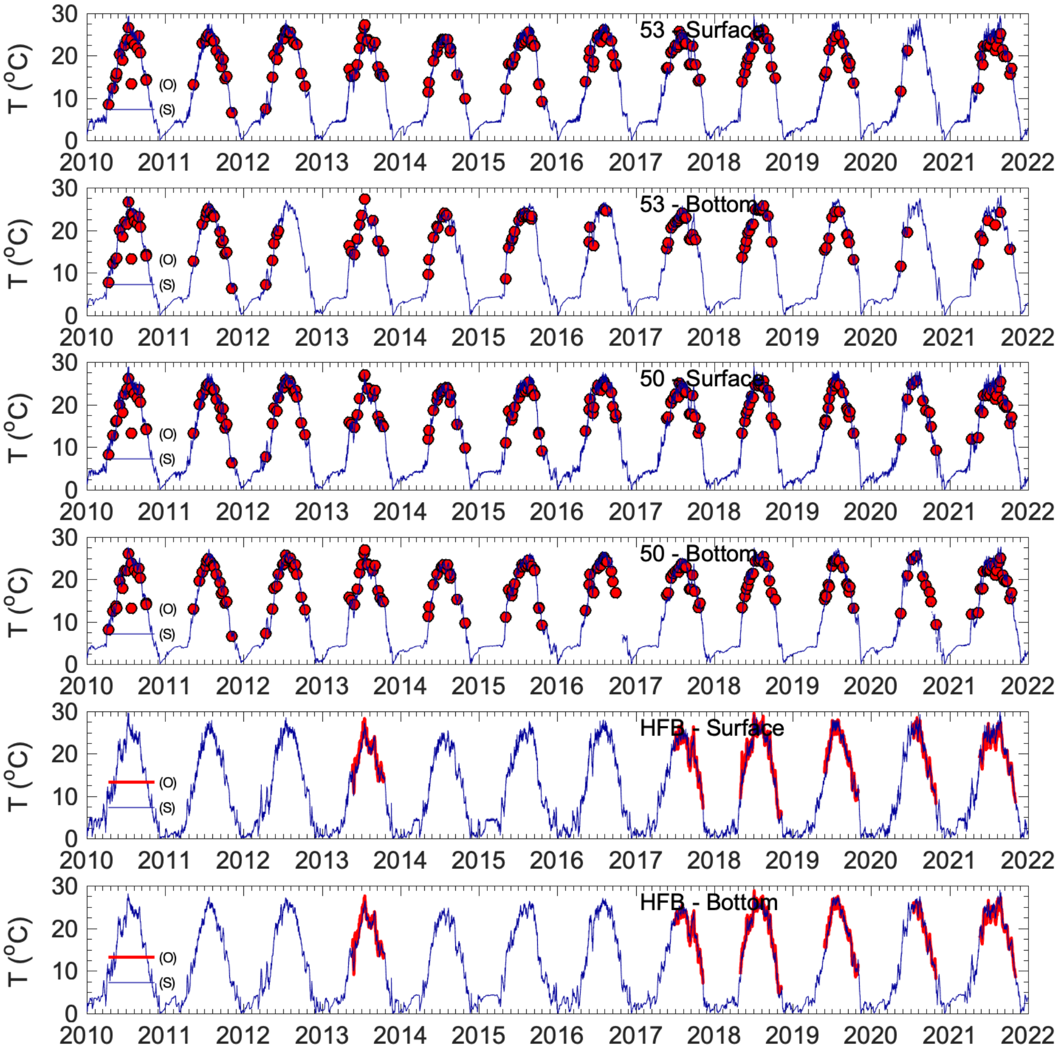

Figure A9. Comparison of model simulation results against field observations (red circles) in the surface (1 m), and bottom waters (0.5 m above the bottom) at different monitoring stations (LTMP stations 53 and 50, and VT EPSCoR BREE HFB) in Missisquoi Bay during the baseline period (2010-2021) for water temperature.

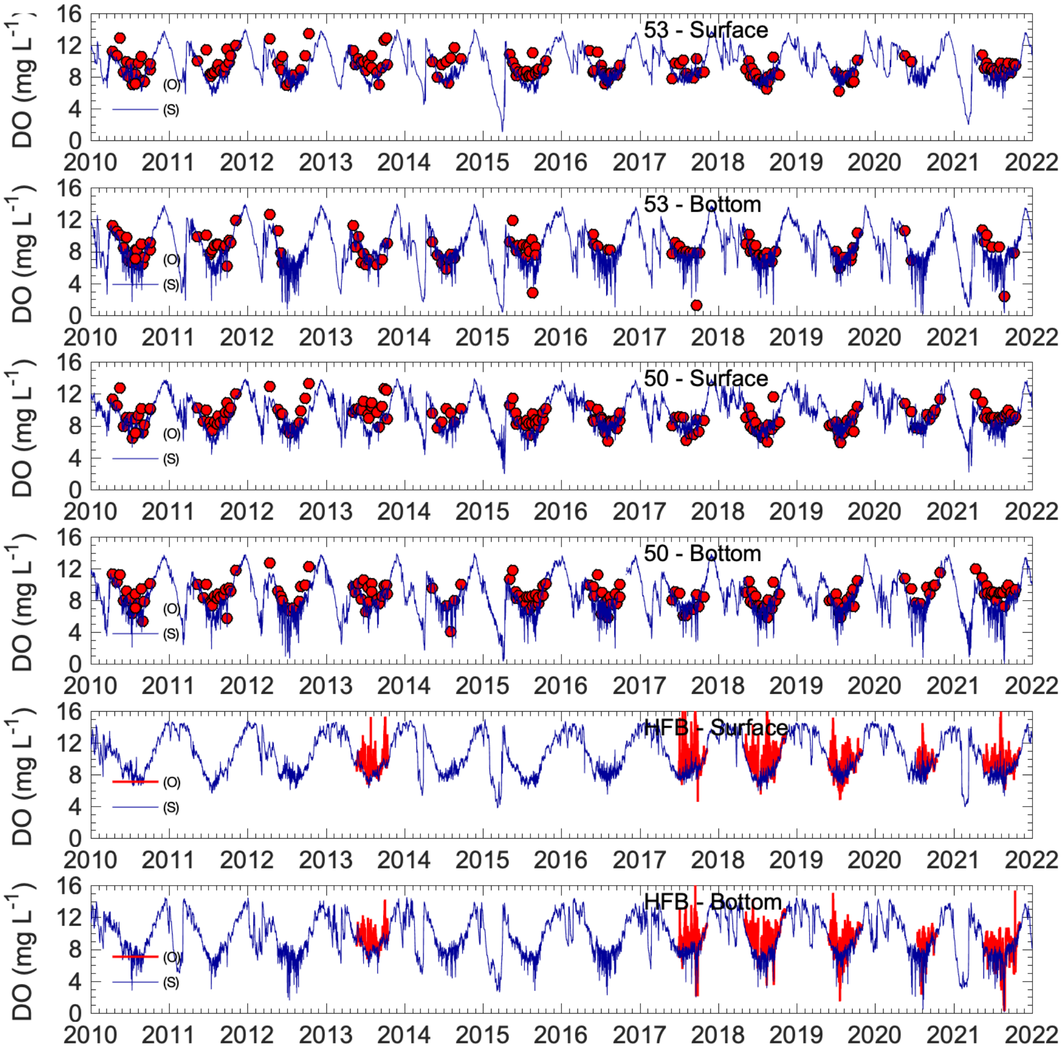

Figure A10. Comparison of model simulation results against field observations (red circles) in the surface (1 m), and bottom waters (0.5 m above the bottom) at different monitoring stations (LTMP stations 53 and 50, and VT EPSCoR BREE HFB) in Missisquoi Bay during the baseline period (2010-2021) for dissolved oxygen.

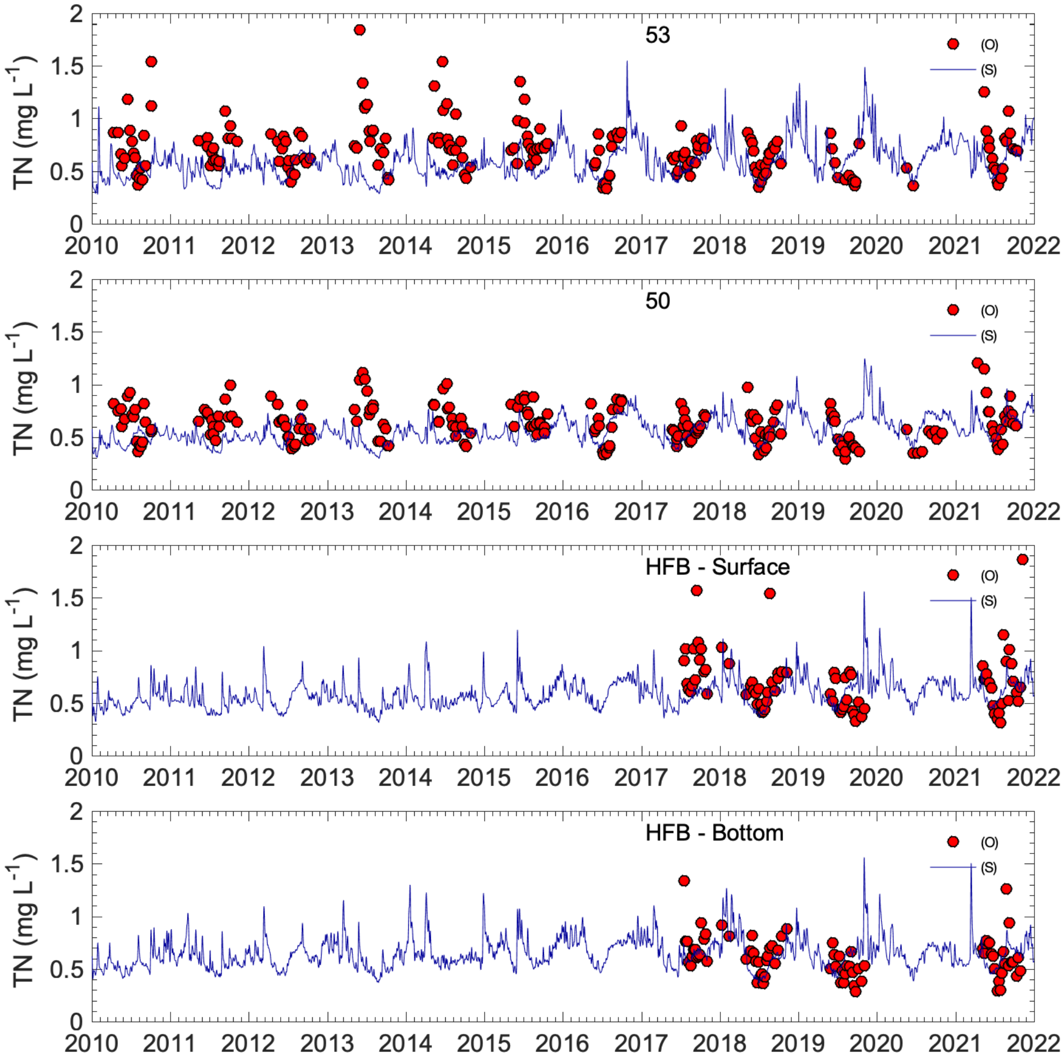

Figure A11. Comparison of model simulation results against field observations (red circles) at different monitoring stations (LTMP stations 53 and 50 – euphotic zone, and VT EPSCoR BREE HFB - the surface (1 m) and bottom waters (0.5 m above the bottom)) in Missisquoi Bay during the baseline period (2010-2021) for Total Nitrogen.

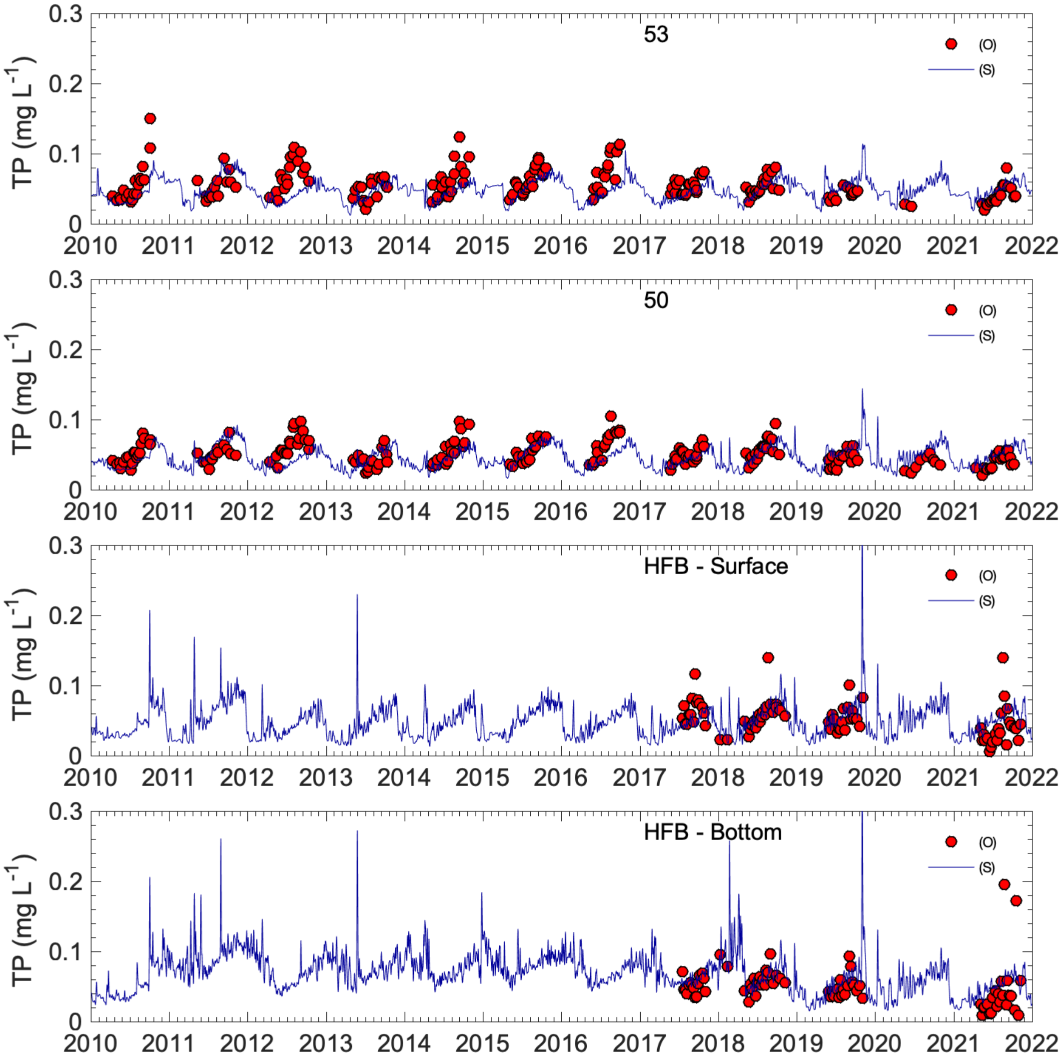

Figure A12. Comparison of model simulation results against field observations (red circles) at different monitoring stations (LTMP stations 53 and 50 – euphotic zone, and VT EPSCoR BREE HFB - the surface (1 m) and bottom waters (0.5 m above the bottom)) in Missisquoi Bay during the baseline period (2010-2021) for Total Phosphorus.

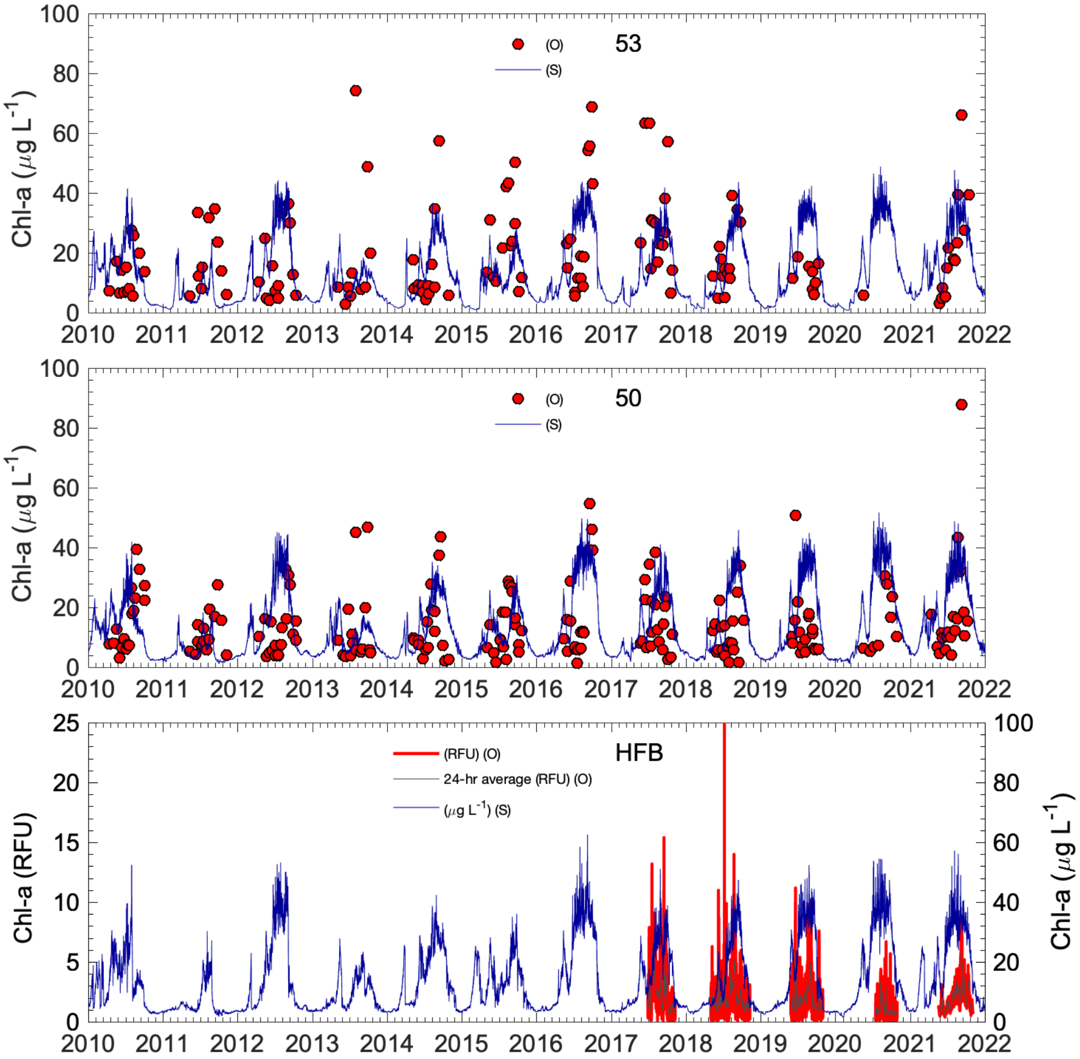

Figure A13. Comparison of model simulation results against field observations (red circles) in the euphotic zone at different monitoring stations (LTMP stations 53 and 50, and VT EPSCoR BREE HFB) in Missisquoi Bay during the baseline period (2010-2021) for chlorophyll *a*.